



Universidade Federal da Paraíba
Centro de Ciências Exatas e da Natureza

Programa de Pós-Graduação *Stricto Sensu* em Física

**Neutral and Electrically Charged
Localized Structures**

Matheus Moreira de Assis Paganelly

Tese de Doutorado

João Pessoa
2023

Universidade Federal da Paraíba
Centro de Ciências Exatas e da Natureza

Matheus Moreira de Assis Paganelly

Neutral and Electrically Charged Localized Structures

Trabalho apresentado ao Programa de Pós-Graduação Stricto Sensu em Física do Centro de Ciências Exatas e da Natureza da Universidade Federal da Paraíba como requisito parcial para obtenção do grau de Doutor em Física na Área de Concentração de Física das Partículas Elementares e Campos.

Orientador: *Dionísio Bazeia Filho*
Co-orientador: *Matheus Araújo Marques*

João Pessoa
2023

Catálogo na publicação
Seção de Catalogação e Classificação

P128n Paganelly, Matheus Moreira de Assis.
Neutral and electrically charged localized
structures / Matheus Moreira de Assis Paganelly. - João
Pessoa, 2023.

116 f. : il.

Orientação: Dionísio Bazeia Filho.

Coorientação: Matheus Araújo Marques.

Tese (Doutorado) - UFPB/CCEN.

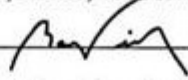
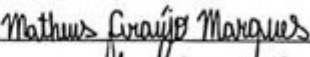
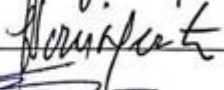

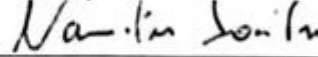
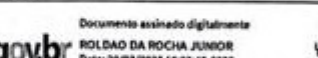
1. Física. 2. Parede de Bloch. 3. Monopolo global.
4. Estruturas carregadas. I. Bazeia Filho, Dionísio.
II. Marques, Matheus Araújo. III. Título.

UFPB/BC

CDU 53(043)

Ata da Sessão Pública da Defesa de tese de Doutorado do aluno Matheus Moreira de Assis Paganelly, candidato ao Título de Doutor em Física na Área de Concentração Física de Partículas Elementares e Campos.

Aos vinte e quatro dias do mês de fevereiro do ano de dois mil e vinte e três, às 14:00, nas dependências do Centro de Ciências Exatas e da Natureza da Universidade Federal da Paraíba, reuniram-se os membros da Banca Examinadora constituída para avaliar a tese de Doutorado, na área de Física de Partículas Elementares e Campos, de **Matheus Moreira de Assis Paganelly**. A banca foi composta pelos(as) professores(as) doutores(as): Dionísio Bazeia Filho (PPGF/UFPB), orientador e presidente da banca examinadora, Matheus Araújo Marques (UFPB), coorientador, José Roberto Soares do Nascimento (PPGF/UFPB), Albert Petrov (PPGF/UFPB), Nami Fux Svaiter (CBPF) e Roldão da Rocha (UFABC). Dando início aos trabalhos, o Prof. Dionísio Bazeia Filho comunicou aos presentes a finalidade da reunião. A seguir, passou a palavra para o candidato para que o mesmo fizesse, oralmente, a exposição da pesquisa de tese intitulada "*Neutral and Electrically Charged Localized Structures*". Concluída a exposição, o candidato foi arguido pela Banca Examinadora, que emitiu o parecer "**aprovado**". Assim sendo, deve a Universidade Federal da Paraíba expedir o respectivo diploma de Doutor em Física na forma da lei. E para constar, Danilo Wilson Lemos Menezes, Técnico em Assuntos Educacionais, redigiu a presente ata que vai assinada pelos membros da Banca Examinadora. João Pessoa, Paraíba, 24 de fevereiro de 2023.

Prof. Dr. Dionísio Bazeia Filho Orientador – PPGF/UFPB	
Prof. Dr. Matheus Araújo Marques Coorientador - UFPB	
Prof. Dr. José Roberto Soares do Nascimento PPGF/UFPB	
Prof. Dr. Albert Petrov PPGF/UFPB	
Prof. Dr. Nami Fux Svaiter CBPF	
Prof. Dr. Roldão da Rocha UFABC	

gouver

Documento assinado digitalmente
ROLDÃO DA ROCHA JUNIOR
Data: 20/02/2023 10:22:45-0300
Verifique em <https://validar.jf.gov.br>

Dedico essa Tese a minha filha Amélie.

Acknowledgements

Gostaria de expressar meus mais sinceros agradecimentos àqueles que foram minha base e suporte ao longo desta jornada. Em primeiro lugar, agradeço a Deus por me guiar e me dar forças em todos os momentos desta jornada. Minha gratidão à minha mãe, ao meu pai e ao meu irmão Pedro, cujo amor incondicional foi fundamental para meu crescimento e amadurecimento.

Aos amigos que estiveram presentes mesmo à distância, Thiago, Júnior, Toneta e Edgar, e ao irmão que a vida me presenteou, George, sou imensamente grato por todas as experiências compartilhadas. Meu primo Adonel e Léo Carreta também têm meu agradecimento especial por terem sido fontes de apoio e incentivo.

Minha estadia na UFPB foi enriquecida pelos diversos colegas que conheci, em particular, Fabiano, Igor Oliveira, Klécio, Susane, João Carlos, Allan e Bongestab. Sua acolhida calorosa e valiosas contribuições foram fundamentais para minha caminhada acadêmica.

Quero destacar e agradecer profundamente aos dedicados professores da pós-graduação da UFPB, que tornaram o departamento uma referência. Em especial, ao professor Sérgio, que além de ser um mentor exemplar, também se tornou um grande amigo e conselheiro.

Meus mestres, não posso deixar de mencioná-los. Agradeço ao meu coorientador Matheus Marques e ao meu orientador Dionísio Bazeia, cuja orientação e incentivo foram imprescindíveis para a realização deste trabalho.

Em João Pessoa, encontrei uma família que me acolheu calorosamente. A Alysson e a Vouban, agradeço por fazerem parte desse capítulo importante da minha vida.

Por fim, um agradecimento especial à minha companheira e meu amor, Isabela, que esteve ao meu lado, dando suporte e força durante a reta final deste processo. E à minha querida Amélie, minha fonte de inspiração.

A todos vocês, meu profundo reconhecimento por terem contribuído de forma significativa para que esta tese se tornasse uma realidade.

E a tarefa da filosofia é mesmo a de revelar aos homens a utilidade do inútil ou, em outras palavras, ensiná-los a distinguir entre os dois sentidos da palavra "útil".

—PIERRE HADOT

Resumo

Esta tese centra-se na investigação de estruturas localizadas em diferentes cenários. Começamos com uma revisão de teoria de campos para um campo escalar em uma dimensão espacial e outra temporal, incluindo uma ação com densidade Lagrangiana padrão e uma discussão de temas-chave, como o procedimento de Bogomol'nyi, formalismo de primeira ordem para minimização de energia, estabilidade de soluções e estruturas como kinks, lumps, paredes de domínio do tipo Néel e Bloch. Introduzimos um modelo de dois campos escalares acoplados que podem ser usados para descrever Bloch Walls e investigamos modificações na sua estrutura interna em um modelo campo de três escalares com um acoplamento não mínimo. Nessa tese também apresentamos o método da órbita tentativa, usado para encontrar órbitas que desacoplam as equações de primeira ordem. Apresentamos uma nova forma de construir estruturas topológicas com simetria global em D dimensões espaciais, contornando o teorema de Derrick e Hobart. O procedimento nos leva a estruturas localizadas como monopolos globais com energia regularizada. Também investigamos configurações de multicampos eletricamente carregadas, onde consideramos uma permissividade elétrica controlada por campos escalares que descrevem uma parede do tipo Bloch capaz de regularizar a divergência do campo elétrico na origem dando origem a estruturas do tipo anel e casca para duas e três dimensões, respectivamente.

Palavras-chave: Kinks, Parede de Bloch, Monopolo global, Estruturas carregadas.

Abstract

This thesis focuses on the investigation of localized structures in different scenarios. We start with a review of the scalar field theory in one spatial and one temporal dimension, including a standard Lagrangian density action and a discussion of key topics such as the Bogomol'nyi procedure, first-order formalism for energy minimization, stability of solutions and structures like kinks, lumps, Néel and Bloch domain walls. We introduce a two-coupled scalar field model that can be used to describe Bloch Walls and investigate modifications in its internal structure in a three-scalar field model with a non-minimum coupling. This thesis also presents the trial orbit method for orbits that decouple the first-order equations. We present a new way to construct topological structures with global symmetry in D spatial dimensions, bypassing the Derrick and Hobart theorem. The procedure leads us to localized structures like global monopoles with regularized energy. We also investigate electrically charged multi-field configurations, where we consider an electric permittivity controlled by scalar fields that describe a Bloch-type wall capable of regulating the electric field divergence at the origin, giving rise to ring and shell structures for two and three dimensions, respectively.

Keywords: Kinks, Bloch Wall, Global Monopole, Charged Structures.

Contents

1	Introduction	1
2	Domain Walls	5
2.1	The scalar field	5
2.1.1	BPS models	7
2.1.2	Linear stability	8
2.2	Kinks	11
2.3	A brief comment on topology	13
2.4	Lumps	14
2.5	Bloch Wall	15
2.5.1	BPS for two scalar fields	16
2.5.2	BNRT model	17
2.5.3	Trial orbit method	18
3	Internal Structure of Bloch Walls	21
3.1	Manipulating the internal structure	21
3.1.1	First Model	25
3.1.2	Second Model	27
3.1.3	Third Model	30
4	Spatially localized structures	33
4.1	Circumventing the Theorem	33
4.2	Global Monopole	36
4.2.1	The $ \phi^4 $ model	41
4.2.2	The $ \phi^6 $ model	42
4.3	Extended global monopole	44
4.3.1	The second extend model	49
5	Electrically charged multi-field configurations	53
5.1	A single point charge	53
5.2	Charged configurations	56
5.2.1	Two spatial dimensions	58
5.2.2	Three spatial dimensions	59
5.3	Internal structure of charged configurations	61
5.3.1	Two spatial dimensions	64
5.3.1.1	First model	65

5.3.1.2	Second model	66
5.3.2	Three spatial dimensions	69
5.3.2.1	First model	70
5.3.2.2	Second model	71
5.4	Global Monopole in the presence of electric charge	72
6	Conclusions and perspectives	79
A	Integrating factor for BPS equations	81
A.1	Integrating factor	81
A	Conserved quantities	85
A.1	Noether Current	85
A.2	Energy-momentum tensor	89

List of Figures

1.1	Néel wall (top) and Bloch wall (bottom).	2
2.1	The potential $V(\phi)$, in Eq.(2.34).	11
2.2	The solution $\phi(x)$ in Eq. (2.37).	12
2.3	The Néel Wall.	12
2.4	The energy density ρ in Eq. (2.38).	13
2.5	The potential $V(\phi)$ in Eq. (2.42).	14
2.6	The lump solution $\phi(x)$ (left) in Eq. (2.44) and the energy density ρ (right) in Eq. (2.45).	15
2.7	The Bloch Wall.	16
2.8	The solutions $\phi(x)$ (red, dotted line) and $\chi_+(x)$ (blue, solid line) in Eqs. (2.62) and (2.63), depicted for $k = 1/3$.	18
3.1	The solution $\psi(x)$ (left) in Eq. (3.30) and the energy density ρ_2 (right) in Eq. (3.31) depicted for $\alpha = 0.2$ (solid, blue line) and $\alpha = 0.8$ (dotted, red line).	25
3.2	The solutions $\phi(x)$ (left) and $\chi(x)$ (right) associated to the model in Sec. 3.1.1, for $r = 1/3$ and $\alpha = 0.2$ (solid, blue line), and 0.8 (dotted, red line).	26
3.3	The energy density ρ_1 associate to model in Sec. 3.1.1, for $r = 1/3$ and $\alpha = 0.2$ (solid, blue line), and 0.8 (dotted, red line).	27
3.4	The solutions $\phi(x)$ and $\chi(x)$ for the model in Sec. 3.1.2, with $f(\psi) = \sec^2(n\pi\psi)$, depicted with $r = 1/3$ and for $\alpha = 0.2$ (solid, blue line) and 0.6 (dotted, red line) and with $n = 1$ (top) and $n = 2$ (bottom). The insets highlight the behavior of the χ -field configurations near the origin.	28
3.5	The solutions $\phi(x)$ and $\chi(x)$ for the model in Sec. 3.1.2, with $f(\psi) = \csc^2((n + 1/2)\pi\psi)$, depicted with the same values used in Fig. 3.4, for comparison. The insets highlight the behavior of the χ -field configurations near the origin.	29
3.6	The solutions $\phi(x)$ (top panel) and $\chi(x)$ (bottom panel) for the model in Sec. 3.1.3, with $f(\psi) = 1/J_1^2(a\psi)$, depicted with $r = 1/3$ and for $\alpha = 0.2$ and with $a = 5$ (red, dotted line) and $a = 9$ (blue, solid line). The inset highlights the behavior of the χ -field configurations near the origin.	31
3.7	The energy density for $f(\psi)$ being controlled by the cos-secant (blue) and the Bessel (red) functions, depicted for $r = 1/3$, $\alpha = 0.2$, and for $n = 1$ and $a = 5$, respectively.	31

- 4.1 The solution in Eq. (4.55) (top left) and the energy density (4.56) (top right), and the planar section passing through the center of the energy density (bottom), for $D = 3$. 43
- 4.2 Solution in Eq. (4.61) (top left), the energy density in Eq. (4.62) (top right) and planar section passing through the center of the energy density (bottom), for $D = 3$. 44
- 4.3 Solutions H and \mathcal{H} in Eq. (4.85) and (4.86) (left) and the energy density in Eq. (4.87) (right) for $s = 1/3$ and with $D = 3$. The thinner line represents $H(r)$ and the thicker one stands for $\mathcal{H}(r)$. 48
- 4.4 Planar section of the energy density (42) passing through its center, for $D = 3$ and $s = 0.2$ (left), $s = 0.3$ (center), $s = 0.4$ (right). 48
- 4.5 Solution $H(r)$ (left) in Eq. (51a) its associated energy density (23) (right) for $D = 3$ and $n = 1, 4$ and 16 . The darkness of the color increases with n . 51
- 4.6 Planar section passing through the center of the energy density (23) for $D = 3$ and $n = 1$ (left), 4 (center) and 16 (right). The darkness of the color increases with n . 51
- 5.1 The solutions $\phi(r)$ (left) and $\chi(r)$ (right) associated to the model in Sec. 5.2.1 for $\sigma = 5$, with $k = 1$ (solid, blue line) and 2 (dotted, red line). 58
- 5.2 The radial component of the electric field (left) for $e = 1$ and the energy density (right) associated to the model in Sec. 5.2.1 for $\sigma = 5$, with $k = 1$ (solid, blue line) and 2 (dotted, red line). 59
- 5.3 The radial component of the electric field (left, blue) with $e = 1$ and the energy density (right, orange) associated to the model in Sec. 5.2.1 depicted in the plane for $\sigma = 5$, with $k = 1$ (top), and $k = 2$ (bottom). The intensity of the blue and orange colors increases with the increasing of the electric field and energy density, respectively. 60
- 5.4 The solutions $\phi(r)$ (left) and $\chi(r)$ (right) associated to the model in Sec. 5.2.2 for $\sigma = 5$, with $k = 1$ (solid, blue line) and 2 (dotted, red line). 61
- 5.5 The radial component of the electric field (left) with $e = 1$ and the energy density (right) associated to the model in Sec. 5.2.2 for $\sigma = 5$, with $k = 1$ (solid, blue line) and 2 (dotted, red line). The inset in the bottom figure shows the interval $\rho \in [0, 0.04]$. 61
- 5.6 The electric field in the plane (left, blue) with $e = 1$ and the energy density (right, orange) associated to the model in Sec. 5.2.2 for $\sigma = 5$ and $k = 1$. The intensity of the blue and orange colors increases with the increasing of the electric field and energy density, respectively. 62
- 5.7 The solutions $\psi(r)$ in Eq. (5.55) (left), and the energy density in Eq. (5.56) (right) for $\alpha = 2$. 65
- 5.8 The solutions $\phi(r)$ (left) and $\chi(r)$ (right) associated to the model in Sec. 5.3.1.1 for $\sigma = 5$ and $\alpha = 2$, with $k = 1$ (solid, blue line) and 2 (dotted, red line). 66
- 5.9 The radial component of the electric field (left) with $e = 1$ and the energy density (right) associated to the model in Sec. 5.3.1.1 for $\sigma = 5$, $\alpha = 2$, with $k = 1$ (solid, blue line) and 2 (dotted, red line). 66

- 5.10 The radial component of the electric field (left, blue) with $e = 1$ and the energy density (right, orange) associated to the model in Sec. 5.3.1.1 depicted in the plane for $\sigma = 5$ and $\alpha = 2$, with $k = 1$ (top), and $k = 2$ (bottom). The intensity of the blue and orange colors increases with the increasing of the electric field and energy density, respectively. 67
- 5.11 The solutions $\phi(r)$ (left) and $\chi(r)$ (right) associated to the model in Sec. 5.3.1.2 for $\sigma = 5$, $\alpha = 2$ and $n = 2$, with $k = 1$ (solid, blue line) and 2 (dotted, red line). The inset in the bottom figure shows the interval $r \in [0.5, 1.5]$ for $k = 2$. 68
- 5.12 The radial component of the electric field (left) with $e = 1$ and the energy density (right) associated to the model in Sec. 5.3.1.2 for $\sigma = 5$, $\alpha = 2$ and $n = 2$, with $k = 1$ (solid, blue line) and $k = 2$ (dotted, red line). 68
- 5.13 The electric field (left, blue) with $e = 1$ and the energy density (right, orange) associated to the model in Sec. 5.3.1.2 depicted in the plane for $\sigma = 5$, $\alpha = 2$ and $n = 2$, with $k = 1$ (top) and 2 (bottom). The intensity of the blue and orange colors increases with the increasing of the electric field and energy density, respectively. 69
- 5.14 The solution $\psi(r)$ in Eq. (5.68) (left) and the energy density ρ_2 in Eq. (5.69) (right) for $\alpha = 2$. The inset in the top figure shows the solution near the origin. 70
- 5.15 The solution $\phi(r)$ (left) and $\chi(r)$ (right) associated to the model in Sec. 5.3.2.1 for $\sigma = 5$ and $\alpha = 2$ with $k = 1$ (solid, blue line) and 2 (dotted, red line). 70
- 5.16 The radial component of the electric field (left) with $e = 1$ and the energy density (right) associated to the model in Sec. 5.3.2.1 for $\sigma = 5$, $\alpha = 2$, and $k = 1$ (solid, blue line) and 2 (dotted, red line). 71
- 5.17 The section passing through the center of the structure, representing the electric field (left, blue) with $e = 1$ and the energy density (right, orange) associated to the model in Sec. 5.3.2.1 for $\sigma = 5$, $\alpha = 2$ and $k = 2$. The intensity of the blue and orange colors increases with the increasing of the electric field and energy density, respectively. 71
- 5.18 The solutions $\phi(r)$ (left) and $\chi(r)$ (right) associated to the model in Sec. 5.3.2.2 for $\sigma = 5$, $\alpha = 2$ and $n = 2$ with $k = 1$ (solid, blue line) and 2 (dotted, red line). The inset in the top figure shows the behavior for small r . 72
- 5.19 The radial component of the electric field (left) with $e = 1$ and energy density (right) associated to the model in Sec. 5.3.2.2 for $\sigma = 5$, $\alpha = 2$ and $n = 2$, with $k = 1$ (solid, blue line) and 2 (dotted, red line). For $k = 2$, we have depicted $2E_r$ and $2\rho_1$ to illustrate the behavior better. 73
- 5.20 The section passing through the center of the structure, representing the electric field (left, blue) with $e = 1$ and the energy density (right, orange) associated to the model in Sec. 5.3.2.2 for $\sigma = 5$, $\alpha = 2$, with $k = 1$ (top) and 2 (bottom). The intensity of the blue and orange colors increases with the increasing of the electric field and energy density, respectively. 73
- 5.21 Gauge field (left) and the radial component of the electric field in Eq.(5.90) (right) associated to the system with electric permittivity in Eq.(5.89), for $D = 3$ and $e = 1$.** 76

- 5.22 Section of the electric field passing through the center of the structure in the interval $r \in [0, 3]$ for $D = 3$ and $e = 1$. White, blue and purple are used to represent $E_r = 0$, $E_r = 0.079$ and $E_r = 2$, respectively. 76
- 5.23 Gauge field (left) and the electric field in Eq. (5.92) (right) associated to the system with electric permittivity in Eq. (5.91), for $D = 3$ and $e = 1$. The inset in the right panel highlights the behavior of the electric field near the origin. 77
- 5.24 Section of the electric field passing through the center of the structure in the interval $r \in [0, 3]$ for $D = 3$ and $e = 1$. White, blue and purple are used to represent $E_r = 0$, $E_r = 0.034$ and $E_r = 1$, respectively. 78

Introduction

Following the approach outlined in Ref. [38], we consider that physics aims to describe a natural phenomenon mathematically and then infer results about experiments that have not been performed. Math seems to speak the language of nature, then why not use it as a starting point? In other words, instead of observing the phenomenon and describing it mathematically, we can use math as a starting point, develop it, and investigate if the results match experiments. In this thesis, we do a bit of both. We use field theory to describe phenomena observed in nature and also propose new results from math which should lead to phenomena not yet observed but which are of interest to several areas of science and technology. For that, we use field theory to investigate topological structures through a branch of math known as topology.

In classical field theory, topological structures are non-trivial solutions of the field equations, which can exhibit stability due to quantized topological properties. These structures emerge as a consequence of the topology of the underlying space and remain independent of the specific details of the field's dynamics. Notably, they are characterized by conserved topological charges that remain unchanged under smooth deformations of the field configuration.

Topological structures are mathematical objects that find applications in many areas, such as physics, mathematics, biology, and computer science. These structures can also be called topological defects. The simplest objects are the kinks, which emerge in one spatial dimension in systems with spontaneous breaking symmetry, which are named domain walls when immersed in more dimensions. Domain walls are stable structures with a topological charge connecting two degenerate potential minima. This structure can be identified in magnetic materials as the configuration between two regions with different magnetizations. Ferromagnetic materials in low temperatures tend to direct spins up or down, giving rise to a non-null magnetization featuring a spontaneous symmetry breaking. These systems present a degenerate ground state, i.e., there are two configurations with minimum energy: all spins up or all spins down. The two cases can coexist, generating two regions with different vacuums. The configuration between these regions gives rise to a localized structure known as the Néel and Bloch wall, which can be identified as a topological structure or domain wall in the context of field theory.

In Ch. 2, we review scalar field theory, where we study the BPS formalism that leads to first-order equations with stable solutions of minimum energy. We show that the procedure can be used to investigate localized structures, which are used to describe the Néel Wall (one scalar field) and Bloch Walls (two scalar fields). In Fig. 1.1, are illustrated these two kinds of walls [30]. This chapter will serve as a starting point for the development of this thesis.

In Ch. 3, we present a procedure that we devolved that leads to modifications in the internal structure of Bloch Walls caused by a function coupled to the dynamical term that simulates geometrical constrictions in a model with three scalar fields introduced by us in Ref. [21]. The

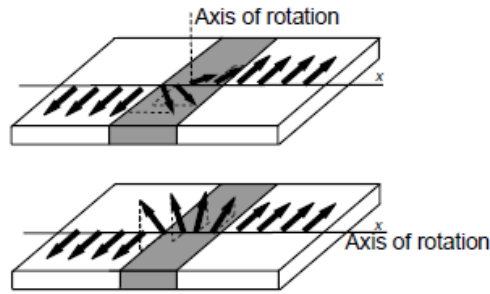


Figure 1.1 Néel wall (top) and Bloch wall (bottom).
Coey, 2010, p. 240.

model investigated deals with a Lagrangian density with three scalar fields and non-minimal coupling between fields done through a function that depends on an independent scalar field. The intriguing consequences of this procedure give rise to captivating effects within the walls, making it a valuable tool for investigating magnetic materials. These findings open new avenues for exploring the behavior of magnetic materials under intricate conditions, especially at the nanometric scale.

Moving on to Chapter 4, we shift our attention to monopoles, another class of topological structures that emerge in three spatial dimensions. Originally introduced by Dirac [37] and further developed by t’Hooft and Polyakov [2][70], monopoles are found in grand unified theories and are considered stable due to local symmetries. This chapter presents new localized structures involving monopoles with global symmetry developed by us in Ref. [19]. In our investigation, we have revealed that the global monopole possesses infinite energy [8]. However, through our developed procedure that leads to first-order formalism, we successfully regularize this infinite energy, offering new insights into the structure’s behavior and properties. Furthermore, we go beyond the standard model and explore the implications of extended models involving two families of scalar fields.

In addition to the discussed topological structures, it is worth noting that models with multiple spatial dimensions and diverse fields can give rise to various other intriguing topological objects. Notably, Skyrmions introduced in Refs.[81][80], cosmic strings [86] and vortices[1] are among these fascinating structures. While these objects hold significant interest and importance, they fall beyond the scope of the current thesis and will not be discussed further herein. Nonetheless, their exploration remains an exciting avenue for future research and investigation in the realm of topological phenomena.

The vortices and monopoles in the ’70s paved the way for the investigation of topological structures charged. In the next years, theoretical physics devoted itself to exploring such objects as Dyons, structures with magnetic and electric charge [53], and vortices with Chern-Simons dynamics [47][51], which play a crucial role in the presence of magnetic vortices that carry an electric charge. In Chapter 5, we explore the possibility of the new charged localized structures. In the investigation, we consider a point charge in a medium with electric permittivity controlled by scalar fields, which describes Bloch walls. The procedure regularizes the electric

field divergence at the origin. Furthermore, we investigate a similar model, where we consider a set of scalar fields and electric permittivity controlled by the modulus of the family of scalar fields.

We ended our work in Ch. 6, summarizing the results obtained and discussing future perspectives.

This present thesis considers natural unity, which uses the following definition for the constants $c = \hbar = k_B = 1$. The spacetime coordinates in these physical units have an inverse energy dimension, while the action defined as $S = \int \mathcal{L} d^{D+1}x$ has a null energy dimension. Here, $D + 1$ represents D spatial dimensions and one time dimension.

Domain Walls

In the 20th century, Lev Landau took the first step towards spontaneous symmetry breaking in his study of the statistical physics of phase transition [59]. Later these concepts were adopted in field theory.

It can be said that the study of the real scalar field is the most elementary problem in a field theory and the simplest model that allows symmetry breaking and topological solutions. In $(1, 1)$ spacetime dimensions, models with spontaneous symmetry breaking can lead to localized topological structures called kinks. When they are immersed in more than one dimension, they are called domain walls.

In this chapter, we will study kinks, lumps, and the energy-momentum tensor for these structures, describe the first-order formalism that minimizes the energy, and analyze their linear stability. In addition, we present a model with two coupled scalar fields that mimic the domain wall with an internal structure.

2.1 The scalar field

The scalar field is a mathematical function that associates a scalar value with each point in space. Its applications are widespread, encompassing various fields of study. For instance, in general scenarios, the scalar field can be employed to describe the temperature distribution in a room, the humidity in a given space, the frequency of lightning strikes in a region, or even the population density in a country, among others.

In the realm of physics, scalar fields find diverse and fundamental applications. They are used to represent the electric potential in electrostatic scenarios, the gravitational potential, and the pressure variation in regions traversed by sound waves.

Moreover, in condensed matter physics, scalar fields are instrumental in describing the order parameter in ferromagnetic materials [21]. They provide critical insights into the behavior and properties of these materials at a microscopic level.

Additionally, scalar fields serve as essential tools in understanding and describing branes in cosmology. Within the braneworld scenario, the observable universe is represented by a hypersurface in $(3, 1)$ spacetime dimensions, known as the brane. This brane exists within a higher-dimensional space denoted by $(3, 1, d)$, commonly referred to as the bulk [74]. In this particular model, the scalar field assumes a crucial role in modeling the extra dimension. Notably, in reference [11], the authors put forth a system incorporating two scalar fields, effectively generating a brane with an intriguing internal structure.

Among these applications, a particularly intriguing one involves utilizing scalar fields to

describe the phenomenon of spontaneous symmetry breaking, which leads to interesting effects such as phase transitions, the emergence of new excitations, and the formation of topological structures, among others [58]. In our investigation, we focus on studying localized structures like kinks and lumps, for which a scalar field theory serves as a powerful tool.

Let us start with the model for the real scalar field described by the canonical Lagrangian density given by

$$\mathcal{L} = \frac{1}{2} \partial_\mu \phi \partial^\mu \phi - V(\phi), \quad (2.1)$$

where ϕ is the real scalar field, the derivatives are written in the form $\partial_\mu \phi = \partial \phi / \partial x^\mu$, $V(\phi)$ is the potential density, although we call it a potential. Here, x^μ is identified as the components of the coordinate system, where $\mu = 0, 1, \dots, D$, with x^0 being the temporal part and x^i the spatial, with $i = 1, \dots, D$. In our investigation, we are considering the Minkowski flat space with metric tensor given by $\eta_{\mu\nu}$, and components $\eta_{00} = 1$ and $\eta_{ij} = -\delta_{ij}$, where $j = 1, \dots, D$.

In this chapter, we focus the investigations on the $(1, 1)$ spacetime dimensions. The action in this case is given by $S = \int \mathcal{L} d^2x$. As it has a null energy dimension, the Lagrangian density must have a squared energy dimension since d^2x has an inverse squared energy dimension. Note that the term $\partial_\mu \phi \partial^\mu \phi$ and the Lagrangian density have the same dimension, and the partial derivative ∂_μ has an energy dimension, which leads to the scalar field ϕ dimensionless.

The equation of motion obtained by varying the action associated (see Appendix A) has the form

$$\partial_\mu \partial^\mu \phi + V_\phi = 0, \quad (2.2)$$

where $V_\phi = dV/d\phi$. Writing the above equation in terms of components, we get

$$\ddot{\phi}(x, t) - \phi''(x, t) + V_\phi = 0. \quad (2.3)$$

Here, we use the compact notation that follows $\phi'' = \partial^2 \phi / \partial x^2$ and $\ddot{\phi} = \partial^2 \phi / \partial t^2$.

The localized structures we are looking for are time-independent, that is, are the solutions of the equation of motion constant in time. In order to investigate these static configurations, we take $\phi(x, t) = \phi(x)$. In this situation, the equation of motion in Eq. (2.3) becomes

$$\phi''(x) = V_\phi. \quad (2.4)$$

The Lagrangian density in Eq. (2.1) is a functional of the fields and their derivatives. In other words, the Lagrangian density can be written as $\mathcal{L} = \mathcal{L}(\phi, \partial_\mu \phi)$, not explicitly depending on the coordinates x^μ . In variational calculus models of this type, translation invariants, allow us to define a tensor called the energy-momentum tensor. Below we write it for a general case of $(D, 1)$ -dimensions:

$$T_{\mu\nu} = \frac{\partial \mathcal{L}}{\partial(\partial^\mu \phi)} \partial_\nu \phi(x) - \eta_{\mu\nu} \mathcal{L}. \quad (2.5)$$

This expression in components terms can be written in matrix form as follows

$$T_{\mu\nu} = \begin{pmatrix} \frac{\dot{\phi}^2}{2} + \frac{\phi'^2}{2} + V(\phi) & \phi' \dot{\phi} \\ \phi' \dot{\phi} & \frac{\dot{\phi}^2}{2} + \frac{\phi'^2}{2} - V(\phi) \end{pmatrix}. \quad (2.6)$$

The steps for getting it can be seen in Appendix A. Here, T_{00} is identified as the energy density ρ and T_{11} denotes pressure or stress. The components T_{01} and T_{10} are the flux density and momentum density, respectively. The static configurations scenario in (1, 1) leads us to the disappearance of the other components T_{01} and T_{10} , while the others become

$$T_{00} = \frac{\phi'^2}{2} + V(\phi), \quad (2.7)$$

$$T_{11} = \frac{\phi'^2}{2} - V(\phi). \quad (2.8)$$

2.1.1 BPS models

In this section, we delve into a significant challenge posed by the second-order equation in (2.4) governing the scalar field ϕ . Obtaining analytical solutions for this equation is not a straightforward task, and in certain cases, numerical methods are the only viable option. However, an insightful alternative to simplify the problem arises through the method introduced by Bogomol'nyi [27], Prasad, and Sommerfield [71], known as BPS (Bogomol'nyi-Prasad-Sommerfield). This remarkable method enables the reduction of second-order equations to first-order equations, thus offering a more manageable approach.

The essence of the BPS procedure seems to resonate with Dirac's principle of simplicity [38], as it involves "completing the square on energy density." Despite its apparent simplicity, the implications of the BPS approach are profound, as it leads to solutions with minimal energy.

Here, we present the BPS procedure in the context of a scalar field in (1, 1) spacetime dimensions. Furthermore, in the subsequent chapter, we showcase its versatile application in higher dimensions and various fields, highlighting its significance as a powerful tool for investigating topological structures in different physical systems.

The Bogomol'nyi formalism consists in to include an auxiliary function $W(\phi)$ in the energy density in Eq. (2.7) as follows

$$\rho = \frac{1}{2} \left(\phi' \mp W_\phi \right)^2 + V(\phi) - \frac{W_\phi^2}{2} \pm W', \quad (2.9)$$

where $W' = dW/dx$ e $W_\phi = dW/d\phi$. Then, we take the potential $V(\phi)$ in terms of the auxiliary function and recognize it as a non-negative

$$V(\phi) = \frac{1}{2} W_\phi^2. \quad (2.10)$$

In this way, the energy density takes the form

$$\rho = \frac{1}{2} \left(\phi' \mp W_\phi \right)^2 + W'. \quad (2.11)$$

By integration, we get the energy

$$E = \frac{1}{2} \int_{-\infty}^{+\infty} [(\phi' \mp W_\phi)^2 + W'] dx. \quad (2.12)$$

Notice that the second term is surface integral, so it can be rewritten as follows

$$\begin{aligned} E &= \frac{1}{2} \int_{-\infty}^{+\infty} (\phi' \mp W_\phi)^2 dx + \int_{-\infty}^{+\infty} \frac{dW}{dx} dx \\ &= \frac{1}{2} \int_{-\infty}^{+\infty} (\phi' \mp W_\phi)^2 dx + E_B, \end{aligned} \quad (2.13)$$

where

$$E_B = |W(\phi(+\infty)) - W(\phi(-\infty))| \quad (2.14)$$

or just $E_B = |\Delta W|$. Note that the first term in this equation can be positive or null once it is squared. Therefore, we can conclude that the energy has a lower bound, $E \geq E_B$, where E_B is called Bogomol'nyi energy. The minimum energy is reached when the first term is null, in this case, $E = E_B$, and for this to happen, the first-order equation must be written as

$$\phi' = \pm W_\phi. \quad (2.15)$$

This expression reduces the energy density in Eq. (2.11) to $\rho = W'$, minimizing the energy. The first-order equation solutions are known as BPS state or BPS solutions. Notice that for these configurations to exist the condition $\phi(+\infty) \neq \phi(-\infty)$ must be met, otherwise from the Bogomol'nyi E_B in Eq. (2.14) becomes null, that is, the ground state theory must be degenerate. In topology, we say that the homotopy group needs to be non-trivial. Therefore, BPS solutions are naturally Furthermore, these states produce configurations with null stress, as can be seen by replacing the first-order equation (2.15) in Eq.(2.8), which leads to

$$\begin{aligned} T_{11} &= \frac{W_\phi^2}{2} - V(\phi) \\ &= \frac{W_\phi^2}{2} - \frac{W_\phi^2}{2} \\ &= 0. \end{aligned} \quad (2.16)$$

One of the advantages of the method is that it features minimum energy states, which can be obtained knowing only the boundary conditions for the scalar field ϕ . In this case, we need to know $\phi(x \rightarrow \pm\infty)$ and calculate $|\Delta W(\phi)|$ in these limits. Note that the adjacent minimum must be degenerate, so there is Bogomol'nyi energy.

2.1.2 Linear stability

In order to investigate the configuration stability under small perturbations, we write the scalar field as $\phi(x,t) = \phi(x) + \eta(x,t)$, where $\phi(x)$ is the static solution and $\eta(x,t)$ represents the fluctuations around it. Replacing in the equation of motion (2.2) we get

$$\partial_\mu \partial^\mu \phi(x) + \partial_\mu \partial^\mu \eta(x,t) + V_\phi + V_{\phi\phi} \eta(x,t) = 0, \quad (2.17)$$

where the potential derivative was expanded considering $\eta(x, t)$ until the first-order, as follows

$$V_{\phi(x,t)} = \left. \frac{dV}{d\phi} \right|_{\phi(x)} + \left. \frac{d^2V}{d\phi^2} \right|_{\phi(x)} (\phi(x, t) - \phi(x)) , \quad (2.18)$$

or yet in a compact form

$$V_{\phi(x,t)} = V_{\phi} + V_{\phi\phi}\eta(x, t) . \quad (2.19)$$

Notice that the sum of the first and the third term in Eq. (2.17) can be identified as the equation of motion (2.2) for the static case, and since this term is null, we can eliminate it. Thus, the stability equation, in coordinate terms, can be rewritten as

$$\ddot{\eta}(x, t) - \eta''(x, t) + U(x)\eta(x, t) = 0 , \quad (2.20)$$

where stability potential is defined by

$$U(x) = V_{\phi\phi} . \quad (2.21)$$

In order to solve the partial second-order equation in (2.20), one can rewrite the fluctuation $\eta(x, t)$ using the separation of variables, where the spatial and temporal parts are written in terms of $\eta(x)$ and $\cos(w_i t)$ functions, as follows

$$\eta(x, t) = \sum_i \xi_i(x) \cos(w_i t) . \quad (2.22)$$

In this way, Eq. (2.20) becomes

$$\left(-\frac{d^2}{dx^2} + U(x) \right) \xi_i = w_i^2 \xi_i . \quad (2.23)$$

Notice that this expression can be identified as a eigenvalues and eigenvectors problem, where H is the linear operator given by $H = -d^2/dx^2 + U(x)$ and ξ_i is the eigenfunction with eigenvalue w_i^2 , as follows

$$H\xi_i = w_i^2 \xi_i . \quad (2.24)$$

We can do the trick to get the zero modes of the stability equation differentiating the equation of motion in (2.2) concerning the x coordinate, which leads us to

$$\left(-\frac{d^2}{dx^2} + U(x) \right) \phi' = 0 . \quad (2.25)$$

Comparing the above equation with (2.23), we can identify the zero modes as a spatial derivative of the scalar field $\xi_0 = A\phi'$, where A is a constant and the eigenvalue is $w_0^2 = 0$. This trick will not always be efficient, and sometimes will be necessary to factor the operator and calculate the zero modes.

Notice that if $w_i^2 < 0$, then the values for w_i will be complex but remember that the temporal part in Eq. (2.22) is given by $\cos(wt)$. It turns out that the cosine argument of complex value makes it a hyperbolic cosine, and analyzing the hyperbolic cosine, we see that it diverges asymptotically. To avoid divergences in the temporal part, we should look for eigenvalues $w_i^2 > 0$, so that w_i is real and the temporal part of the stability equation float around the static solution giving rise to stable solutions.

Consider the H operator, if it can be factored and rewritten as $H = SS^\dagger$, where S is an operator and S^\dagger is its supersymmetric partner, so the equation (2.24) becomes

$$S^\dagger S \xi_i = w_i^2 \xi_i, \quad (2.26)$$

multiplying by ξ_i^\dagger left and integrating we can show that

$$\int_{-\infty}^{+\infty} \xi_i^\dagger S^\dagger S \xi_i dx = \int_{-\infty}^{+\infty} \xi_i^\dagger w_i^2 \xi_i dx, \quad (2.27)$$

or yet

$$w_i^2 = \frac{\int_{-\infty}^{+\infty} |S \xi_i|^2 dx}{\int_{-\infty}^{+\infty} |\xi_i|^2 dx}, \quad (2.28)$$

that is, $w_i^2 > 0$. Therefore, showing that the operator H can be written in the form $H = SS^\dagger$, we can ensure w_i real, in that way to obtain stable solutions.

The above results were obtained for a general case of a scalar field in (1,1) spacetime dimensions. Since the target of our investigation are BPS solutions, we take the operator H in Eq.(2.23) in terms of an auxiliary function $W(\phi)$ in order to evaluate the stability of the configuration, as follows

$$H = \frac{d^2}{dx^2} + W_{\phi\phi}^2 + W_\phi W_{\phi\phi}. \quad (2.29)$$

Note that the above expression can be written as

$$S^\dagger S = \frac{d^2}{dx^2} + W_{\phi\phi}^2 + W_\phi W_{\phi\phi}, \quad (2.30)$$

if we identify

$$S = -\frac{d}{dx} + W_{\phi\phi}, \quad (2.31)$$

$$S^\dagger = \frac{d}{dx} + W_{\phi\phi}. \quad (2.32)$$

Therefore, we conclude that the operator H for the BPS case can be factored, $H = S^\dagger S$. This means that BPS configurations produce positive eigenvalues and hence are stable. It is worth remembering that BPS configurations are solutions of minimum energy and, therefore, cannot decay into a less energetic solution. In this sense, it was expected that they would be stable.

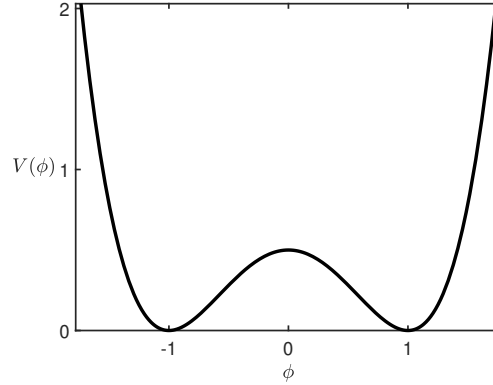


Figure 2.1 The potential $V(\phi)$, in Eq.(2.34).

2.2 Kinks

Kinks are localized structures that arise from spontaneous symmetry breaking in a scalar field theory with one spatial dimension. The symmetry break occurs in models where the ground state is degenerate. When immersed in high dimensions, kinks become domain walls; see Refs.[86][83][31][63]. The symmetry break occurs in models where the ground state is degenerate.

A well-known model that supports these conditions is the $\lambda\phi^4$ described by the potential

$$V(\phi) = \frac{1}{2}\lambda^2(a^2 - \phi^2)^2. \quad (2.33)$$

where a and λ are parameters. As we saw earlier, in natural unity, the potential has a square energy dimension as the Lagrangian and the scalar field is dimensionless. In this case, λ must have an energy dimension, and a must be dimensionless.

We can execute a transformation that eliminates the parameters taking the scalar field $\phi \rightarrow a\phi$, the coordinate $x^\mu \rightarrow x^\mu/a\lambda$ and Lagrangian density $\mathcal{L} \rightarrow \lambda^2 a^4 \mathcal{L}$, which leads us to write the potential as

$$V(\phi) = \frac{1}{2}(1 - \phi^2)^2. \quad (2.34)$$

Notice that the ground state of this model is degenerate. The potential has two different minimum energy states on $\phi = -1$ and $\phi = 1$, as seen in Fig.2.1. The topological sector is the patch that connects the potential minima. The field configuration that arises between the two minima due to spontaneous symmetry breaking is known as kink.

The auxiliary function associated with this model is obtained through the equation in (2.10) that relates $W(\phi)$ with the potential $V(\phi)$:

$$W(\phi) = \phi - \frac{\phi^3}{3}. \quad (2.35)$$

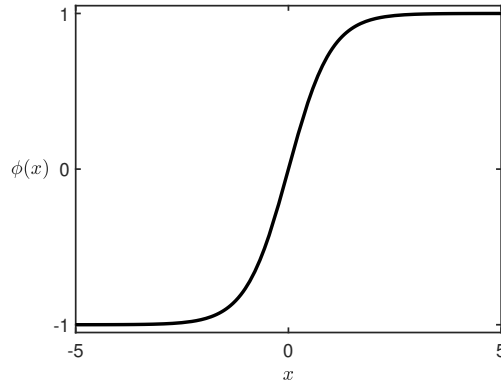


Figure 2.2 The solution $\phi(x)$ in Eq. (2.37).

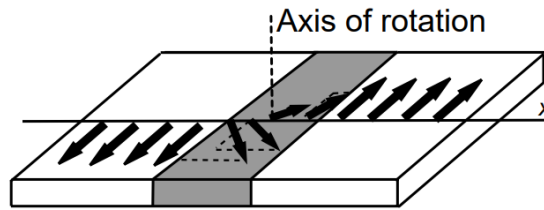


Figure 2.3 The Néel Wall.
Coey, 2010, p.240.

In this scenario, the first-order equation in (2.15) takes the form

$$\phi' = \pm(1 - \phi^2). \quad (2.36)$$

This equation supports kink-type solutions for the positive sign and anti-kinks for the negative case given by

$$\phi(x) = \pm \tanh(x). \quad (2.37)$$

Notice that $\phi(x) = \tanh(x + b)$ is also a solution for the first-order equation, where b is a constant that plays the role of locating the center of the solution. As the Lagrangian density is invariant by translation, we can take $b = 0$ without loss of generality.

Kinks can be used to describe structures known as Néel Walls, which are characterized by the spin rotation in their own plane through an angle π [30]. In Fig. 2.2 we depicted the kink centered at the origin and in Fig. 2.3 the Néel Wall. The energy density associated with this configuration is given by

$$\rho = \text{sech}^4(x), \quad (2.38)$$

by integration, we get the energy $E = 2/3$, which match with the expression $E_B = |\Delta W|$.

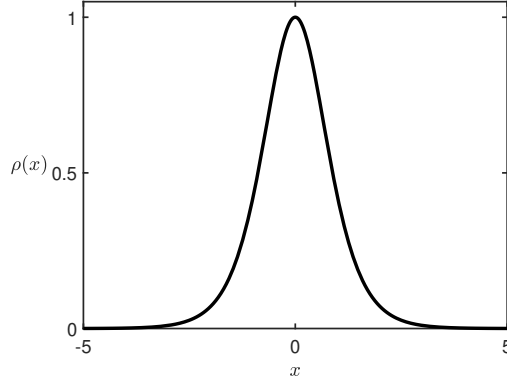


Figure 2.4 The energy density ρ in Eq. (2.38).

2.3 A brief comment on topology

When we study a field from a geometric point of view, we deal with physical quantities such as sizes, angles, lines, shapes, the dimensions of an object, and any other things that might involve the metric. If we calculate the distance between two points on a rubber plane, for instance, and then stretch this plane, we know that the distance will never be the same. For the geometry, these objects are different. On the other hand, for topology, these objects are topologically equivalent. Topology is a mathematics branch that deals with continuous transformations, such as stretching, bending, and the properties preserved under these transformations.

Topological objects may arise in a field theory with spontaneous symmetry breaking and are called topological defects, as discussed in Refs [77][58][39] and in for a more mathematical approach[67]. Defects can be introduced in a field theory through the fundamental fields, which are the sum of a regular field and a singular multivalued part; see Ref. [28].

As seen, the kink connects the two vacuums presented in the model. Such field configuration allows defining a quantity Q given by

$$Q = \phi(+\infty) - \phi(-\infty) . \quad (2.39)$$

Notice that this quantity is not null only for the cases in which the ground state is degenerate. Moreover, Q is independent of Noether's Theorem, which relates continuous symmetries in Lagrangian density to conserved quantities. Therefore, the quantity Q is independent of symmetries, and its conservation depends only on the topology, and that's why it is called topological charge. In this way, one can define a topological conserved current

$$J^\mu = \varepsilon^{\mu\nu} \partial_\nu \phi , \quad (2.40)$$

where $\varepsilon^{\mu\nu}$ is the Levi-Civita symbol and J^0 is identified as the charge density, such that $\partial_\mu J^\mu =$

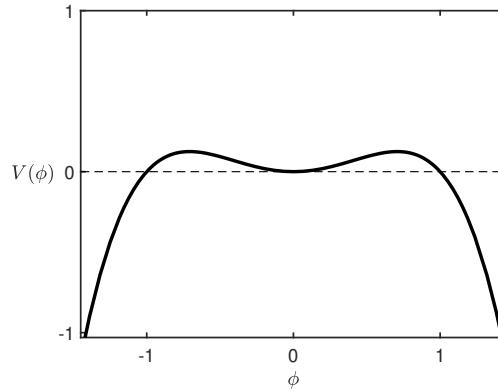


Figure 2.5 The potential $V(\phi)$ in Eq. (2.42).

0. In this sense, the expression for the topological charge is obtained by integration

$$\begin{aligned}
 Q &= \int_{-\infty}^{+\infty} J^0 dx \\
 &= \int_{-\infty}^{+\infty} \varepsilon^{01} \partial_1 \phi dx \\
 &= \phi(+\infty) - \phi(-\infty) .
 \end{aligned} \tag{2.41}$$

Well-behaved fields possess a non-degenerate vacuum that nullifies the above expression. In this case, there is no BPS energy. Defects may still exist, but these are the non-topological type, such as the lump we will see next.

2.4 Lumps

Lumps are non-topological configurations with null topological charges. Although these structures are unstable, they still arouse interest in the description of some physical, such as bright solitons in optic phenomena [44]. The author in Ref. [64] proposes new models that present an unusual decay. In Ref. [6] are exhibited lump-like structures that have their profile controlled by parameters. Another important application for the lumps occurs in non-topological structures called Q-ball [32]. Q-balls are stable structures described for a complex scalar field and carry a conserved global charge due to continuous symmetry.

A model that leads to configurations lump type is the inverse ϕ^4 with potential given by

$$V(\phi) = \frac{1}{2}\phi^2 - \frac{1}{2}\phi^4 . \tag{2.42}$$

In order to obtain time-independent solutions, we consider static configurations, which leads the equation of motion in (2.2) to

$$\phi'' = \phi(1 - 2\phi^2) . \tag{2.43}$$

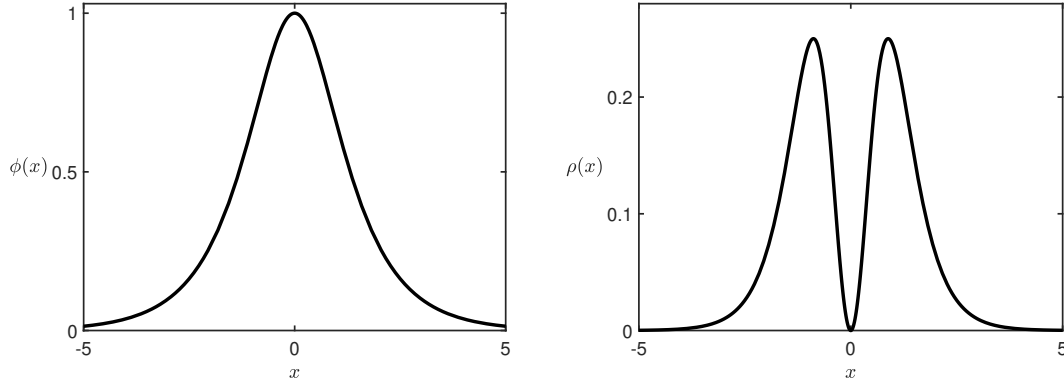


Figure 2.6 The lump solution $\phi(x)$ (left) in Eq. (2.44) and the energy density ρ (right) in Eq. (2.45).

Notice that, different from the previous example, this potential crosses the zero taking negative values, as can be seen in Fig. 2.5. On the other hand, the potential for BPS solutions must be positive from the $V = W_\phi^2/2$ in Eq. (2.10). Therefore, BPS solutions are incompatible with lumps. The equation of motion (2.43) supports the solution

$$\phi(x) = \pm \text{sech}(x) , \quad (2.44)$$

and the energy density of this structure is given by

$$\rho = \text{sech}^2(x) \tanh^2(x) . \quad (2.45)$$

In fig.2.6, we depicted the lump solution and its energy density. Notice that this configuration tends to zero for $x \rightarrow \pm\infty$, which implies in Bogomol'nyi energy E_B null. The energy of this structure is $E = 2/3$.

2.5 Bloch Wall

In this investigation, we examine a specific type of domain wall known as the Bloch Wall. These structures possess an internal structure and are characterized by spins that rotate outside the plane in which they are contained, as depicted in Fig. 2.7. To accurately describe Bloch Wall structures, scalar field theories must be formulated using two scalar fields. The Lagrangian density that accommodates these configurations can be represented by

$$\mathcal{L} = \frac{1}{2} \partial_\mu \phi \partial^\mu \phi + \frac{1}{2} \partial_\mu \chi \partial^\mu \chi - V(\phi, \chi) , \quad (2.46)$$

where χ is the scalar field and now the potential $V(\phi, \chi)$ depends on ϕ and χ . The next steps are to proceed with the same method of handling as for the Néel Wall.

The equations of motion associated with this model are given by

$$\begin{aligned} \partial_\mu \partial^\mu \phi + V_\phi &= 0, \\ \partial_\mu \partial^\mu \chi + V_\chi &= 0 . \end{aligned} \quad (2.47)$$

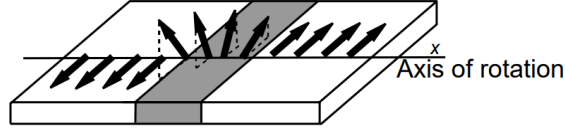


Figure 2.7 The Bloch Wall.
Coey, 2010, p.240.

The above equations for static configurations become

$$\phi'' = V_\phi, \quad (2.48)$$

$$\chi'' = V_\chi. \quad (2.49)$$

The energy density for this configuration is

$$\rho = \frac{\phi'^2}{2} + \frac{\chi'^2}{2} + V(\phi, \chi). \quad (2.50)$$

2.5.1 BPS for two scalar fields

In order to perform the Bogomol'nyi procedure for two scalar fields, we set a new auxiliary function $W(\phi, \chi)$. Following the lines of Eq. (2.9), we rewrite the energy density in Eq.(2.50) in the form

$$\rho = \frac{1}{2} \left(\phi' \mp W_\phi \right)^2 + \frac{1}{2} \left(\chi' \mp W_\chi \right)^2 + V(\phi, \chi) - \frac{1}{2} W_\phi^2 - \frac{1}{2} W_\chi^2 \pm W', \quad (2.51)$$

where

$$\begin{aligned} W' &= \frac{\partial W}{\partial \phi} \frac{d\phi}{dx} + \frac{\partial W}{\partial \chi} \frac{d\chi}{dx} \\ &= W_\phi \frac{d\phi}{dx} + W_\chi \frac{d\chi}{dx}. \end{aligned} \quad (2.52)$$

In this case, we identify the potential as

$$V = \frac{1}{2} W_\phi^2 + \frac{1}{2} W_\chi^2, \quad (2.53)$$

the energy density becomes

$$\rho = \frac{1}{2} \left(\phi' \mp W_\phi \right)^2 + \frac{1}{2} \left(\chi' \mp W_\chi \right)^2 \pm W'. \quad (2.54)$$

By integrating, we get the energy

$$\begin{aligned} E &= \int \frac{1}{2} \left[\left(\phi' \mp W_\phi \right)^2 + \left(\chi' \mp W_\chi \right)^2 \right] dx + \int W' dx \\ &= \int \frac{1}{2} \left[\left(\phi' \mp W_\phi \right)^2 + \left(\chi' \mp W_\chi \right)^2 \right] dx + E_B \end{aligned} \quad (2.55)$$

Notice the energy is bounded by a Bogomol'nyi energy E_B that depends on the two field configuration at the infinity

$$E_B = |W(\phi(\infty), \chi(\infty)) - W(\phi(-\infty), \chi(-\infty))|. \quad (2.56)$$

Now for that, the energy can be minimized for configurations it must obey the two first-order equations bellow

$$\phi' = \pm W_\phi, \quad (2.57)$$

$$\chi' = \pm W_\chi. \quad (2.58)$$

Next, we illustrate this procedure with a famous model.

2.5.2 BNRT model

When selecting models for the auxiliary function, it is crucial to exercise caution. Using a simple auxiliary function such as the sum of powers of ϕ and χ , for example, $W(\phi, \chi) = \phi + \chi$, can result in a trivial potential (2.53). An alternative choice, such as $W(\phi, \chi) = \phi - \phi^3 + \chi^2$, results in a non-constant potential, but it will lack an interaction term between the fields, so the equations of motion become independent, leading to a non-interact scalar fields scenario. Therefore, it is essential to have a cross-term that couples the scalar fields. A suitable choice would be

$$W = \phi - \frac{1}{3}\phi^3 - k\phi\chi^2, \quad (2.59)$$

with k serving as a controlling parameter for the intensity of coupling between the scalar fields. Moreover, as we progress, we will discover that k also governs the width of the Bloch wall and influences the amplitude of the χ solution. This captivating model was first introduced in reference [9] and is commonly referred to as BNRT, a nomenclature originating from its association with Ref. [25].

By employing the positive sign in the first-order equations (2.57) and (2.58), we obtain the following outcome:

$$\phi' = 1 - \phi^2 - k\chi^2, \quad (2.60)$$

$$\chi' = -2k\phi\chi. \quad (2.61)$$

These equations support the solutions

$$\phi(x) = \tanh(2kx), \quad (2.62)$$

$$\chi(x) = \pm \sqrt{\frac{1}{k} - 2} \operatorname{sech}(2kx). \quad (2.63)$$

Note that as the parameter k increases, the argument of the hyperbolic tangent in ϕ grows rapidly, resulting in a thin domain wall that resembles a step function. Conversely, for small values of k , the solution becomes thicker. The effects of k on the solution χ are manifested

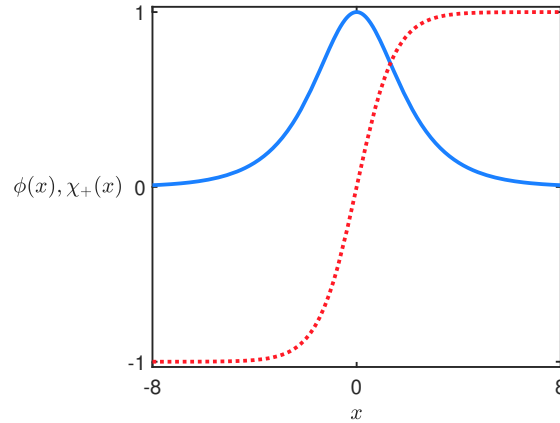


Figure 2.8 The solutions $\phi(x)$ (red, dotted line) and $\chi_+(x)$ (blue, solid line) in Eqs. (2.62) and (2.63), depicted for $k = 1/3$.

through the amplitude of the function $\sqrt{(k^{-1} - 2)}$, which decreases for larger values of k and increases for smaller ones. The width of χ is affected in a manner similar to ϕ .

In the following section, we will delve into the specific steps for obtaining solutions for Bloch walls. However, for now, we will only provide a qualitative overview.

It is important to note that the values of k cannot be arbitrary. First, one must take $k \neq 0$ to avoid divergences, and beyond that $k < 1/2$ in order for $\chi(x)$ to be a real value. The solutions come in pairs $(\phi(x), \chi_+(x))$ and $(\phi(x), \chi_-(x))$, which can be used to describe the left and right chiralities in magnetization as those investigated in recent works [29][69]. The pair (ϕ, χ) can be related to the order parameter of the Bloch wall, which projects $\phi(x)$ in the ϕ axis and $\chi(x)$ in the χ axis. In Fig. 2.8, we have plotted the fields $(\phi(x), \chi_+(x))$ for $k = 1/3$. By analyzing this figure in comparison to Fig. 2.7, one can see $\phi(x)$ is associated with the rotation for an angle π going from $-1(\downarrow)$ to $+1(\uparrow)$, while $\chi(x)$ is related to the twist that occurs out of the plane starting at 0, increasing, and then returning to 0. These structures have also been found to have applications in describing hydrogen-bonded chains and crystalline polyethylene, as detailed in references [24][26].

2.5.3 Trial orbit method

As previously mentioned, solving non-linear coupled differential equations can be a challenging task. The trial orbit method aims to simplify this process by decoupling the differential equations and making them more tractable to solve; see Refs. [73] [10]. This method involves several steps, the first of which is identifying the minima of the potential.

Here we show the method using the BNRT as an example. The potential in Eq. (2.53) for the auxiliary function $W(\phi, \chi)$ in Eq. (2.59) has the form

$$V(\phi, \chi) = \frac{1}{2}(1 - \phi^2)^2 - k\chi^2 + k(1 + 2k)\phi^2\chi^2 + \frac{1}{2}k^2\chi^4, \quad (2.64)$$

its minimums are put like an ordered pair (ϕ, χ) , being $(\pm 1, 0)$ considering $k < 0$, and $(\pm 1, 0)$

and $(0, \pm 1/\sqrt{k})$ for $k > 0$.

We explore the case where $k > 0$. In this situation the potential has four minimums given by $W_1 = W(1, 0) = 2/3$, $W_2 = W(-1, 0) = -2/3$, $W_3 = W(0, 1/\sqrt{k}) = 0$ and $W_4 = W(0, -1/\sqrt{k}) = 0$. The arrangement them must be able to produce BPS energy, for that $W(\phi_i, \chi_i) \neq W(\phi_j, \chi_j)$, giving rise to BPS sectors. A combination W_1 with W_2 , for example, produces the energy $E_B^{12} = 4/3$, W_1 with the other two minimums produce the same energy $E_B^{13} = E_B^{14} = 2/3$, the same occurs with W_2 that gives rising $E_B^{23} = E_B^{24} = 2/3$. The last combination is W_3 with W_4 , but this combination has no BPS energy $E_B^{34} = 0$. Next, we need to choose an orbit that connects the fields, and this is done through a constant function $F(\phi, \chi) = C$ that depends on the fields, where C is a constant. It also must support the first-order equations (2.60) and (2.61) in the topological sector analyzed. We start out considering the BPS sector formed by $W_1=(1,0)$ and $W_2 = (-1, 0)$, and we suggest the orbit $a\phi^2 + b\chi^2 = C$, where a , b and C are parameters to be determined. In this BPS sector, ϕ must be equal to ± 1 for $\chi = 0$, which leads us to identify $a = c = 1$. Thus the orbit takes the form $\phi^2 + b\chi^2 = 1$, differentiating with relation to x , we get

$$\phi\phi' + b\chi\chi' = 0, \quad (2.65)$$

replacing (2.60) and (2.61) the equation takes the form

$$\phi^2 + k(1 + 2b)\chi^2 = 1. \quad (2.66)$$

Finally, we can identify $b = k/(1 - 2k)$, for $k \in (0, 1/2)$, and write the expression for the orbit

$$\phi^2 + \frac{1}{1/k - 2}\chi^2 = 1. \quad (2.67)$$

We can then use the orbit in (2.60) to decouple the equation and write

$$\phi' = 2k(1 - \phi^2). \quad (2.68)$$

This equation supports the solution

$$\phi(x) = \tanh(2kx). \quad (2.69)$$

In order to get the solution $\chi(x)$, we replace the above equation in the orbit equation (2.67):

$$\tanh(2kx)^2 + \frac{1}{1/k - 2}\chi^2 = 1. \quad (2.70)$$

Finally, we get the solution

$$\chi(x) = \pm \sqrt{\frac{1}{k} - 2} \operatorname{sech}(2kx). \quad (2.71)$$

In conclusion, we have explored the trial orbit method as a valuable approach to simplifying the resolution of non-linear coupled differential equations, which can be challenging tasks. Decoupling the differential equations makes them more tractable to solve, facilitating the identification of their minima.

In conclusion, this chapter has been devoted to the in-depth exploration of domain walls and the rich phenomena they entail. Our journey began with studying the scalar field and examining the energy-momentum tensor associated with localized configurations. This foundational knowledge provided crucial insights into these structures.

We then delved into the first-order formalism, known as the BPS model, which emerged as a powerful and indispensable tool for investigating topological structures. Demonstrating the stability of solutions under this formalism.

Moreover, we shed light on the remarkable capability of these localized structures to accurately describe domain walls, commonly referred to as Bloch walls, which exhibit intriguing internal structures. The profound interplay between these structures and their representation by kinks and lumps serves as an initial step for other discussions that will come throughout the other chapters.

Internal Structure of Bloch Walls

As we saw earlier, kinks are topological solutions for first-order equations that support BPS energy. In the introductory case, we analyze the Néel Wall, showing how it emerges in a scenario of spontaneous symmetry breaking for one scalar field. We also saw that rich structures that arise in two scalar fields context can be identified as Bloch Walls, where the second field plays the role of the degree of freedom. In Ref. [52], the authors show experimentally that geometrical constrictions could modify the profile of kink-like structures giving rise to a plateau in the core of the configuration. In a recent study (Ref. [12]), the authors examined a model with two scalar fields and a function that alters the kinematics term in Lagrangian density, resulting in effects of deformation of the medium that can be characterized as such geometrical constriction. In [21], we developed a procedure with three scalar fields capable of manipulating the internal structure of Bloch walls through a first-order formalism that minimizes the solutions' energy. The modifications bring to light internal structures for solutions never seen before and may be of interest in studying magnetic materials.

3.1 Manipulating the internal structure

We start with the Lagrangian density inspired by the work [12], where we consider three real scalar fields ϕ , χ , and ψ , and a function coupled to the dynamic terms of ϕ and χ in (1,1)-dimension

$$\mathcal{L} = \frac{1}{2}f(\psi)\partial_\mu\phi\partial^\mu\phi + \frac{1}{2}f(\psi)\partial_\mu\chi\partial^\mu\chi + \frac{1}{2}\partial_\mu\psi\partial^\mu\psi - V(\phi, \chi, \psi). \quad (3.1)$$

Here $f(\psi)$ denotes a real and positive function that depends only on ψ and $V(\phi, \chi, \psi)$ is the potential. Notice that $f(\psi)$ modifies the kinematic terms that involve ϕ and χ , while ψ stays standard. The equations of motion for this model are given by

$$\partial_\mu(f\partial^\mu\phi) + V_\phi = 0, \quad (3.2)$$

$$\partial_\mu(f\partial^\mu\chi) + V_\chi = 0, \quad (3.3)$$

$$\partial_\mu\partial^\mu\psi - \frac{1}{2}f_\psi(\partial_\mu\phi\partial^\mu\phi + \partial_\mu\chi\partial^\mu\chi) + V_\psi = 0, \quad (3.4)$$

where $f_\psi = df/d\psi$. The energy-momentum tensor (2.5) can be easily extended to three fields problem, as follows

$$T_{\mu\nu} = \frac{\partial\mathcal{L}}{\partial(\partial^\mu\phi)}\partial_\nu\phi(x) + \frac{\partial\mathcal{L}}{\partial(\partial^\mu\chi)}\partial_\nu\chi(x) + \frac{\partial\mathcal{L}}{\partial(\partial^\mu\psi)}\partial_\nu\psi(x) - \eta_{\mu\nu}\mathcal{L}. \quad (3.5)$$

Feeding the above expression with the Lagrangian density in Eq. (3.1), we get

$$T_{\mu\nu} = f(\psi)(\partial_\mu\phi\partial_\nu\phi + \partial_\mu\chi\partial_\nu\chi) + \partial_\mu\psi\partial_\nu\psi - \eta_{\mu\nu}\mathcal{L}. \quad (3.6)$$

Since we are looking for structures that describe Bloch Walls, we follow the lines in the previous chapter, and we will consider static configurations. Thereby, the set of the equation of motions (3.2), (3.3), and (3.4) become

$$(f\phi')' = V_\phi, \quad (3.7)$$

$$(f\chi')' = V_\chi, \quad (3.8)$$

$$\psi'' - \frac{1}{2}f_\psi(\phi'^2 + \chi'^2) = V_\psi. \quad (3.9)$$

The scenario of (1, 1)-dimension implies in four components for the energy-momentum tensor in Eq. (3.6), these being T_{00} , T_{11} , T_{01} and T_{10} . As discussed in Ch. 2, the components T_{01} and T_{10} are null for static configurations, which leaves us with T_{00} and T_{11} , respectively

$$\rho = \frac{1}{2}f(\psi)(\phi'^2 + \chi'^2) + \frac{1}{2}\psi'^2 + V(\phi, \chi, \psi), \quad (3.10a)$$

$$p = \frac{1}{2}f(\psi)(\phi'^2 + \chi'^2) + \frac{1}{2}\psi'^2 - V(\phi, \chi, \psi). \quad (3.10b)$$

To implement the Bogomol'nyi procedure, we introduce an auxiliary function $W(\phi, \chi, \psi)$ into the energy density in Eq. (3.10a), following the approach outlined in Eq. (2.51):

$$\begin{aligned} \rho &= \frac{f}{2} \left(\phi' \mp \frac{W_\phi}{f} \right)^2 + \frac{f}{2} \left(\chi' \mp \frac{W_\chi}{f} \right)^2 + \frac{1}{2} (\psi' \mp W_\psi)^2 \\ &+ V - \frac{1}{2} \left(\frac{W_\phi^2}{f} + \frac{W_\chi^2}{f} + W_\psi^2 \right) \pm W'. \end{aligned} \quad (3.11)$$

Here, the subscripts represent partial derivatives with respect to scalar fields, and the prime indicates differentiation with respect to the spatial coordinate x , as shown below

$$W' = \frac{dW}{dx} = \frac{\partial W}{\partial\phi} \frac{d\phi}{dx} + \frac{\partial W}{\partial\chi} \frac{d\chi}{dx} + \frac{\partial W}{\partial\psi} \frac{d\psi}{dx} \quad (3.12)$$

$$= W_\phi\phi' + W_\chi\chi' + W_\psi\psi'. \quad (3.13)$$

Identifying the potential as

$$V = \frac{1}{2} \left(\frac{W_\phi^2}{f} + \frac{W_\chi^2}{f} + W_\psi^2 \right), \quad (3.14)$$

we get the energy density in Eq. (3.11) in the form

$$\rho = \frac{f}{2} \left(\phi' \mp \frac{W_\phi}{f} \right)^2 + \frac{f}{2} \left(\chi' \mp \frac{W_\chi}{f} \right)^2 + \frac{1}{2} (\psi' \mp W_\psi)^2 \pm W'. \quad (3.15)$$

In this situation, the energy obtained by integration becomes bounded, that is

$$\begin{aligned} E &= \int \left[\frac{f}{2} \left(\phi' \mp \frac{W_\phi}{f} \right)^2 + \frac{f}{2} \left(\chi' \mp \frac{W_\chi}{f} \right)^2 + \frac{1}{2} (\psi' \mp W_\psi)^2 \pm W' \right] dx \\ &= \int \left[\frac{f}{2} \left(\phi' \mp \frac{W_\phi}{f} \right)^2 + \frac{f}{2} \left(\chi' \mp \frac{W_\chi}{f} \right)^2 + \frac{1}{2} (\psi' \mp W_\psi)^2 \right] dx + E_B, \end{aligned} \quad (3.16)$$

where $E \geq E_B = \Delta W$ or yet

$$E_B = |W(\phi(\infty), \chi(\infty), \psi(\infty)) - W(\phi(-\infty), \chi(-\infty), \psi(-\infty))|. \quad (3.17)$$

The minimum energy state E_B is reached for configurations that support the first-order equations

$$\phi' = \pm \frac{W_\phi}{f}, \quad (3.18)$$

$$\chi' = \pm \frac{W_\chi}{f}, \quad (3.19)$$

$$\psi' = \pm W_\psi, \quad (3.20)$$

leading the energy density (3.15) to $\rho = W'$. The authors in Ref. [14] demonstrated that defect structures in generalized models, described by a real scalar field in (1,1) spacetime dimensions, could be stable against contractions and dilations as long as they meet the null pressure condition. This statement has also been proven to be valid for a generalized model of n scalar fields, as stated in Ref. [13]. In Sec. 4.1 we show a brief discussion about it. The above arguments are sufficient to ensure the stability of the solutions for the first-order equations (3.18), (3.19), and (3.20).

In principle, the auxiliary function $W(\phi, \chi, \psi)$ can take into account the coupling between the three real scalar fields. However, it is essential to note that the first-order equations (3.18) and (3.19) depend on f , a function of the scalar field ψ , and on the auxiliary derivatives W_ϕ and W_χ , respectively. While the first-order equation (3.20) considers only the derivative W_ψ . This condition allows us to write the auxiliary function in a particular form

$$W(\phi, \chi, \psi) = W_1(\phi, \chi) + W_2(\psi). \quad (3.21)$$

Thus, the solution ψ can be obtained independently. Therefore, knowing ψ , one can use it to feed the function $f(\psi)$ in first-order equations (3.18) and (3.19) and solve them. This way, the scalar field ψ can be understood as a source that feeds the other solutions ϕ and χ . The energy density for this configuration can be written as the sum of two parts ρ_1 and ρ_2 , being the second independent of ϕ and χ :

$$\begin{aligned} \rho &= f(\phi'^2 + \chi'^2) + \psi'^2 \\ &= \rho_1 + \rho_2, \end{aligned} \quad (3.22)$$

where one we identify

$$\rho_1 = f(\phi'^2 + \chi'^2), \quad (3.23)$$

$$\rho_2 = \psi'^2. \quad (3.24)$$

By integration, we can obtain the total energy E as sum $E = E_1 + E_2$ arising from the energy densities, respectively. Since the energy density equation was obtained taking into account the BPS solutions, the total energy must match the expression $E = E_B$. Although the energy density ρ_1 depends on f , the same no occurs with the energy E_1 , as seen in Eq. (3.17). Therefore, different configurations generated by functions $f(\psi)$ must present the same energy. The energy density, denoted as ρ_2 , describes how the mass of the source is distributed. Here, ρ_1 can be understood as the structure's mass affected by the source arranged. In Ref. [21], we investigated how the other scalar fields feel the effects of $f(\psi)$.

In order to illustrate the procedure, we take ϕ and χ describing structures of Bloch walls type, so we considered the model of two scalar fields investigated in Refs. [9] [25] and revised in section 2.5.2 for W_1 . For W_2 , we take the ϕ^4 model as follows

$$W_1 = \phi - \frac{1}{3}\phi^3 - k\phi\chi^2, \quad (3.25)$$

$$W_2 = \alpha\psi - \alpha\frac{1}{3}\psi^3, \quad (3.26)$$

where k and α are parameters. In this situation, the first-order equations (3.18), (3.19) and (3.20) become

$$\phi' = \pm \frac{1 - \phi^2 - r\chi^2}{f(\psi)}, \quad (3.27)$$

$$\chi' = \mp \frac{2r\phi\chi}{f(\psi)}, \quad (3.28)$$

$$\psi' = \pm\alpha(1 - \psi^2). \quad (3.29)$$

The first-order equation (3.29) can be solved independently. The solution is as follows:

$$\psi(x) = \pm \tanh(\alpha x). \quad (3.30)$$

Feeding the energy density in Eq. (3.24) with the above expression, we get

$$\rho_2 = \alpha^2 \text{sech}^4(\alpha x). \quad (3.31)$$

In Fig.3.1, we present the solution and its energy density for different values of α . The energy associated with the source is $E_2 = 4\alpha/3$ and can be obtained by integrating ρ_2 . As observed in the figure, α regulates the width of the solution and energy, resulting in thinner widths as higher values are used.

To solve the remaining first-order equations (3.27) and (3.28), we can employ the trial orbit method, previously discussed in Sec. 2.5.3, to obtain an orbit that decouples the equations. This approach leads us to the well-known orbit in Eq. (2.67):

$$\phi^2 + \frac{1}{1/k - 2}\chi^2 = 1. \quad (3.32)$$

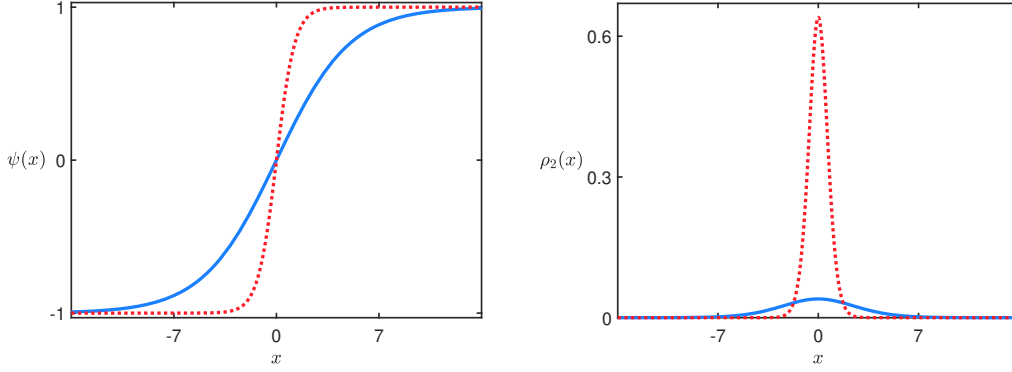


Figure 3.1 The solution $\psi(x)$ (left) in Eq. (3.30) and the energy density ρ_2 (right) in Eq. (3.31) depicted for $\alpha = 0.2$ (solid, blue line) and $\alpha = 0.8$ (dotted, red line).

Notice that although the coupled first-order equations depend on $f(\psi)$, the same no occurs with the orbit, which is written only in terms of ϕ and χ . Replacing the above orbit equation in Eq. (2.15) leads us to

$$\phi' = \pm \frac{2r(1 - \phi^2)}{f(\psi)}. \quad (3.33)$$

The investigations in Refs.[23] and [12] lead to similar equations. A function coupled to the dynamic term in Lagrangian density is used to modify the kink profile. Here, we use $f(\psi)$ to simulate geometrical constrictions in Bloch Walls. Notice that f is a function of ψ , and this is a function of x , so why not just consider $f = f(x)$? Why a third scalar field? If we take $f = f(x)$, the Lagrangian density loses translational invariance, which no occurs with the third field ψ . Therefore, including a third field enables modifications to the core of Bloch Wall structures while maintaining translation invariance and preserving the stability of solutions. Next, we investigate some possibilities for the function $f(\psi)$.

3.1.1 First Model

As we saw earlier, $f(\psi)$ must be real and positive, so as the first model we take $f(\psi) = 1/\psi^2$. In this case, the potential (3.14) in terms of scalar fields takes the form

$$V(\phi, \chi, \psi) = \frac{1}{2} \psi^2 (1 - \phi^2 - r\chi^2)^2 + 2r^2 \phi^2 \chi^2 \psi^2 + \frac{1}{2} \alpha^2 (1 - \psi^2)^2. \quad (3.34)$$

In order to get the ϕ and χ solution, we use the first-order equation (3.33) obtained from the trial orbit method feeding it with $f(\psi) = 1/\psi^2$, as follows

$$\phi' = \pm 2r(1 - \phi^2)\psi^2, \quad (3.35)$$

or yet

$$\phi' = \pm 2r(1 - \phi^2) \tanh(\alpha x)^2. \quad (3.36)$$

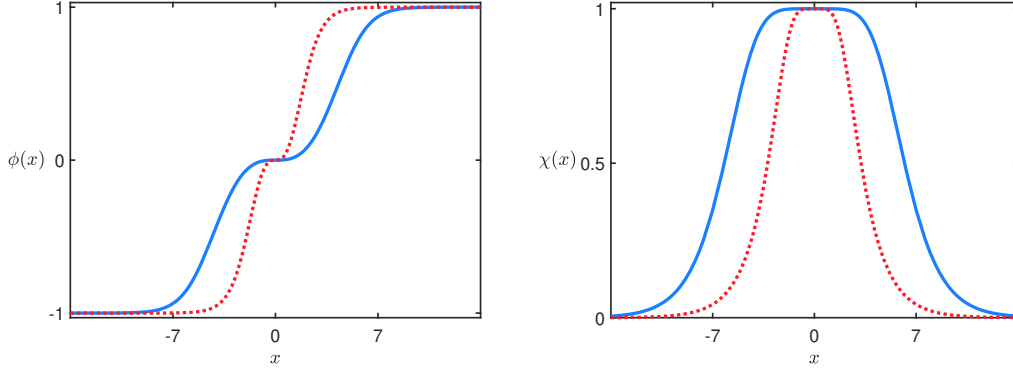


Figure 3.2 The solutions $\phi(x)$ (left) and $\chi(x)$ (right) associated to the model in Sec. 3.1.1, for $r = 1/3$ and $\alpha = 0.2$ (solid, blue line), and 0.8 (dotted, red line).

This equation supports the solution

$$\phi(x) = \pm \tanh(\xi(x)), \quad (3.37)$$

where $\xi(x)$ plays the role of geometrical coordinate and is given by

$$\xi(x) = 2r(x - \tanh(\alpha x)/\alpha). \quad (3.38)$$

The orbit in Eq. (3.32) fed with the solution $\phi(x)$ in Eq. (3.37) becomes

$$\tanh(\xi(x))^2 + \frac{1}{1/r - 2} \chi^2 = 1, \quad (3.39)$$

which leads to

$$\chi(x) = \pm \sqrt{\frac{1}{r} - 2} \operatorname{sech}(\xi(x)). \quad (3.40)$$

In Fig. 3.2, we plot the scalar fields ϕ and χ for α different values to investigate as the intensity of this coupling modifies the behavior solutions. It can be seen that stronger couplings tend to reduce the width of the solutions. In addition, one can see how the geometrical coordinate changes the profile solutions giving rise to a plateau in the core of configurations in ϕ and a plateau in χ . This structure can be used to describe magnetic domain walls that arise in micrometer-sized $\mathbf{Fe}_{20}\mathbf{Ni}_{80}$, where the emergence of plateaus occurs in the presence of geometrical constriction; see Ref. [52]. The energy density in Eq. (3.23) for this structure is given by

$$\rho_1 = 4r^2 \tanh^2(\alpha x) \operatorname{sech}^2(\xi) \left[\operatorname{sech}^2(\xi) + \tanh^2(\xi) \left(\frac{1}{r} - 2 \right) \right]. \quad (3.41)$$

Notice that α controls the width of the energy density, as seen in Fig. 3.3. The energy density ρ_1 depends on α , but the same non-occurs with the energy associated that is independent, as expected from (3.17). In this way, one can say that α modifies the shape of energy density, squeezing it without changing the energy giving rise to structures with degenerate energy. The total energy, considering source and structure, is given by $E = E_1 + E_2$, where $E_1 = 4/3$ and $E_2 = 4\alpha/3$.

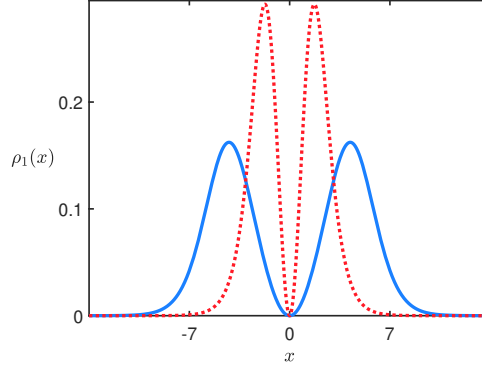


Figure 3.3 The energy density ρ_1 associate to model in Sec. 3.1.1, for $r = 1/3$ and $\alpha = 0.2$ (solid, blue line), and 0.8 (dotted, red line).

3.1.2 Second Model

In the second model, another possibility is explored, inspired by [52] and the work in Ref. [23], which considers fermions in the presence of topological structures under geometrical constrictions. Here, the function is denoted by $f(\psi) = \sec^2(n\pi\psi)$, where n is an integer. In this case, the first-order equation becomes

$$\phi' = 2r(1 - \phi^2) \cos^2(n\pi \tanh(\alpha x)). \quad (3.42)$$

This equation is similar to the first-order equation in (3.36), which gives a clue about the solution. Then following the first case, we get a solution $\phi = \tanh(\eta(x))$ type, where $\eta(x)$ is the new geometrical coordinate given by

$$\eta(x) = rx + \frac{r}{2\alpha} (\text{Ci}(\xi_+(x)) - \text{Ci}(\xi_-(x))), \quad (3.43)$$

and $\xi_{\pm}(x) = 2n\pi(1 \pm \tanh(\alpha x))$. In this way, $\chi(x)$ supports the solution in Eq. (3.40) with the geometrical coordinate $\xi(x)$ replaced by $\eta(x)$. The term $\text{Ci}(z)$ that appears in Eq. (3.43) is known as cosine integral and is defined as

$$\text{Ci}(z) = \gamma + \ln(z) + \int_0^z \frac{\cos(y) - 1}{y} dy, \quad (3.44)$$

where the first term in $\text{Ci}(z)$ is called Euler–Mascheroni constant and its value is approximately $\gamma \approx 0,58$. For small z , this function behaves as

$$\text{Ci}(z) = \gamma + \ln(z) - \frac{z^2}{4} + \mathcal{O}(z^4), \quad (3.45)$$

while for large z it takes the form

$$\text{Ci}(z) = \frac{\sin(z)}{z} - \frac{\cos(z)}{z^2} + \mathcal{O}(1/z^3). \quad (3.46)$$

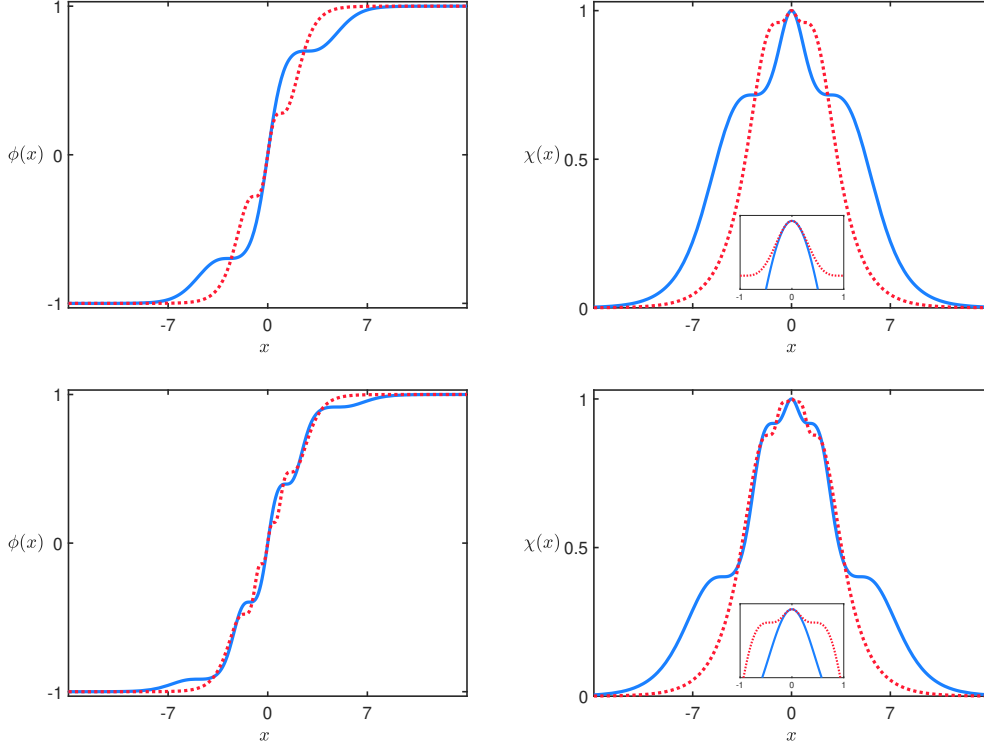


Figure 3.4 The solutions $\phi(x)$ and $\chi(x)$ for the model in Sec. 3.1.2, with $f(\psi) = \sec^2(n\pi\psi)$, depicted with $r = 1/3$ and for $\alpha = 0.2$ (solid, blue line) and 0.6 (dotted, red line) and with $n = 1$ (top) and $n = 2$ (bottom). The insets highlight the behavior of the χ -field configurations near the origin.

In order to investigate how α and n modify the solution profile, k was fixed while the other parameters varied. The kinklike $\phi(x)$ and lumplike $\chi(x)$ configurations show a structure with $2n$ plateaus that have their width associated with α , as seen in Fig 3.4.

In the inflection point, the derivative of the solution is zero. The solution is approximately constant near this point, giving rise to a plateau. Then in this region, its derivative is approximately zero. To understand better, we analyze the roots of the first-order equation (3.42). The term $\cos^2(n\pi \tanh(\alpha x))$, which comes to the function $f(\psi) = \sec^2(n\pi\psi)$, has roots in $n\pi \tanh(\alpha x) = \pm(n\pi - \pi/2)$, that is these roots are reached for $\tanh(\alpha x) = \pm(1 - 1/2n)$. Therefore, for $n = 1$, we have roots in $\tanh(\alpha x) = \pm 1/2$, for $n = 2$, the roots will be $\tanh(\alpha x) = \pm 1/2$ and $\pm 3/4$, thus for n , there will be $2n$ roots and consequently $2n$ plateaus.

Note that the energy density of ρ_2 remains the same since it depends on ψ . On the other hand, the energy density ρ_1 in (3.23) for this model becomes

$$\rho_1 = 4r^2 \cos^2(n\pi \tanh(\alpha x)) \operatorname{sech}^2(\eta) \left[\operatorname{sech}^2(\eta) + \tanh^2(\eta) \left(\frac{1}{r} - 2 \right) \right]. \quad (3.47)$$

Although the energy density ρ_1 depends on $f(\psi)$, the same does not occur with the energy $E_1 = 4/3$, which matches with (3.17). In this way, the total energy is given by $E = 4\alpha/3 + 4/3$, equal to the first model.

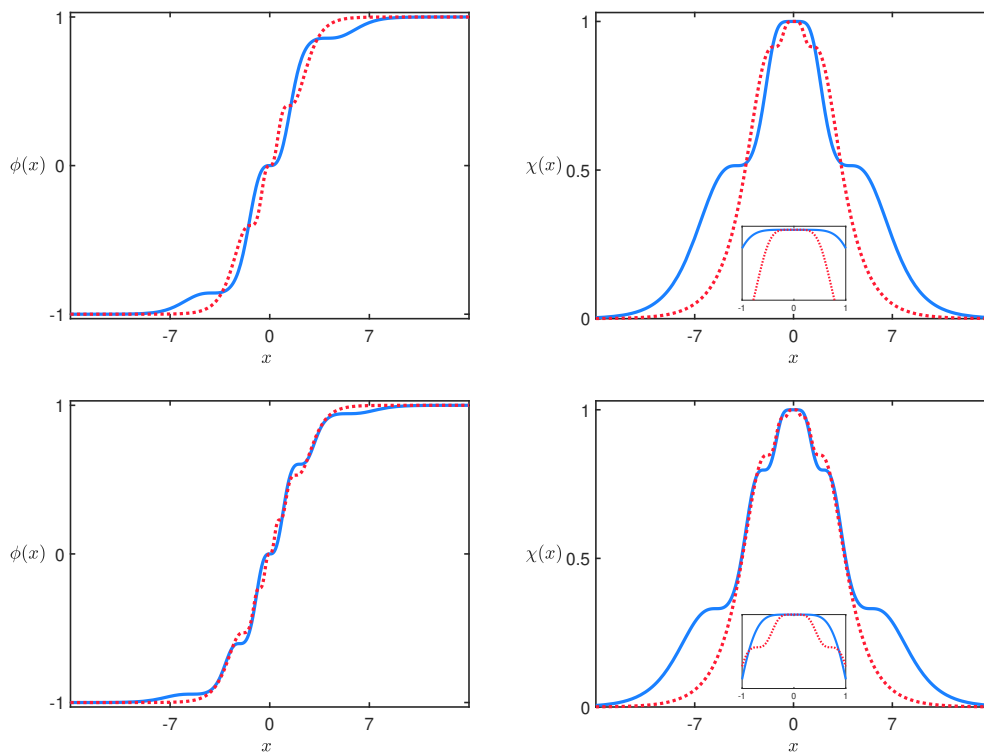


Figure 3.5 The solutions $\phi(x)$ and $\chi(x)$ for the model in Sec. 3.1.2, with $f(\psi) = \csc^2((n + 1/2)\pi\psi)$, depicted with the same values used in Fig. 3.4, for comparison. The insets highlight the behavior of the χ -field configurations near the origin.

Another possibility to consider is a similar function $f(\psi) = \csc^2((n + 1/2)\pi\psi)$. In this case, we get

$$\phi' = 2r(1 - \phi^2) \sin^2((n + 1/2)\pi \tanh(\alpha x)). \quad (3.48)$$

The argument about the plateaus and inflection points can also be used here. In this case, the term $\sin^2((n + 1/2)\pi \tanh(\alpha x))$ possesses zero at the origin. Then it is natural that there is one plateau there. In this way, the number of plateaus for kinklike and lumplike configurations is $2n + 1$, as can be seen in Fig. 3.5. Here, ϕ and χ support solutions (3.36) and (3.40) with geometrical coordinate $\eta(x)$ in Eq. (3.43), where $\xi_{\pm}(x) = 2n\pi(1 \pm \tanh(\alpha x))$ is replaced by new $\xi_{\pm}(x) = (2n + 1)\pi(1 \pm \tanh(\alpha x))$. The modifications in the shape of solutions are significant and show different structures with the same energy.

3.1.3 Third Model

In Refs. [54, 65, 56, 55, 36] were investigated models with a vortex in Bessel optical lattices. Inspired by these works, we propose the function $f(\psi)$ given by $f(\psi) = 1/J_1^2(a\psi)$, where J_1 stands for the Bessel function of the first kind, and a is a real and positive parameter. We investigated the Bloch wall structures in $(1, 1)$ -dimension in the medium geometrically constrained by the Bessel function. Here, the stability of the configurations is ensured by the first-order procedure that minimizes the energy. For this case, the first-order equation in (3.33) takes the form

$$\phi' = 2r(1 - \phi^2)J_1^2(a \tanh(\alpha x)). \quad (3.49)$$

We solve this equation numerically and then get χ through the orbit in Eq. (3.32) fed by the numerical solution ϕ . As we saw earlier, the configurations in Sec. 3.1.1 and 3.1.2 share a similar size, but the same does not occur with the third model. Notice that the Bessel function produces plateaus in the internal structure of the configurations. In Sec. 3.1.3, one can note that ϕ and χ solutions are wider and their profiles look stretched; see Fig 3.6. Furthermore, the energy density is diffuse, in the sense of being much less concentrated around its center, as can be seen in Fig. 3.7, where we depicted the energy density for $f(\psi) = \csc^2((n + 1/2)\pi\psi)$ and $f(\psi) = 1/J_1^2(a\psi)$. The energy is the same as the other models. In this way, we can identify the Bessel function as a tool that helps increase the size of the wall, stretching it.

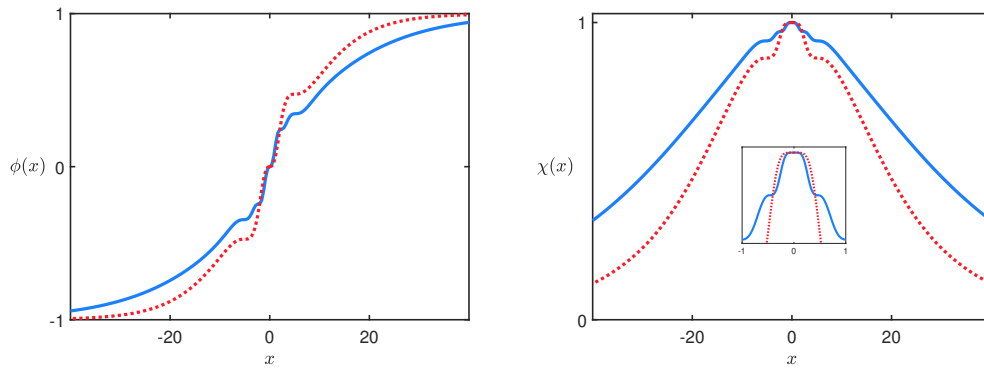


Figure 3.6 The solutions $\phi(x)$ (top panel) and $\chi(x)$ (bottom panel) for the model in Sec. 3.1.3, with $f(\psi) = 1/J_1^2(a\psi)$, depicted with $r = 1/3$ and for $\alpha = 0.2$ and with $a = 5$ (red, dotted line) and $a = 9$ (blue, solid line). The inset highlights the behavior of the χ -field configurations near the origin.

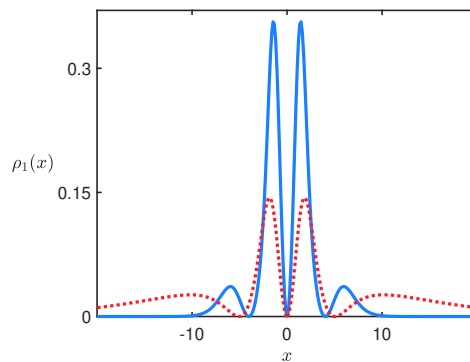


Figure 3.7 The energy density for $f(\psi)$ being controlled by the cos-secant (blue) and the Bessel (red) functions, depicted for $r = 1/3$, $\alpha = 0.2$, and for $n = 1$ and $a = 5$, respectively.

Spatially localized structures

Topological structures, such as kinks, vortices, and monopoles, are objects of significant interest across various fields of physics. These structures arise in different spatial dimensions, with kinks appearing in one dimension, vortices in two dimensions, and monopoles in three dimensions. Vortices, for instance, are topological defects introduced by Nielsen–Olesen [1] that arise in two-dimensional systems and can find applications in magnetic materials [79][87], superfluid Helium [75], and Bose-Einstein condensate [62]. Monopoles emerge as topological structures in three spatial dimensions in grand unified theories [72], although Dirac’s first version was made in Ref. [37]. From Derrick and Hobart’s Theorem, time-independent topological structures for scalar field models in dimensions greater than one are unstable or divergent; see [35] [45]. Therefore, Vortices and Monopoles with global symmetry are usually unstable, and their energy diverges. However, However, some possibilities exist to evade the theorem [86], such as considering local symmetries. In Ref. [15], the authors showed that vortices models scale invariant can present stability, and in a recent work [19], we introduce a way to find Global Monopoles with finite energy.

In this chapter, we study a procedure that evades Derrick-Hobart’s theorem, allowing us to find localized structures with finite energy. Next, we investigate the global monopole and introduce first-order formalism that stabilizes the solution. In order to illustrate the procedure, we take some examples. We investigate an extended model that deals with the dark and hidden sector in the context of the Higgs portal. Finally, we investigate a second extended model where the Global Monopole is inserted in a medium with geometrical constrictions.

4.1 Circumventing the Theorem

In the first step, we demonstrate that Derrick’s and Hobart’s theorem forbid topological defects time-independent in dimensions more than one in a canonical scalar field theory. The procedure that leads to the theorem analyzes the change in the energy scale. For that, we consider the Lagrangian density for N scalar fields below

$$\mathcal{L}(\phi^a, \partial_i \phi^a), \quad (4.1)$$

where the field index is given by $a = 1, \dots, N$. Here, ϕ^a denotes a N -plet of fields. The energy associated with this model is obtained by integration, as follows

$$E = \int T_{00} d^D x. \quad (4.2)$$

The energy-momentum tensor component T_{00} for static configurations can be written as

$$T_{00} = -\mathcal{L}, \quad (4.3)$$

which lead us to

$$E = - \int \mathcal{L}(\phi^a, \partial_i \phi^a) d^D x, \quad (4.4)$$

where $i = 1, \dots, D$. Consider the energy with the change of scale $E \rightarrow E_\lambda$ and $x^i \rightarrow \lambda x^i$, where λ is the scale parameter. In same way, the fields $\phi^a(x)$ become $\phi^a(x)^\lambda = \phi^a(\lambda x)$, and the derivatives take the form $\partial x_i \rightarrow \lambda \partial x_i$. The infinitesimal volume element $d^D x$ becomes

$$d^D x = \left(\frac{dx_1}{\lambda} \right) \left(\frac{dx_2}{\lambda} \right) \dots \left(\frac{dx_D}{\lambda} \right) = \frac{1}{\lambda^D} d^D x. \quad (4.5)$$

Replacing the above equation in the energy in Eq. (4.4), we get

$$E_\lambda = - \int d^D x \lambda^{-D} \mathcal{L}(\phi^a, \lambda \partial_i \phi^a). \quad (4.6)$$

The solutions $\phi^a(x)^\lambda$ will be constricted for $\lambda > 1$ and enlarged for $\lambda < 1$. The standard case is recovered for $E_{\lambda=1} = E$. In order to analyze the energy variation in terms of λ , we take

$$\begin{aligned} \frac{\partial E_\lambda}{\partial \lambda} &= - \int d^D x \left[\lambda^{-D} \frac{\partial \mathcal{L}}{\partial \lambda} - \lambda^{-D-1} D \mathcal{L} \right] \\ &= - \int d^D x \left[\lambda^{-D} \frac{\partial \mathcal{L}}{\partial (\lambda \partial_i \phi^a)} \frac{\partial (\lambda \partial_i \phi^a)}{\partial \lambda} - \lambda^{-D-1} D \mathcal{L} \right] \\ &= - \int d^D x \lambda^{-D-1} \left[\lambda \frac{\partial \mathcal{L}}{\partial (\lambda \partial_i \phi^a)} \partial_i \phi^a - D \mathcal{L} \right]. \end{aligned} \quad (4.7)$$

Since $\lambda = 1$ recovers the energy without contractions or dilations, the above equation must be null in this situation as follows

$$\left. \frac{\partial E_\lambda}{\partial \lambda} \right|_{\lambda=1} = - \int d^D x \left[\frac{\partial \mathcal{L}}{\partial (\partial_i \phi^a)} \partial_i \phi^a - D \mathcal{L} \right] = 0, \quad (4.8)$$

which leads us to

$$\frac{\partial \mathcal{L}}{\partial (\partial_i \phi^a)} \partial_i \phi^a - D \mathcal{L} = 0. \quad (4.9)$$

In order to investigate the energy-momentum tensor components we consider the stress in Eq. (2.5) for one scalar field in (1, 1)-dimension, which is given by

$$T_{11} = \frac{\partial \mathcal{L}}{\partial (\partial^1 \phi)} \partial_1 \phi(x) - \eta_{11} \mathcal{L}, \quad (4.10)$$

if we consider more dimensions, it is necessary to sum the other components in the calculus for the total stress. Thus, from the expression in Eq. (4.9) we can identify the stress in D spatial dimensions for a family of fields $\phi^a(x)$ as $T_{11} + T_{22} + \dots + T_{DD}$

$$\frac{\partial \mathcal{L}}{\partial(\partial^i \phi^a)} \partial_i \phi^a - D\mathcal{L} = \sum_i T_i^i = 0. \quad (4.11)$$

This expression reveals that models stables by scale variation must have average pressure null.

Consider the canonical Lagrangian density for N scalar fields with scale variation in coordinates given by

$$\mathcal{L} = \lambda^2 \frac{1}{2} \partial_\mu \phi^a \partial^\mu \phi^a - V(\phi_1^\lambda, \dots, \phi_D^\lambda), \quad (4.12)$$

where $a = 1, \dots, N$. In this case, the expression for energy variation in Eq. (4.7) takes the form

$$\begin{aligned} \frac{\partial E_\lambda}{\partial \lambda} &= - \int d^D x \lambda^{-D-1} \left[\lambda^2 \partial^i \phi^a \partial_i \phi^a - D \frac{\lambda^2}{2} \partial_j \phi^a \partial^j \phi^a + DV(\phi_1^\lambda, \dots, \phi_D^\lambda) \right] \\ &= - \int d^D x \lambda^{-D-1} \left[\frac{\lambda^2}{2} (D-2) (\partial_j \phi^a)^2 + DV \right], \end{aligned} \quad (4.13)$$

for $\lambda = 1$ we get

$$\left. \frac{\partial E_\lambda}{\partial \lambda} \right|_{\lambda=1} = - \int d^D x \left[\frac{1}{2} (D-2) (\partial_j \phi^a)^2 + DV \right] = 0 \quad (4.14)$$

or yet

$$\left. \frac{\partial E_\lambda}{\partial \lambda} \right|_{\lambda=1} = (2-D)E_G - DE_P = 0, \quad (4.15)$$

where E_G and E_P are the energy gradient and potential, respectively, representing positive quantities. Then, so that the above relation is respected, the first term must be positive, in this sense $(2-D) > 0$. Thus, for $D = 2$, we get $E_P = 0$, which is the trivial case. On the other hand, $D = 1$ implies $E_G = E_P$, which leads to the null pressure condition. If we consider $D \geq 3$, the expression in Eq. (4.15) is not respected, showing the impossibility of getting topological objects time-independent in high dimensions.

There are some possibilities to evade this theorem [86]. One can consider terms with high derivatives in Lagrangian density as in skyrmion models [81][80]. Another way is to consider time dependence as in non-topological solutions called Q-balls [60][41][40][31]. Models with more symmetries can also be stables, as vortices in two-dimension with local $U(1)$ symmetry or monopoles with $SU(2)$ in three dimensions [2][70].

Next, we focus on another special case where the Lagrangian density has explicit dependence on the coordinate term. Inspired by Ref. [22], we introduce a procedure that allows us to find structures in D spatial dimensions with finite energy.

4.2 Global Monopole

The magnetic monopole was initially proposed by Dirac in Ref. [37] as a singularity in the gauge field, producing a non-divergence in the magnetic field. In modern theories such as those proposed by t'Hooft [2] and Polyakov [70], the monopole arises as a topological object in a triplet of scalar field coupled to a non-Abelian gauge field in three spatial dimensions, and its energy regularization is due to local symmetry $SU(2)$. While the structures known as global monopoles emerge from the spontaneous breaking of a global symmetry $O(3)$ and its infinite energy.

According to Grand Unified Theories, global monopoles could have emerged during the early Universe [57]. In Reference [8], an investigation was carried out on the gravitational impact of a monopole, revealing that global monopoles do not gravitationally interact with non-relativistic matter. The paper also explores the annihilation efficiency between global monopoles and antimonopoles, which could potentially account for the observed absence of global monopoles in the Universe. In a recent work Ref. [34], the authors investigated the influence of a global monopole on generalized Klein–Gordon relativistic quantum oscillator for bosonic fields in the presence of a non-central potential. The Refs. [42] [76] [68] are a sequence of works where the stability is discussed.

In our procedure, we propose a first-order formalism that minimizes the energy, evading the Derrick and Hobart theorem and finding structures with finite energy. For that, we initially consider $(D, 1)$ flat spacetime, with $D \geq 3$, and next, we study the particular case for $D = 3$. The Lagrangian density which governs this model is given by

$$\mathcal{L} = -\frac{1}{2}\partial_\mu\phi^a\partial^\mu\phi^a - V(|\phi|), \quad (4.16)$$

where $|\phi| = \sqrt{\phi^a\phi^a}$. For convenience, in this chapter we use the metric with $\text{diag}(\eta_{\mu\nu}) = (-, +, +, \dots, +)$ to avoid problems with the field and metric index. The equation of motion obtained by varying the action has the form

$$\partial_\mu\partial^\mu\phi^a = \frac{\phi^a}{|\phi|}V_{|\phi|}, \quad (4.17)$$

where $V_{|\phi|} = dV/d|\phi|$. In order to find static configurations, we consider the ansatz with radial symmetry

$$\phi^a = \frac{x^a}{r}H(r). \quad (4.18)$$

where $|\phi| = H(r)$ and r is the radial coordinate. The implicit sum allow us to write $x_i x^i = r^2 = x^a x^a$. In this way, the equation of motion (4.17) takes the form

$$\partial_i\partial^i\phi^a = \frac{x^a}{r}V_H. \quad (4.19)$$

As ϕ^a depends only on the radial coordinate r , its derivative can be written as

$$\begin{aligned}\partial^i \phi^a &= \frac{\partial}{\partial x_i} \left(\frac{x^a}{r} H \right) \\ &= \frac{H}{r} \frac{\partial x^a}{\partial x_i} + H x^a \frac{\partial}{\partial x_i} \left(\frac{1}{r} \right) + \frac{x^a}{r} \frac{\partial H}{\partial x_i} \\ &= \frac{H}{r} \delta^{ia} + H x^a \left(-\frac{x^i}{r^3} \right) + \frac{x^a x^i}{r^2} \frac{\partial H}{\partial r}.\end{aligned}\quad (4.20)$$

Thereby, the first term in the equation of motion (4.17) can be calculated as follow

$$\begin{aligned}\partial_i \partial^i \phi^a &= \frac{\partial}{\partial x^i} \left(\frac{H}{r} \delta^{ia} + H x^a \left(-\frac{x^i}{r^3} \right) + \frac{x^a x^i}{r^2} \frac{\partial H}{\partial r} \right) \\ &= \frac{\delta^{ia}}{r} \frac{\partial H}{\partial x^i} + H \delta^{ia} \frac{\partial}{\partial x^i} \left(\frac{1}{r} \right) - \frac{x^a x^i}{r^3} \frac{\partial H}{\partial x^i} - \frac{H x^i}{r^3} \frac{\partial x^a}{\partial x^i} - \frac{H x^a}{r^3} \frac{\partial x^i}{\partial x^i} \\ &\quad - H x^a x^i \frac{\partial}{\partial x^i} \left(\frac{1}{r^3} \right) + \frac{x^i}{r^2} \frac{\partial H}{\partial r} \frac{\partial x^a}{\partial x^i} + \frac{x^a}{r^2} \frac{\partial H}{\partial r} \frac{\partial x^i}{\partial x^i} + x^a x^i \frac{\partial H}{\partial r} \frac{\partial}{\partial x^i} \left(\frac{1}{r^2} \right) \\ &\quad + \frac{x^a x^i}{r^2} \frac{\partial}{\partial x^i} \left(\frac{\partial H}{\partial r} \right),\end{aligned}\quad (4.21)$$

or yet

$$\begin{aligned}\partial_i \partial^i \phi^a &= \frac{x_i \delta^{ia}}{r^2} \frac{\partial H}{\partial r} + H \delta^{ia} \left(-\frac{x_i}{r^3} \right) - \frac{x^a x^i x_i}{r^4} \frac{\partial H}{\partial r} - \frac{H x^i}{r^3} \delta_i^a - \frac{H x^a}{r^3} D \\ &\quad + 3H x^a \frac{x^i x_i}{r^5} + \delta_i^a \frac{x^i}{r^2} \frac{\partial H}{\partial r} + D \frac{x^a}{r^2} \frac{\partial H}{\partial r} - 2x^a \frac{x^i x_i}{r^4} \frac{\partial H}{\partial r} + \frac{x^a x^i x_i}{r^3} \frac{\partial^2 H}{\partial r^2} \\ &= \frac{x^a}{r^2} \frac{\partial H}{\partial r} - H \frac{x^a}{r^3} - \frac{x^a}{r^2} \frac{\partial H}{\partial r} - \frac{H x^a}{r^3} - \frac{H x^a}{r^3} D \\ &\quad + 3H \frac{x^a}{r^3} + \frac{x^a}{r^2} \frac{\partial H}{\partial r} + D \frac{x^a}{r^2} \frac{\partial H}{\partial r} - 2 \frac{x^a}{r^2} \frac{\partial H}{\partial r} + \frac{x^a}{r} \frac{\partial^2 H}{\partial r^2},\end{aligned}\quad (4.22)$$

and finally

$$\partial_i \partial^i \phi^a = \frac{x^a}{r} \frac{\partial^2 H}{\partial r^2} + \left[\frac{x^a}{r^2} \frac{\partial H}{\partial r} - H \frac{x^a}{r^3} \right] (D-1). \quad (4.24)$$

Thus, the equation of motion (4.17) takes the form

$$\frac{x^a}{r} \frac{\partial^2 H}{\partial r^2} + \left[\frac{x^a}{r^2} \frac{\partial H}{\partial r} - H \frac{x^a}{r^3} \right] (D-1) = \frac{x^a}{r} V_H. \quad (4.25)$$

Multiplying both sides by x^a/r we get

$$\frac{\partial^2 H}{\partial r^2} + \left[\frac{1}{r} \frac{\partial H}{\partial r} - H \frac{1}{r^2} \right] (D-1) = V_H, \quad (4.26)$$

or better

$$\frac{1}{r^{D-1}} (r^{D-1} H')' = (D-1) \frac{H}{r^2} + V_H. \quad (4.27)$$

Here we are using the prime subscript to indicate the derivative in radial coordinate, $H' = \partial H / \partial r$, and so on. Note that in D spatial dimensions arise more a term in the equation of motion with dependence on dimension.

The energy density is calculated following Eq. (4.3). Although the metric has an inverse signal, the expression is still the same $\rho = \eta_{00} \mathcal{L}$. Using the derivative in Eq. (4.20), we can write the energy density in the form

$$\rho = \frac{1}{2} \left[\frac{H}{r} \delta_i^a + H x^a \left(-\frac{x_i}{r^3} \right) + \frac{x^a x_i}{r^2} \frac{\partial H}{\partial r} \right] \left[\frac{H}{r} \delta^{ia} + H x^a \left(-\frac{x^i}{r^3} \right) + \frac{x^a x^i}{r^2} \frac{\partial H}{\partial r} \right] + V_H, \quad (4.28)$$

which lead us to

$$\rho = \frac{1}{2} \left[\frac{H^2}{r^2} D - 2 \frac{H^2}{r^2} + 2 \frac{H}{r} \frac{\partial H}{\partial r} + \frac{H^2}{r^2} + \left(\frac{\partial H}{\partial r} \right)^2 - 2 \frac{H}{r} \frac{\partial H}{\partial r} \right] + V_H, \quad (4.29)$$

or yet

$$\rho = \frac{1}{2} H'^2 + \frac{D-1}{2} \frac{H^2}{r^2} + V(H). \quad (4.30)$$

One can define a core structure with size r_{core} , such that asymptotically, that is, $r \gg r_{core}$, the solution H goes to a constant value η . In this way, $H \approx \eta$, $H' \approx 0$, and $V(H) \approx 0$. Realize that in this scenario, the energy density takes the form $\rho \propto 1/r^2$, and when integrated, this term produces a divergence in the energy, which matches Derrick and Hobart's arguments.

In order to evade the theorem, we introduce an auxiliary function $W(|\phi|)$ in the energy density inspired by the works [27][22], aiming to regularize the energy as follows

$$\rho = \frac{1}{2} \left(H' \mp \frac{W_H}{r^{D-1}} \right)^2 + V(H) + \frac{D-1}{2} \frac{H^2}{r^2} - \frac{1}{2} \frac{W_H^2}{r^{2D-2}} \pm \frac{1}{r^{D-1}} W'. \quad (4.31)$$

Inspired by Ref. [22], we take the potential $V(H)$ with explicit dependence on radial coordinate as follows

$$V(r, H) = \frac{W_H^2}{2r^{2D-2}} - \frac{D-1}{2} \frac{H^2}{r^2}. \quad (4.32)$$

Thereby, the energy density in Eq. (4.31) takes the form

$$\rho = \frac{1}{2} \left(H' \mp \frac{W_H}{r^{D-1}} \right)^2 \pm \frac{1}{r^{D-1}} W'. \quad (4.33)$$

By integration, we get the energy E given by

$$\begin{aligned} E &= \int \left[\frac{1}{2} \left(H' \mp \frac{W_H}{r^{D-1}} \right)^2 \pm \frac{1}{r^{D-1}} W' \right] d^D x \\ &= \int \left[\frac{1}{2} \left(H' \mp \frac{W_H}{r^{D-1}} \right)^2 \pm \frac{1}{r^{D-1}} W' \right] \Omega(D) r^{D-1} dr \\ &= \int \frac{1}{2} \left(H' \mp \frac{W_H}{r^{D-1}} \right)^2 \Omega(D) r^{D-1} dr + E_B, \end{aligned} \quad (4.34)$$

where $\Omega_{(D)} = 2\pi^{D/2}/\Gamma(D/2)$ denotes the D -dimensional solid angle and E_B is the Bogomol'nyi energy. The energy E is bounded by E_B , as follows

$$E \geq E_B = \Omega_{(D)} |W(H(\infty)) - W(H(0))|. \quad (4.35)$$

The configurations that supports the first-order equation below minimize the energy:

$$H' = \pm \frac{W_H}{r^{D-1}}, \quad (4.36)$$

which allows writing the energy density in Eq. (4.33) in the form

$$\rho = \pm \frac{1}{r^{D-1}} W'. \quad (4.37)$$

It is important to comment that this equation matches the equation of motion in (4.27). We can interpret these results in another form. For that, we define a new variable, x , such that

$$dx = \frac{dr}{r^{D-1}}, \quad (4.38)$$

and

$$x = \mp \frac{1}{(D-2)r^{D-2}}. \quad (4.39)$$

In this case, the first-order equation (4.36) takes the form

$$\frac{dH}{dx} = W_H, \quad (4.40)$$

where

$$\begin{aligned} H' &= \frac{dH}{dx} \frac{dx}{dr} \\ &= \frac{dH}{dx} \frac{1}{r^{D-1}}. \end{aligned} \quad (4.41)$$

Notice that the change of variable leads to an equation already seen in Chapter 1 in kinks investigations. In fact, what we have here is the structure in D dimensions being mapped in a kink in $(1, 1)$ -dimension. In addition, one can use the potential in Eq. (4.32) to write the equation of motion in terms of an effective potential as follows

$$\begin{aligned} \frac{1}{r^{D-1}} (r^{D-1} H')' &= (D-1) \frac{H}{r^2} + \frac{\partial}{\partial H} \left[\frac{W_H^2}{2r^{2D-2}} - \frac{D-1}{2} \frac{H^2}{r^2} \right] \\ &= (D-1) \frac{H}{r^2} + \frac{W_H W_{HH}}{r^{2D-2}} - (D-1) \frac{H^2}{r^2} \\ &= \frac{W_H W_{HH}}{r^{2D-2}}, \end{aligned} \quad (4.42)$$

or better

$$r^{D-1} (r^{D-1} H')' = U_H, \quad (4.43)$$

where $U_H = W_H W_{HH}$ and the effective potential

$$U(H) = \frac{1}{2W_H^2}, \quad (4.44)$$

which has its connected minima by the kink solution related to the global monopole by the change of variable. In this case, the energy density can be written as

$$\rho = \frac{1}{2} H'^2 + \frac{1}{r^{2D-2}} U(H). \quad (4.45)$$

The formalism we presented, introduced in Ref. [19], has proven effective in regularizing the energy of global monopoles, revealing structures with finite energy that were unprecedented in the literature. By utilizing an auxiliary function, we successfully eliminated the problematic second term in the energy density (4.30) that was causing divergence in the energy. To achieve this, we needed to consider a potential with radial dependence, which led to sacrificing translational invariance. Despite this trade-off, models with broken translational invariance hold significant relevance in physics.

In holographic models, where gravity is linked to a strongly coupled nongravitational theory, properties such as optical conductivity in lattices with broken translational invariance have been studied (Ref. [49]). Additionally, authors in Ref. [84] have explored breaking translational invariance through the framework of massive gravity in the context of describing strongly coupled quantum fields. Moreover, the presence of electric and magnetic impurities in BPS vortices has also been associated with breaking translation invariance (Ref. [82]). Recent work in Ref. [61] has achieved the realization of a supersolid exhibiting translational symmetry breaking along one direction in a quantum gas.

Overall, the incorporation of break translational invariance offers fascinating avenues for investigating diverse physical phenomena and is a subject of significant interest and exploration in various areas of research.

As we saw earlier, the effective potential given by $U(H) = 1/2W_H^2$ is positive. On the other hand, the potential in Eq. (4.32) there is a negative term, which could cause instability of the solutions of Eq. (4.36). In this way, it is recommended to investigate the stability of these solutions under small fluctuations.

Following the lines of Sec. 2.1.2, we write the scalar fields as static part $\phi^a(r)$ and a small perturbation time-dependent $\eta^a(r, t)$:

$$\phi^a(r, t) = \phi^a(r) + \eta^a(r, t). \quad (4.46)$$

Replacing in equation of motion (4.17) we get

$$\partial_\mu \partial^\mu \eta^a(r, t) - V_{|\phi|} \eta^a(r, t) = 0. \quad (4.47)$$

The radial part of $\eta(r, t)$ can be written similarly to the ansatz of the static configurations in Eq. (4.18) as follows

$$\eta^a(r, t) = \frac{x^a}{r} \sum_k \xi_k(r) \cos(\omega_k t). \quad (4.48)$$

To calculate the stability equation we replace the above equation in (4.47) and follow the approach outlined in Eq. (4.20) that leads to (4.27)

$$-\frac{1}{r^{D-1}}(r^{D-1}\xi_k')' + \left(\frac{(D-1)}{r^2} + V_{|\phi||\phi|}\right)\xi_k = \omega_k^2 \xi_k. \quad (4.49)$$

Notice that this expression is valid for any solution of the equation of motion (4.27). In order to investigate our first-order formalism, we consider the potential with dependence on radial coordinate as in Eq. (4.32), thereby the stability equation takes the form

$$-\frac{1}{r^{D-1}}(r^{D-1}\xi_k')' + \frac{W_H W_{HHH} + W_{HH}^2}{r^{2D-2}}\xi_k = \omega_k^2 \xi_k. \quad (4.50)$$

As we have seen in Sec. 2.1.2, the solutions are stable if $w_k^2 \geq 0$. For that, it is necessary that the above expression can be written as $L\xi_k = w_k^2 \xi_k$, where the operator is given by $L = S^\dagger S$. The operator factorization in S and its supersymmetric partner S^\dagger ensures that the eigenvalue in Eq. (4.50) only supports non-negative eigenvalues. Here we see that the operators can be written in the form

$$S = -\frac{d}{dr} + \frac{W_{HH}}{r^{D-1}} \quad (4.51a)$$

$$S^\dagger = \frac{d}{dr} + \frac{W_{HH}}{r^{D-1}} + \frac{(D-1)}{r}, \quad (4.51b)$$

which ensures that the solutions of Eq. (4.36) are stable under small fluctuations.

Therefore, the formalism developed can be used to find localized structures in D spatial dimensions stable and with finite energy. Next, we investigate some models in order to illustrate the procedure.

4.2.1 The $|\phi^4|$ model

To illustrate our procedure, we suggest as an example the $|\phi^4|$ model with auxiliary function $W(|\phi|)$ given by

$$W(|\phi|) = |\phi|^2 - \frac{1}{3}|\phi|^3. \quad (4.52)$$

The effective potential $U(H)$ in Eq. (4.44) takes the form

$$\begin{aligned} U(H) &= \frac{1}{2}W_H^2 \\ &= \frac{H^2}{2}(2-H)^2. \end{aligned} \quad (4.53)$$

The minima are localized at $|\phi| = 2$ and $|\phi| = 0$, there is also a maximum located at $|\phi| = 1$, which $U(1) = 1/2$. From the first-order equation (4.36) we get

$$H' = \frac{H(2-H)}{r^{D-1}}. \quad (4.54)$$

This equation supports the solution

$$H(r) = 1 - \tanh\left(\frac{1}{(D-2)r^{D-2}}\right). \quad (4.55)$$

Notice that this solution connects the points $|\phi| = 0$ and $|\phi| = 1$. The energy density associated with the structure in Eq. (4.37) is given by

$$\begin{aligned} \rho &= \frac{1}{r^{D-1}} W' \\ &= \frac{1}{r^{D-1}} W_H H' \\ &= \frac{H^2(2-H)^2}{r^{2D-2}} \\ &= \frac{1}{r^{2D-2}} \operatorname{sech}^4\left(\frac{1}{(D-2)r^{D-2}}\right). \end{aligned} \quad (4.56)$$

By integration, we get the energy $E = \Omega(D)2/3$, which matches with the Bogomol'nyi energy as follows

$$\begin{aligned} E_B &= \Omega(D) |W(H(\infty)) - W(H(0))| \\ &= \Omega(D) |W(1) - W(0)| \\ &= \frac{2}{3} \Omega(D). \end{aligned} \quad (4.57)$$

Fig. 4.1 presents the solution from Eq. (4.55) and its energy density in three spatial dimensions, depicted as a planar section. The energy density exhibits a hole around the origin, resembling the magnetic monopole in Ref. [18].

4.2.2 The $|\phi^6|$ model

Another model studied is the $|\phi|^6$ with an auxiliary function associated given by

$$W(|\phi|) = \frac{1}{2}|\phi|^2 - \frac{1}{4}|\phi|^4. \quad (4.58)$$

Its effective potential in Eq. (4.44) is written in the form

$$U(|\phi|) = \frac{1}{2}|\phi|^2 (1 - |\phi|^2)^2, \quad (4.59)$$

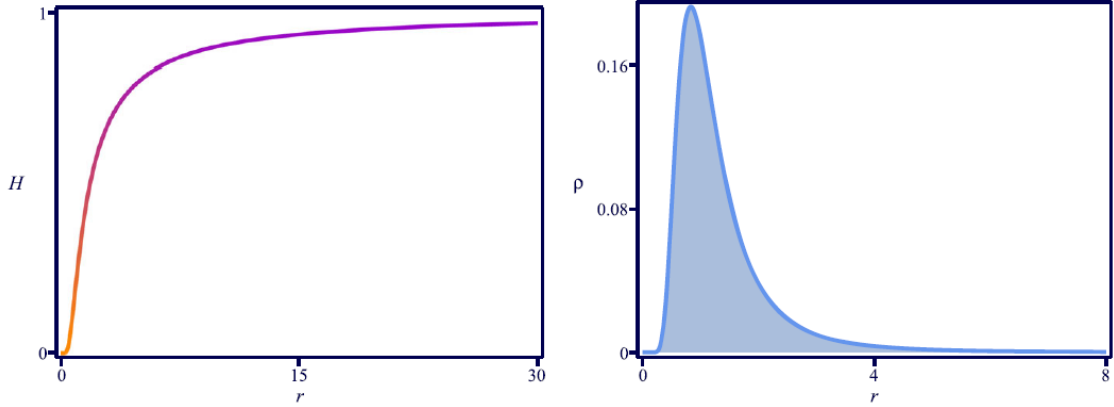


Figure 4.1 The solution in Eq. (4.55) (top left) and the energy density (4.56) (top right), and the planar section passing through the center of the energy density (bottom), for $D = 3$.

with minima at $|\phi| = 0$ and $|\phi| = 1$, and a maximum in $|\phi| = 1/\sqrt{3}$, which implies $U(1/\sqrt{3}) = 2/27$. The first order equation (4.36) takes the form

$$H' = \frac{H(1-H^2)}{r^{D-1}}. \quad (4.60)$$

In this case, the solution supported is given by

$$H(r) = \sqrt{\frac{1}{2} - \frac{1}{2} \tanh\left(\frac{1}{(D-2)r^{D-2}}\right)}. \quad (4.61)$$

It connects the points $|\phi| = 0$ to $|\phi| = 1/\sqrt{2}$. The energy density in Eq. (4.37) takes the form

$$\rho(r) = \frac{1}{8r^{2D-2}} \left(1 + \tanh\left(\frac{1}{(D-2)r^{D-2}}\right)\right) \operatorname{sech}^2\left(\frac{1}{(D-2)r^{D-2}}\right). \quad (4.62)$$

In Fig. 4.2, we plot the solution in Eq.(4.61) and the energy density in Eq. (4.62) for $D = 3$. In addition, we plot the planar section of the energy density, where the blue color indicates the

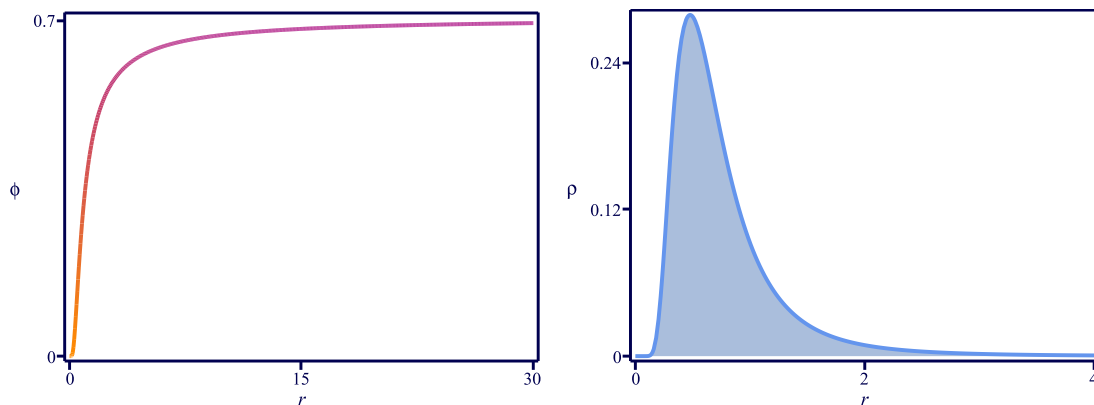


Figure 4.2 Solution in Eq. (4.61) (top left), the energy density in Eq. (4.62) (top right) and planar section passing through the center of the energy density (bottom), for $D = 3$.

energy density height. Since this energy density is higher than in the previous case, it is colored darker blue. This structure also carries a hole in the center, as can be seen. By integration, we get the energy $E = 3\Omega(D)/16$ matching the lower energy bound in Eq.(4.35).

4.3 Extended global monopole

The results obtained above encourage us to explore other possibilities. Recent work in Ref.[5] investigated a model where particles that represent dark matter interact through the Standard Model-like Higgs boson. In this scenario, the Higgs plays the role of a communication channel between the visible sector, i.e., the standard-model particles, and the dark sector or hidden sector. Motivated by this work, we propose a topological model with two distinct global monopoles that may communicate with each other through the Higgs portal. For that, we in-

roduce the Lagrangian density given by

$$\mathcal{L} = -\frac{1}{2}\partial_\mu\phi^a\partial^\mu\phi^a - \frac{1}{2}\partial_\mu\chi^a\partial^\mu\chi^a - V(|\phi|, |\chi|). \quad (4.63)$$

Here, χ^a denotes another family of scalar fields, where $a = 1, \dots, D$, for $D \geq 3$, $V(|\phi|, |\chi|)$ is the potential with dependence on the modulus of the scalar fields, with $|\chi| = \sqrt{\chi^a\chi^a}$. The equations of motions associated with the Lagrangian density in Eq. (4.63) are given by

$$\partial_\mu\partial^\mu\phi^a = \frac{\phi^a}{|\phi|}V_{|\phi|}, \quad (4.64)$$

$$\partial_\mu\partial^\mu\chi^a = \frac{\chi^a}{|\chi|}V_{|\chi|}. \quad (4.65)$$

In order to get another structure with a global monopole profile, we consider the ansatz for χ^a with a shape similar to Eq. (4.18) as follows

$$\chi^a = \frac{x^a}{r}\mathcal{H}(r). \quad (4.66)$$

Since the fields depend only on the radial component r , the equations of motion are written in the form

$$\frac{1}{r^{D-1}}(r^{D-1}H')' = (D-1)\frac{H}{r^2} + V_H, \quad (4.67)$$

$$\frac{1}{r^{D-1}}(r^{D-1}\mathcal{H}')' = (D-1)\frac{\mathcal{H}}{r^2} + V_{\mathcal{H}}. \quad (4.68)$$

The energy density associated with these structures is calculated standardly. It is the previous energy density plus the new contributions from the other field as follows

$$\rho = \frac{1}{2}H'^2 + \frac{1}{2}\mathcal{H}'^2 + \frac{D-1}{2r^2}(H^2 + \mathcal{H}^2) + V(H, \mathcal{H}). \quad (4.69)$$

In order to explore the first-order formalism, we introduce an auxiliary function $W(|\phi|, |\chi|)$ in the energy density following the steps of the previous case

$$\begin{aligned} \rho = & \frac{1}{2}\left(H' \mp \frac{W_H}{r^{D-1}}\right)^2 + \frac{1}{2}\left(\mathcal{H}' \mp \frac{W_{\mathcal{H}}}{r^{D-1}}\right)^2 + V(H, \mathcal{H}) + \frac{D-1}{2r^2}(H^2 + \mathcal{H}^2) \\ & - \frac{1}{2r^{2D-2}}(W_H^2 + W_{\mathcal{H}}^2) \pm \frac{1}{r^{D-1}}W', \end{aligned} \quad (4.70)$$

where

$$\begin{aligned} W' &= \frac{dW}{dr} \\ &= \frac{\partial W}{\partial|\phi|}\frac{d|\phi|}{dr} + \frac{\partial W}{\partial|\chi|}\frac{d|\chi|}{dr} \\ &= W_H H' + W_{\mathcal{H}} \mathcal{H}'. \end{aligned} \quad (4.71)$$

If we consider the potential in the form

$$V(H, \mathcal{H}) = \frac{1}{2r^{2D-2}}(W_H^2 + W_{\mathcal{H}}^2) - \frac{D-1}{2r^2}(H^2 + \mathcal{H}^2), \quad (4.72)$$

the energy density in Eq. (4.70) becomes

$$\rho = \frac{1}{2} \left(H' \mp \frac{W_H}{r^{D-1}} \right)^2 + \frac{1}{2} \left(\mathcal{H}' \mp \frac{W_{\mathcal{H}}}{r^{D-1}} \right)^2 \pm \frac{1}{r^{D-1}} W'. \quad (4.73)$$

From this expression we can see that the energy is bounded, that is, $E \geq E_B$, where

$$E_B = \Omega(D) |W(H(\infty), \mathcal{H}(\infty)) - W(H(0), \mathcal{H}(0))|. \quad (4.74)$$

The minimum energy is reached for solutions that obey the first-order equations

$$H' = \pm \frac{W_H}{r^{D-1}}, \quad (4.75)$$

$$\mathcal{H}' = \pm \frac{W_{\mathcal{H}}}{r^{D-1}}, \quad (4.76)$$

which allows writing the energy density in the form $\rho = W'/r^{D-1}$, leading the energy $E = E_B$. The auxiliary function $W(|\phi|, |\chi|)$ is inspired by the model introduced in Ref. [9] and studied in Sec. 2.5.2:

$$W(|\phi|, |\chi|) = |\phi|^2 - \frac{1}{3}|\phi|^3 - s(|\phi| - 1)|\chi|^2, \quad (4.77)$$

where s is a real parameter that controls the interaction intensity between the families of scalar fields, in other words, the Higgs portal. In this case, the first-order equations in Eqs.(4.75) and (4.76) becomes

$$H' = \frac{H(2-H) - s\mathcal{H}^2}{r^{D-1}}, \quad (4.78)$$

$$\mathcal{H}' = -\frac{2s(H-1)\mathcal{H}}{r^{D-1}}. \quad (4.79)$$

To decouple these equations, we will use some tools obtained in Ch. 2. Perform the trial orbit method here may not be such an easy task, so we do a change variable of

$$H = u + 1, \quad (4.80)$$

which leads to $H' = u'$. In this case, the set of first-order equations become

$$u' = \frac{1 - u^2 - s\mathcal{H}^2}{r^{D-1}}, \quad (4.81)$$

$$\mathcal{H}' = -\frac{2su\mathcal{H}}{r^{D-1}}. \quad (4.82)$$

The above expressions are very similar to the first-order equations in (2.60) and (2.61) and lead to the same orbit (2.67) seen previously:

$$u^2 + \frac{1}{1/s-2} \mathcal{H}^2 = 1. \quad (4.83)$$

We can use this expression to decouple the fields. Replacing it in first-order equation (4.81) leads us to

$$u' = 2s(1 - u^2), \quad (4.84)$$

This equation supports the analytical solution written in terms of H

$$H = 1 - \tanh\left(\frac{2s}{(D-2)r^{D-2}}\right). \quad (4.85)$$

In this case, the solution \mathcal{H} can be written as

$$\mathcal{H} = \sqrt{\frac{1-2s}{s}} \operatorname{sech}\left(\frac{2s}{(D-2)r^{D-2}}\right), \quad (4.86)$$

where $s \in (0, 1/2]$. The energy density for this structure is written as

$$\rho = \frac{4sS^2}{r^{2D-2}} (1 - 2s - (1 - 3s)S^2), \quad (4.87)$$

where $S = \operatorname{sech}(2s/((D-2)r^{D-2}))$. By a change variable of r for x as in Eq. (4.38), we can understand the first-order equations in (4.78) and (4.79) as $r^{D-1}(dH/dr) = dH/dx$ and $r^{D-1}(d\mathcal{H}/dr) = d\mathcal{H}/dx$, or yet

$$\frac{dH}{dx} = H(2 - H) - s\mathcal{H}^2, \quad (4.88)$$

$$\frac{d\mathcal{H}}{dx} = -2s(H - 1)\mathcal{H}. \quad (4.89)$$

Although these equations resemble the BNRT, we must be careful. In this case, $H \in [0, 1]$ while the kink seen in Ch.2 belongs to the interval $[-1, 1]$.

From Eq. (4.74), we get $E = 2\Omega(D)/3$. One can realize that the energy is independent s , which allows us to control the Higgs portal without changing the energy. In Fig. 4.3 are plotted the solutions H and \mathcal{H} , and the energy density in Eq. (4.87) for $s = 1/3$ and $D = 3$. Notice that the energy density presents a hole around the origin, yet in this graph, we can see that this structure has its matter more concentrated. Therefore, the energy density has a height greater than this chapter's other models. In order to investigate the influence of s on the profile of the global monopoles, we plot in the planar section for energy density with $s = 0.2, 0.3, \text{ and } 0.4$; see Fig. 4.4. One can notice that s may control the distribution of matter inside the structure.

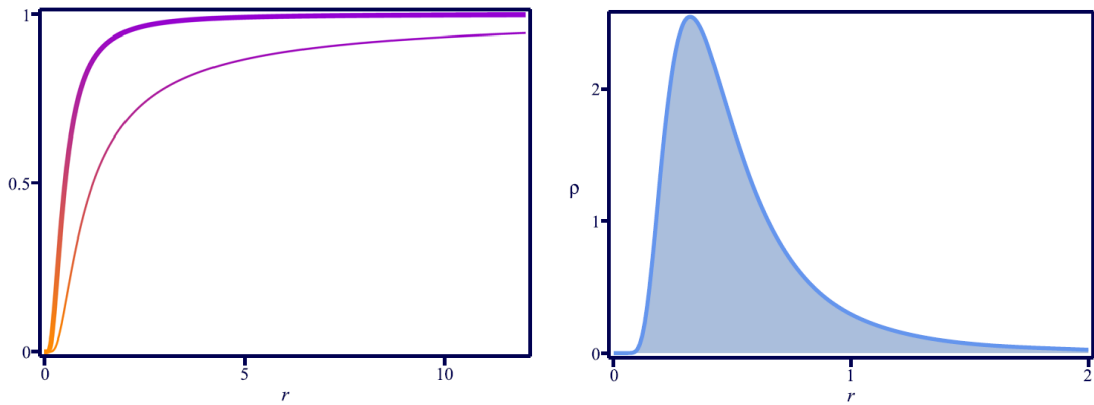


Figure 4.3 Solutions H and \mathcal{H} in Eq. (4.85) and (4.86) (left) and the energy density in Eq. (4.87) (right) for $s = 1/3$ and with $D = 3$. The thinner line represents $H(r)$ and the thicker one stands for $\mathcal{H}(r)$.



Figure 4.4 Planar section of the energy density (42) passing through its center, for $D = 3$ and $s = 0.2$ (left), $s = 0.3$ (center), $s = 0.4$ (right).

4.3.1 The second extend model

We propose another model with a scalar field χ , where the dynamical part of the global monopole is coupled to this new field through a function $f(\chi)$ as follows

$$\mathcal{L} = -\frac{1}{2}f(\chi)\partial_\mu\phi^a\partial^\mu\phi^a - \frac{1}{2}\partial_\mu\chi\partial^\mu\chi - V(|\phi|, \chi). \quad (4.90)$$

This procedure is similar to performing in Ch. 3, where we investigated the possibilities of controlling the internal structures of Bloch Walls by geometrical constrictions. The equations of motion associated with this model are given by

$$\partial_\mu(f\partial^\mu\phi^a) = \frac{\phi^a}{\phi}V_{|\phi|}, \quad (4.91)$$

$$\partial_\mu\partial^\mu\chi = \frac{1}{2}f_\chi\partial_\mu\phi^a\partial^\mu\phi^a + V_\chi. \quad (4.92)$$

Here we consider static configurations and the ansatz in Eq. (4.18). The scalar field is written as $\chi = \chi(r)$. Thus, the equations of motion take the form

$$\frac{1}{r^{D-1}}(fr^{D-1}H')' = (D-1)\frac{fH}{r^2} + V_H, \quad (4.93)$$

$$\frac{1}{r^{D-1}}(r^{D-1}\chi')' = \frac{1}{2}f_\chi\left(H'^2 + (D-1)\frac{H^2}{r^2}\right) + V_\chi. \quad (4.94)$$

In this case, the Bogomol'nyi procedure leads to the energy E bounded below by

$$E_B = \Omega(D)|W(H(\infty), \chi(\infty)) - W(H(0), \chi(0))|, \quad (4.95)$$

for potential with explicit radial dependence written in the form

$$V(|\phi|, \chi, r) = \frac{1}{2r^{2D-2}}\left(\frac{W_{|\phi|}^2}{f(\chi)} + W_\chi^2\right) - \frac{D-1}{2r^2}f(\chi)|\phi|^2. \quad (4.96)$$

The energy minimum energy is reached for configurations that support the first-order equations

$$H' = \frac{W_H}{r^{D-1}f(\chi)}, \quad (4.97)$$

$$\chi' = \frac{W_\chi}{r^{D-1}}. \quad (4.98)$$

In order to investigate effects in global monopole behavior by a geometrical constriction, we take the auxiliary function in the form

$$W(|\phi|, |\chi|) = |\phi|^2 - \frac{1}{3}|\phi|^3 + \chi^2 - \frac{1}{3}\chi^3. \quad (4.99)$$

The first-order equations for $f(\chi) = (1 - \chi)^{-2n}$ take the form

$$H' = \frac{(1 - \chi)^{2n} H (2 - H)}{r^{D-1}}, \quad (4.100)$$

$$\chi' = \frac{\chi(2 - \chi)}{r^{D-1}}. \quad (4.101)$$

Since the fields in the auxiliary function are decoupled, it can be written as $W(|\phi|, \chi) = W_1(|\phi|) + W_2(\chi)$. In this way, the energy density associated with these structures can be written separately in two distinct contributions given by

$$\rho_1 = \frac{(1 - \chi)^{2n} H^2 (2 - H)^2}{r^{2D-2}}, \quad (4.102)$$

$$\rho_2 = \frac{\chi^2 (2 - \chi)^2}{r^{2D-2}}. \quad (4.103)$$

The first-order (4.101) for $\chi(r)$ can be solved independent as follows

$$\chi(r) = 1 - \tanh\left(\frac{1}{(D-2)r^{D-2}}\right). \quad (4.104)$$

Then we can use it to feed the Eq. (4.100) and get the solution:

$$H(r) = 1 - \tanh \xi, \quad (4.105)$$

where the argument is written as

$$\xi = \frac{1}{(D-2)r^{D-2}} - \sum_{k=1}^n \frac{1}{2k-1} \tanh^{2k-1}\left(\frac{1}{(D-2)r^{D-2}}\right). \quad (4.106)$$

Thus, the energy densities become

$$\rho_1 = \frac{1}{r^{2D-2}} \tanh^{2n}\left(\frac{1}{(D-2)r^{D-2}}\right) \operatorname{sech}^4(\xi), \quad (4.107)$$

$$\rho_2 = \frac{1}{r^{2D-2}} \operatorname{sech}^4\left(\frac{1}{(D-2)r^{D-2}}\right). \quad (4.108)$$

By integration, one can get the total energy $E = E_1 + E_2$, each term referring to one energy density. The structure with energy density ρ_2 is the same as obtained in Eq. (4.56), which leads to $E_2 = 2\Omega(D)/3$, the same energy for E_1 . As expected, these values for the energies match the minimum value E_B . Fig. 4.5 are depicted the solution H and the energy density ρ_1 to investigate the influence of n in the structure. One can see that large values of n make the solution H less smooth, which leads to shrink structures. Notice that the energy density forms a structure shell-like that may control by n ; see Fig. 4.6.

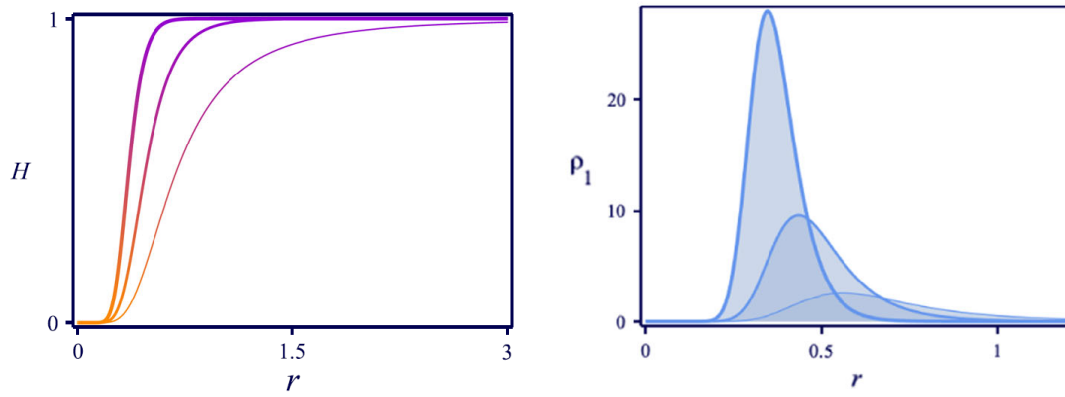


Figure 4.5 Solution $H(r)$ (left) in Eq. (51a) its associated energy density (23) (right) for $D = 3$ and $n = 1, 4$ and 16 . The darkness of the color increases with n .



Figure 4.6 Planar section passing through the center of the energy density (23) for $D = 3$ and $n = 1$ (left), 4 (center) and 16 (right). The darkness of the color increases with n .

Electrically charged multi-field configurations

In this chapter are investigated electrically charged structures that are localized in two and three spatial dimensions. Here, the Maxwell term in Lagrangian density is coupled to the scalar field in an unusual way giving rise to charged structures in $D \geq 2$ dimensions. We developed a procedure in Ref. [20], inspired by the work in Ref. [16], that considers a single point charge in a medium with the electric permittivity controlled by scalar fields, which leads to first-order equations with stable solutions of minimum energy. Moreover, other possibilities are investigated considering modifications in scalar fields kinematics simulating geometrical constrictions, similar to those seen in Ch. 3. We also investigate the electrical permittivity controlled by a family of scalar fields studied in the previous chapter.

5.1 A single point charge

It is known that the electric field generated by a charge grows quickly near the charge's location, diverging at the point. Recent work in Ref. [16] showed that the electric field behavior could be regularized by an electric permittivity controlled by a scalar field. To present this procedure, we start with the standard electromagnetic field in the presence of an external charged source in $(D + 1)$ -dimensions described by the Lagrangian density

$$\mathcal{L} = -\frac{1}{4}F_{\mu\nu}F^{\mu\nu} - A_\mu j^\mu, \quad (5.1)$$

where $F_{\mu\nu} = \partial_\mu A_\nu - \partial_\nu A_\mu$ is the electromagnetic strength tensor, A_μ is the gauge field and j^μ is a (conserved) source current. In this chapter, we are considering the flat space in $(D + 1)$ -dimensions, with diagonal of metric $\text{diag}(\eta_{\mu\nu}) = (+, -, -, \dots, -)$. The equation of motion obtained in a standard way is given by

$$\partial_\mu F^{\mu\nu} = j^\nu. \quad (5.2)$$

Consider the electrostatics scenario of a single point charge e at the origin in the absence of currents, taking j^μ in the form

$$j^0 = e\Omega(D)\delta(\mathbf{r}) \quad \text{and} \quad j^i = 0, \quad (5.3)$$

where $\Omega(D) = 2\pi^{D/2}/\Gamma(D/2)$ denotes the D -dimensional solid angle introduced in this expression for convenience and $\Gamma(D/2)$ is the gamma function. Here, $\delta(\mathbf{r})$ represents the Dirac

delta function of radial vector $\mathbf{r} = r\hat{r}$, with \hat{r} denoting the unit vector in the radial direction. The Dirac delta can also be written as

$$\delta(\mathbf{r}) = \frac{\delta(r)}{\Omega(D)r^{D-1}}, \quad (5.4)$$

such that for $D = 3$ in spherical coordinates, for instance

$$\begin{aligned} \int \delta(\mathbf{r}) d\mathbf{r} &= \int \frac{\delta(r)}{\Omega(3)r^2} d\mathbf{r} \\ &= \int \int \int \frac{\delta(r)}{4\pi r^2} r^2 \sin(\theta) d\theta d\varphi dr \\ &= \int \frac{\delta(r)}{4\pi r^2} 4\pi r^2 dr \\ &= 1. \end{aligned} \quad (5.5)$$

There is no magnetic field in this case, and the electric field is written as $E^i = F^{i0}$. One can show that Gauss's law in Eq. (5.2) takes the form

$$\partial_i F^{i0} = j^0, \quad (5.6)$$

which leads to

$$\mathbf{E}(r) = \frac{e}{r^{D-1}} \hat{r}, \quad (5.7)$$

where $\mathbf{E}(r) = E_r \hat{r}$ is the electric field vector with divergence at the origin.

The procedure developed by the authors in Ref. [16] that regularizes the electric field behavior considers a scalar field non-minimally coupled to the gauge field by a function that describes the electric permittivity as follows

$$\mathcal{L} = -\frac{1}{4}P(\phi)F_{\mu\nu}F^{\mu\nu} + \frac{1}{2}\partial_\mu\phi\partial^\mu\phi - A_\mu j^\mu. \quad (5.8)$$

Here, $P(\phi)$ denotes the electric permittivity controlled by the scalar field ϕ . The equations of motion associated are given by

$$\partial_\mu\partial^\mu\phi + \frac{1}{4}P_\phi F_{\mu\nu}F^{\mu\nu} = 0 \quad (5.9)$$

$$\partial_\mu(P(\phi)F^{\mu\nu}) - j^\nu = 0, \quad (5.10)$$

where $P_\phi = dP/d\phi$. Here we also consider the same scenario of a single-point charge e at the origin in the absence of currents described by Eq (5.3). In this situation, Gauss's law in Eq. (5.10) leads to the electric field

$$\mathbf{E}(r) = \frac{e}{P(\phi)r^{D-1}} \hat{r}. \quad (5.11)$$

Notice that this expression can be replaced in the equation of motion (5.9), leading to a new equation, which allows writing the scalar field ϕ independent of the gauge field A_μ . The energy density associated with this configuration follows the steps in the appendix A.

$$\begin{aligned}\rho &= \frac{1}{2}\phi'^2 + \frac{P}{2}|\mathbf{E}|^2 \\ &= \frac{1}{2}\phi'^2 + \frac{1}{2P} \frac{e^2}{r^{2D-2}}.\end{aligned}\quad (5.12)$$

The Bogomol'nyi procedure is performed by introducing an auxiliary function $W(\phi)$ in the energy density, adding zero to the equation as follows

$$\rho = \frac{1}{2} \left(\phi' \mp \frac{W_\phi}{r^{D-1}} \right)^2 + \frac{1}{2r^{2D-2}} \left(\frac{e^2}{P} - W_\phi^2 \right) \pm \frac{1}{r^{D-1}} W', \quad (5.13)$$

where $W' = \phi' W_\phi$ and $W_\phi = dW/d\phi$. Notice that if $P = e^2/W_\phi$, the energy is bounded from below $E \geq E_B$. In this way, the minimum energy is reached for solutions that obey the first-order equation

$$\phi' = \frac{W_\phi}{r^{D-1}}. \quad (5.14)$$

In order to illustrate the procedure, takes the auxiliary function $W(\phi) = \phi - \phi^3/3$ introduced in Ch. 2, Eq. (2.35), for $D = 2$ and $D \geq 3$. The first-order equation in Eq. (5.14) for this case becomes

$$\phi' = \frac{1 - \phi^2}{r^{D-1}}. \quad (5.15)$$

The planar case with $D = 2$ leads to the first-order equation solution below

$$\phi(r) = \frac{(r^2 - r_0^2)}{(r^2 + r_0^2)}. \quad (5.16)$$

Feeding the electric permittivity $P(\phi)$ with the solution allows us to write the electric field in Eq. (5.11) in the form

$$\mathbf{E}(r) = \left[\frac{2rr_0}{(r^2 + r_0^2)} \right]^4 \frac{1}{er} \hat{r}. \quad (5.17)$$

While for $D \geq 3$, the solutions for the first-order equation (5.14) are given by

$$\phi(r) = \tanh \left(\frac{-1}{(D-2)r^{D-2}} \right). \quad (5.18)$$

In this case, the electric field takes the form

$$\mathbf{E}(r) = \operatorname{sech}^4 \left(\frac{-1}{(D-2)r^{D-2}} \right) \frac{1}{er^{D-1}} \hat{r}. \quad (5.19)$$

Notice that the electric permittivity modifies the usual field behavior, regularizing divergence at the origin. Next, we study a model inspired by this work, in which two coupled scalar fields control the permittivity.

5.2 Charged configurations

In Ref. [20] we developed a procedure inspired by the above results, where the electric permittivity is controlled by two scalar fields that describe the domain wall. Here, we use the scalar fields to mimic the Bloch wall structures, as was presented in Ch. 3. The Lagrangian density for this model is inspired by the ones in Eqs. (5.8) and (2.46)

$$\mathcal{L} = -\frac{1}{4}P(\phi, \chi)F_{\mu\nu}F^{\mu\nu} + \frac{1}{2}\partial_\mu\phi\partial^\mu\phi + \frac{1}{2}\partial_\mu\chi\partial^\mu\chi - A_\mu j^\mu, \quad (5.20)$$

where χ is a real scalar field and $P(\phi, \chi)$ is the new permittivity controlled by the fields ϕ and χ . This expression is quite different from the one in Ref. [16], although both models deal with two scalar fields ϕ , and χ , here they are coupled exclusively by the electric permittivity. The equations of motion are given by

$$\partial_\mu\partial^\mu\phi + \frac{P_\phi}{4}F_{\mu\nu}F^{\mu\nu} = 0, \quad (5.21a)$$

$$\partial_\mu\partial^\mu\chi + \frac{P_\chi}{4}F_{\mu\nu}F^{\mu\nu} = 0, \quad (5.21b)$$

$$\partial_\mu(PF^{\mu\nu}) - j^\nu = 0. \quad (5.21c)$$

Consider the electrostatics scenario of a single point charge described by the current in Eq. (5.3). In this case, Gauss's law in Eq. (5.21c) leads to the electric field

$$\mathbf{E} = \frac{e}{r^{D-1}P(\phi, \chi)}\hat{r}, \quad (5.22)$$

similar to expression in Eq. (5.7). The equations of motion (5.21a) and (5.21b) for static scalar fields are given by

$$\frac{1}{r^{D-1}}(r^{D-1}\phi')' - \frac{e^2}{2r^{2D-2}}\frac{\partial}{\partial\phi}\left(\frac{1}{P}\right) = 0, \quad (5.23a)$$

$$\frac{1}{r^{D-1}}(r^{D-1}\chi')' - \frac{e^2}{2r^{2D-2}}\frac{\partial}{\partial\chi}\left(\frac{1}{P}\right) = 0. \quad (5.23b)$$

The energy density for this configuration is given by

$$\begin{aligned} \rho &= \frac{1}{2}\phi'^2 + \frac{1}{2}\chi'^2 + \frac{P}{2}|\mathbf{E}|^2 \\ &= \frac{1}{2}\phi'^2 + \frac{1}{2}\chi'^2 + \frac{1}{2P}\frac{e^2}{r^{2D-2}}. \end{aligned} \quad (5.24)$$

In order to perform the Bogomol'nyi procedure, we introduce an auxiliary function $W(\phi, \chi)$ following the lines of Sec. 5.1 and rewrite the energy density in Eq. (5.24) in the form

$$\rho = \frac{1}{2}\left(\phi' \mp \frac{W_\phi}{r^{D-1}}\right)^2 + \frac{1}{2}\left(\chi' \mp \frac{W_\chi}{r^{D-1}}\right)^2 + \frac{1}{2r^{2D-2}}\left(\frac{e^2}{P} - (W_\phi^2 + W_\chi^2)\right) \pm \frac{1}{r^{D-1}}W'. \quad (5.25)$$

Notice that if the permittivity has the form

$$P(\phi, \chi) = \frac{e^2}{W_\phi^2 + W_\chi^2}, \quad (5.26)$$

then the energy is bounded, that is $E \geq E_B$, where

$$E_B = \Omega(D) |W(\phi(\infty), \chi(\infty)) - W(\phi(0), \chi(0))|. \quad (5.27)$$

For the minimum energy value to be reached the configurations must obey the first-order equations below

$$\phi' = \pm \frac{W_\phi}{r^{D-1}}, \quad (5.28a)$$

$$\chi' = \pm \frac{W_\chi}{r^{D-1}}. \quad (5.28b)$$

In this case, the energy density becomes

$$\rho(r) = \phi'^2 + \chi'^2. \quad (5.29)$$

Since we studied in Ch. 3, the auxiliary function $W(\phi, \chi)$ in Eq. (3.25) leads to scalar fields that describe Bloch wall structure type. In order to investigate the behavior of a single point charge in a medium with the electric permittivity controlled by ϕ and χ fields that mimic domain wall, we consider $W(\phi, \chi)$ in Eq. (3.25) with a new parameter σ as follow

$$W(\phi, \chi) = \sigma\phi - \frac{1}{3}\sigma\phi^3 - k\phi\chi^2, \quad (5.30)$$

where k is a parameter that controls the intensity of the coupling between the fields ϕ and χ . Here, σ denotes a real and positive parameter, which is not required for one spatial dimension. On the other hand, in high dimensions σ play an important role in avoiding divergences in energy density, as we will see further below. In this situation, the first-order equations in (5.28a) and (5.28b) take the form

$$\phi' = \pm \frac{\sigma - \sigma\phi^2 - k\chi^2}{r^{D-1}}, \quad (5.31a)$$

$$\chi' = \mp \frac{2k\phi\chi}{r^{D-1}}. \quad (5.31b)$$

To decouple these equations we can use the elliptic orbit in Eq. (3.32) with a slight difference

$$\phi^2 + \frac{k}{\sigma - 2k}\chi^2 = 1, \quad (5.32)$$

which leads to the first-order equation (5.31a) below

$$\phi' = \pm \frac{2k(1 - \phi^2)}{r^{D-1}}. \quad (5.33)$$

Next, we investigated the scenario for $D = 2$ and $D = 3$. For simplicity, we take the positive equation above.

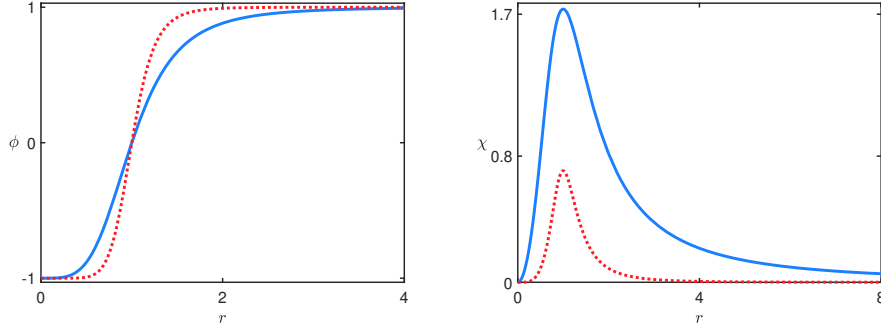


Figure 5.1 The solutions $\phi(r)$ (left) and $\chi(r)$ (right) associated to the model in Sec. 5.2.1 for $\sigma = 5$, with $k = 1$ (solid, blue line) and 2 (dotted, red line).

5.2.1 Two spatial dimensions

In the planar case, with $D = 2$, the first-order equation (5.33) becomes

$$\phi' = \frac{2k(1 - \phi^2)}{r}. \quad (5.34)$$

This equation supports the solution

$$\phi(r) = \frac{r^{4k} - 1}{r^{4k} + 1}. \quad (5.35)$$

To find χ , we feed the orbit equation (5.32) with the above solution to get

$$\chi(r) = 2\sqrt{\frac{\sigma}{k} - 2} \frac{r^{2k}}{r^{4k} + 1}. \quad (5.36)$$

Notice that one must take $\sigma/k > 2$ to respect the condition that χ is a real scalar field and non-vanishing. In Fig 5.1 are plotted the solutions $\phi(r)$ and $\chi(r)$ in Eqs. (5.35) and (5.36). The energy density in Eq. (5.29) becomes

$$\begin{aligned} \rho(r) = \frac{4k^2}{r^2} & \left[\left(\frac{2r^{2k}}{r^{4k} + 1} \right)^4 \right. \\ & \left. + \left(\frac{2r^{2k}}{r^{4k} + 1} \right)^2 \left(\frac{r^{4k} - 1}{r^{4k} + 1} \right)^2 \left(\frac{\sigma}{k} - 2 \right) \right]. \end{aligned} \quad (5.37)$$

The electric field in Eq. (5.22) with the permittivity $P(\phi, \chi)$ in Eq. (5.26) takes the form

$$\begin{aligned} E_r = \frac{4k^2}{er} & \left[\left(\frac{2r^{2k}}{r^{4k} + 1} \right)^4 \right. \\ & \left. + \left(\frac{2r^{2k}}{r^{4k} + 1} \right)^2 \left(\frac{r^{4k} - 1}{r^{4k} + 1} \right)^2 \left(\frac{\sigma}{k} - 2 \right) \right]. \end{aligned} \quad (5.38)$$

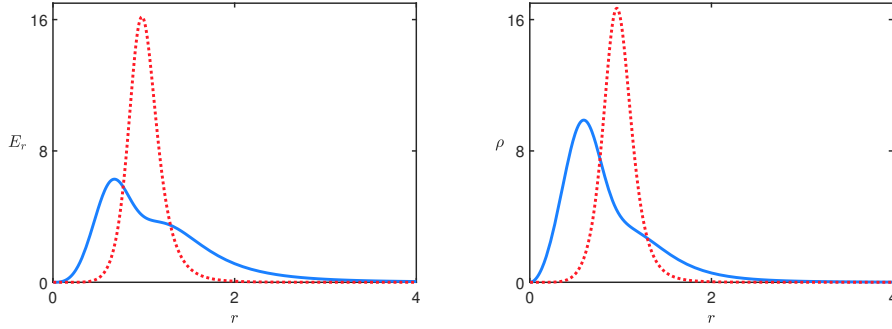


Figure 5.2 The radial component of the electric field (left) for $e = 1$ and the energy density (right) associated to the model in Sec. 5.2.1 for $\sigma = 5$, with $k = 1$ (solid, blue line) and 2 (dotted, red line).

Asymptotically the energy density and the electric field go to zero. On the other hand, near the origin, the first term in energy density $[2r^{2k}/(r^{4k} + 1)]^4$ becomes proportional to r^{8k-2} since, in this situation, $r^{4k} + 1 \approx 1$. Doing the same analysis for the second term, we see that it becomes proportional to r^{4k-2} . Then, for the energy density not to diverge at the origin, one must take $4k - 2 > 0$, this is, $k > 1/2$. Since $\sigma/k > 2$ must be satisfied, this condition imposes that $\sigma > 1$. Similarly, near the origin, the first and second terms in the electric field become proportional to r^{8k-1} and r^{4k-1} , respectively. These terms impose the condition $k > 1/4$. However, this condition is already covered by $k > 1/2$.

In Fig. 5.2 can be seen that the electric field (left) presents a behavior quite different than usual (see Eq. (5.7)), giving rise to a valley around the origin. The same can be observed for the energy density (right). Therefore, the Bloch wall modeled by the scalar fields regularizes the electric field generated by a single-point charge. The planar plot in Fig. 5.3 allows us to visualize the ring-like structure in the electric field and energy density; the hole with a center at the origin is controlled by k . The total energy of this structure is $E = 8\pi\sigma/3$.

5.2.2 Three spatial dimensions

Following the analysis, we take the spatial case with $D = 3$. The first-order equation (5.33), in this case, becomes

$$\phi' = \frac{2k(1 - \phi^2)}{r^2}. \quad (5.39)$$

In this situation, the solutions ϕ and χ are given by

$$\phi(r) = \tanh(\xi(r)) \quad (5.40a)$$

$$\chi(r) = \sqrt{\frac{\sigma}{k} - 2} \operatorname{sech}(\xi(r)), \quad (5.40b)$$

where $\xi(r)$ plays the role of a geometrical coordinate, with

$$\xi(r) = -\frac{2k}{r}, \quad (5.41)$$



Figure 5.3 The radial component of the electric field (left, blue) with $e = 1$ and the energy density (right, orange) associated to the model in Sec. 5.2.1 depicted in the plane for $\sigma = 5$, with $k = 1$ (top), and $k = 2$ (bottom). The intensity of the blue and orange colors increases with the increasing of the electric field and energy density, respectively.

as in Eq. (3.38). In Fig. 5.4 are plotted the solutions ϕ and χ . In this scenario, $\phi(r)$ goes from -1 to 0 . The solution $\chi(r)$ becomes a monotonically increasing function, starting from zero, reaching its maximum value $\sqrt{\sigma/k}$ asymptotically. Moreover, these solutions are more elongated than those of the planar case, as shown in axis r .

The energy density associated is given by

$$\rho(r) = \frac{4k^2}{r^4} \left[\text{sech}(\xi)^4 + \tanh(\xi)^2 \text{sech}(\xi)^2 \left(\frac{\sigma}{k} - 2 \right) \right], \quad (5.42)$$

and the electric field has the form

$$E_r(r) = \frac{4k^2}{er^2} \left[\text{sech}(\xi)^4 + \tanh(\xi)^2 \text{sech}(\xi)^2 \left(\frac{\sigma}{k} - 2 \right) \right], \quad (5.43)$$

where the expressions are written in terms of geometrical coordinate $\xi(r)$. Notice that the energy density and the electric field go to zero asymptotically. The term $\text{sech}(\xi(r)) = \text{sech}(-2k/r)$

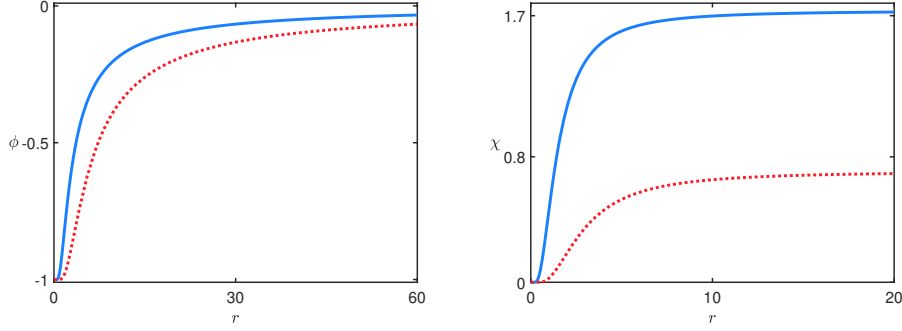


Figure 5.4 The solutions $\phi(r)$ (left) and $\chi(r)$ (right) associated to the model in Sec. 5.2.2 for $\sigma = 5$, with $k = 1$ (solid, blue line) and 2 (dotted, red line).

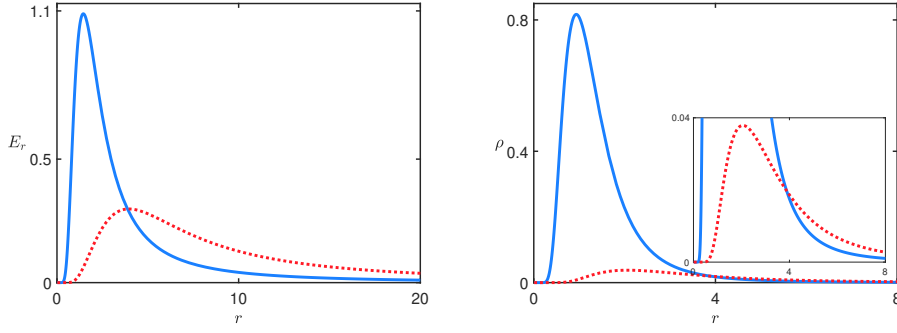


Figure 5.5 The radial component of the electric field (left) with $e = 1$ and the energy density (right) associated to the model in Sec. 5.2.2 for $\sigma = 5$, with $k = 1$ (solid, blue line) and 2 (dotted, red line). The inset in the bottom figure shows the interval $\rho \in [0, 0.04]$.

goes to zero quickly, even before the $1/r^4$ diverges. Therefore, for any allowed value of k , these physical quantities do not diverge at the origin, unlike in the planar case with $D = 2$. Thus, σ is not required here to avoid divergences and to ensure that the electric field is single-valued. In Fig. 5.5 are plotted the energy density and the electric field for some values of k . To better visualize their behavior, we plot them at the plane in Fig. 5.6. The total energy for this structure is $E = 8\pi\sigma/3$.

5.3 Internal structure of charged configurations

In the previous section, we presented a single-point charge in a medium with an electric permittivity controlled by scalar fields, which mimic a Bloch wall. This procedure regularizes the electric field locating it in a ring-like structure. Authors in Ref. [12] presented the effects of deformation in the kink profile through a function that changes the kinematic term in Lagrangian density. In Ref. [21], we describe a procedure to manipulate the internal structure of the Bloch wall, which was presented in Ch. 3. In that sense, we continue the investigation with the idea of modifying the internal structures of charged configurations shown in the previous section.



Figure 5.6 The electric field in the plane (left, blue) with $e = 1$ and the energy density (right, orange) associated to the model in Sec. 5.2.2 for $\sigma = 5$ and $k = 1$. The intensity of the blue and orange colors increases with the increasing of the electric field and energy density, respectively.

For that, in Ref [20], we propose the Lagrangian density

$$\begin{aligned} \mathcal{L} = & -\frac{1}{4}P(\phi, \chi, \psi)F_{\mu\nu}F^{\mu\nu} + \frac{1}{2}f(\psi)\partial_\mu\phi\partial^\mu\phi \\ & + \frac{1}{2}f(\psi)\partial_\mu\chi\partial^\mu\chi + \frac{1}{2}\partial_\mu\psi\partial^\mu\psi - A_\mu j^\mu, \end{aligned} \quad (5.44)$$

where $P(\phi, \chi, \psi)$ is the new electric permittivity, ψ is the scalar field that plays the role of source, $f(\psi)$ is the function that is coupled to the kinematic terms of ϕ and χ associated to the Bloch wall. Here, j^μ is the current in Eq. (5.3). The equations of motion are written as

$$\partial_\mu(f\partial^\mu\phi) + \frac{P_\phi}{4}F_{\mu\nu}F^{\mu\nu} = 0, \quad (5.45a)$$

$$\partial_\mu(f\partial^\mu\chi) + \frac{P_\chi}{4}F_{\mu\nu}F^{\mu\nu} = 0, \quad (5.45b)$$

$$\partial_\mu\partial^\mu\psi + \frac{P_\psi}{4}F_{\mu\nu}F^{\mu\nu} - \frac{f_\psi}{2}(\partial_\mu\phi\partial^\mu\phi + \partial_\mu\chi\partial^\mu\chi) = 0. \quad (5.45c)$$

Gauss's law leads to Eq. (5.11) with the new electric permittivity $P(\phi, \chi, \psi)$. The set of equations of motion for the static field configuration is given by

$$\frac{1}{r^{D-1}}(r^{D-1}f\phi')' - \frac{e^2}{2r^{2D-2}}\frac{\partial}{\partial\phi}\left(\frac{1}{P}\right) = 0, \quad (5.46a)$$

$$\frac{1}{r^{D-1}}(r^{D-1}f\chi')' - \frac{e^2}{2r^{2D-2}}\frac{\partial}{\partial\chi}\left(\frac{1}{P}\right) = 0, \quad (5.46b)$$

$$\frac{1}{r^{D-1}}(r^{D-1}\psi')' - \frac{e^2}{2r^{2D-2}}\frac{\partial}{\partial\psi}\left(\frac{1}{P}\right) - \frac{f_\psi}{2}(\chi'^2 + \phi'^2) = 0. \quad (5.46c)$$

As before, the scalar fields are decoupled from the gauge field due to the electric field. On the other hand, these fields are coupled with each other. The energy density associated with the field configuration has the form

$$\rho = \frac{f}{2}(\phi'^2 + \chi'^2) + \frac{1}{2}\psi'^2 + \frac{1}{2P} \frac{e^2}{r^{2D-2}}. \quad (5.47)$$

In order to perform the first-order formalism, one considers the function $W = W(\phi, \chi, \psi)$ and we rewrite the energy density as

$$\begin{aligned} \rho = & \frac{f}{2} \left(\phi' \mp \frac{W_\phi}{fr^{D-1}} \right)^2 + \frac{f}{2} \left(\chi' \mp \frac{W_\chi}{fr^{D-1}} \right)^2 + \frac{1}{2} \left(\psi' \mp \frac{W_\psi}{r^{D-1}} \right)^2 \\ & + \frac{1}{2r^{2D-2}} \left(\frac{e^2}{P} - \left(\frac{W_\phi^2}{f} + \frac{W_\chi^2}{f} + W_\psi^2 \right) \right) \pm \frac{1}{r^{D-1}} W', \end{aligned}$$

where

$$W' = W_\phi \phi' + W_\chi \chi' + W_\psi \psi'. \quad (5.48)$$

As before, the minimum energy is reached if the permittivity is written in the form

$$P(\phi, \chi, \psi) = e^2 \left(\frac{W_\phi^2}{f} + \frac{W_\chi^2}{f} + W_\psi^2 \right)^{-1}, \quad (5.49)$$

and the equations of motion are compatible with the first-order equations

$$\phi' = \pm \frac{W_\phi}{fr^{D-1}}, \quad (5.50a)$$

$$\chi' = \pm \frac{W_\chi}{fr^{D-1}}, \quad (5.50b)$$

$$\psi' = \pm \frac{W_\psi}{r^{D-1}}. \quad (5.50c)$$

In this case, the energy becomes $E_B = \Omega(D) |W(\phi(\infty), \chi(\infty), \psi(\infty)) - W(\phi(0), \chi(0), \psi(0))|$. Notice that the first-order equations (5.50a) and (5.50b) are given in terms of W_ϕ and W_χ , respectively, and also $f(\psi)$. On the other hand, Eq. (5.50c) depends only on W_ψ , which makes it independent of ϕ and χ . This particular case allows us to write the auxiliary function in the form $W(\phi, \chi, \psi) = W(\phi, \chi) + W(\psi)$. Therefore, the first-order in Eq. (5.50c) can be solved independently. Thus, as in Sec. 3.1, we use its solution to feed the function $f(\psi)$, which plays the role of the source of geometrical constrictions. In this scenario, the energy is written as $\rho = \rho_1 + \rho_2$, where ρ_1 is the part that depends on the $f(\psi)$ and the other fields, and ρ_2 is the energy density associated to the source, as follows

$$\rho_1 = f(\psi)(\phi'^2 + \chi'^2), \quad (5.51a)$$

$$\rho_2 = \psi'^2. \quad (5.51b)$$

In order to investigate the geometrical constrictions effects in the Bloch Wall described by the scalar fields ϕ and χ , we take $W_1(\phi, \chi)$ as the auxiliary function shown in Eq. (5.30). For the source field, we take an auxiliary $W_2(\psi)$ as in Eq. (2.35) as follows

$$W_2 = \alpha\psi - \frac{1}{3}\alpha\psi^3, \quad (5.52a)$$

where α is a real and positive parameter. Then, we get the set of first-order equations (5.50a)-(5.50c)-(5.50b) in the form

$$\phi' = \pm \frac{\sigma - \sigma\phi^2 - k\chi^2}{fr^{D-1}}, \quad (5.53a)$$

$$\chi' = \pm \frac{2k\phi\chi}{fr^{D-1}}, \quad (5.53b)$$

$$\psi' = \pm \frac{\alpha(1 - \psi^2)}{r^{D-1}}. \quad (5.53c)$$

Using the trial orbit method, one can show that the first-order equations (5.53a) and (5.53b) support the orbit elliptic in Eq. (3.32). Thus, we get

$$\phi' = \pm \frac{2k(1 - \phi^2)}{f(\psi)r^{D-1}}. \quad (5.54)$$

This equation is very similar to Eq. (3.33) in Ch. 3 for one dimension, where some possibilities for the function $f(\psi)$ are explored, which leads to modifications in the profile of structures of the Bloch wall type. The following models, in two and three spatial dimensions, are inspired by these results.

5.3.1 Two spatial dimensions

We start with the charged configurations inspired by the structures in Sec. 5.2.1, with $D = 2$. The first step is getting the solution $\psi(r)$, so we can feed the function $f(\psi)$ and replace it in the first-order equations involving ϕ and χ . Eq. (5.53c) supports the solution

$$\psi(r) = \frac{r^{2\alpha} - 1}{r^{2\alpha} + 1}, \quad (5.55)$$

where we have taken the condition $\psi(1) = 0$, for simplicity. The energy density associated to the field source in Eq.(5.51b) has the form

$$\rho_2 = \frac{16\alpha^2 r^{4\alpha-2}}{(r^{2\alpha} + 1)^4}. \quad (5.56)$$

Notice that one must take $4\alpha - 2 > 0$ or yet $\alpha > 0.5$ to prevent the energy density from diverging at the origin. In Fig. 5.7 one can see the solution $\psi(r)$ (left) forms a kink-type structure. It and its energy density present a known profile. Next, distinct possibilities for the function $f(\psi)$ are investigated.

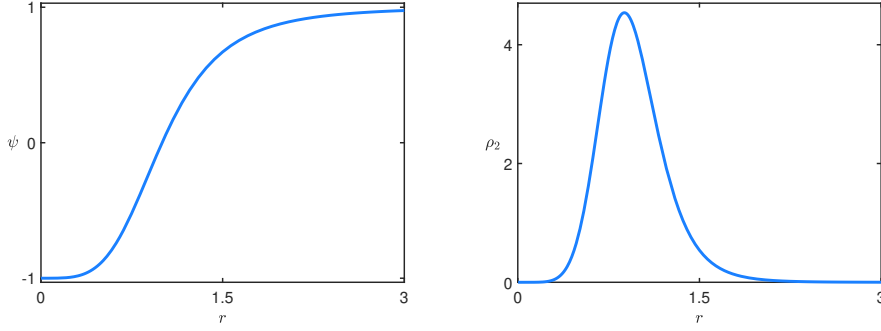


Figure 5.7 The solutions $\psi(r)$ in Eq. (5.55) (left), and the energy density in Eq. (5.56) (right) for $\alpha = 2$.

5.3.1.1 First model

We start out taking $f = 1/\psi^2$. The first-order equation in Eq. (5.54) becomes

$$\phi' = 2k\psi^2 \frac{(1 - \phi^2)}{r}, \quad (5.57)$$

where we consider the upper sign for it. Replacing the solution $\psi(r)$ in Eq. (5.55), we get

$$\phi' = 2k \left(\frac{r^{2\alpha} - 1}{r^{2\alpha} + 1} \right)^2 \frac{(1 - \phi^2)}{r}. \quad (5.58)$$

This equation supports a kink-like solution

$$\phi(r) = \tanh(\xi(r)), \quad (5.59)$$

which leads us to

$$\chi(r) = \sqrt{\frac{\sigma}{k} - 2} \operatorname{sech}(\xi(r)), \quad (5.60)$$

where $\xi(r)$ is the new geometrical coordinate given by

$$\xi(r) = 2k \left(\ln(r) - \frac{1}{\alpha} \frac{r^{2\alpha} - 1}{r^{2\alpha} + 1} \right). \quad (5.61)$$

Notice that the fields $\phi(r)$ and $\chi(r)$ are similar to Eqs.(5.40a) and (5.40b), with another geometrical coordinate. Just like in Ch. 3, the function $f(\psi)$ modifies the internal structure of the Bloch wall. Therefore, a new function $f(\psi)$ still implies a Bloch wall described by $\phi(r)$ and $\chi(r)$, but with a new geometrical coordinate for the scalar fields. In Fig. 5.8, one can see the formation of a plateau in solutions $\phi(r)$ and $\chi(r)$ for $\sigma = 5$, $\alpha = 2$, and some values of k . The energy density associated to this configuration is given by ρ_1 . Below we write it in terms of the geometrical coordinate $\xi(r)$

$$\rho_1 = \frac{4k^2}{r^2} \left(\frac{r^{2\alpha} - 1}{r^{2\alpha} + 1} \right)^2 \left(\operatorname{sech}^4(\xi) + \operatorname{sech}^2(\xi) \tanh^2(\xi) \left(\frac{\sigma}{k} - 2 \right) \right), \quad (5.62)$$

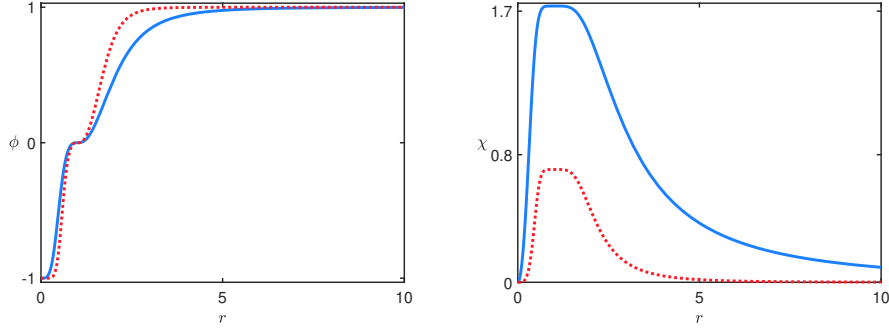


Figure 5.8 The solutions $\phi(r)$ (left) and $\chi(r)$ (right) associated to the model in Sec. 5.3.1.1 for $\sigma = 5$ and $\alpha = 2$, with $k = 1$ (solid, blue line) and 2 (dotted, red line).

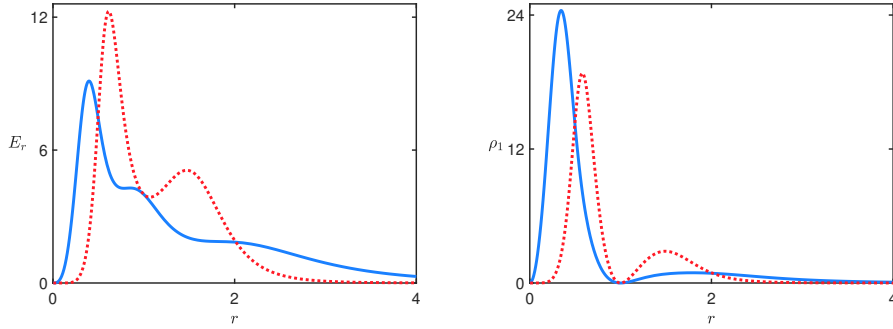


Figure 5.9 The radial component of the electric field (left) with $e = 1$ and the energy density (right) associated to the model in Sec. 5.3.1.1 for $\sigma = 5$, $\alpha = 2$, with $k = 1$ (solid, blue line) and 2 (dotted, red line).

and the electric field in the form

$$E_r = \left[4k^2 \operatorname{sech}^2(\xi) \left(\frac{r^{2\alpha} - 1}{r^{2\alpha} + 1} \right)^2 \left(\operatorname{sech}^2(\xi) + \tanh^2(\xi) \left(\frac{\sigma}{k} - 2 \right) \right) + \frac{16\alpha^2 r^{4\alpha}}{(r^{2\alpha} + 1)^4} \right] \frac{1}{re}. \quad (5.63)$$

In Fig. 5.9, we illustrate the electric field and the energy density. One can see that these new configurations present two peaks, which are controlled by k , the parameter that controls the strength of the coupling between the scalar fields. As k grows, the hole with the center at the origin becomes bigger, squeezing the electric field and energy density and making the peaks higher. In Fig. 5.10, these structures can be seen at the plane. The total energy of the configuration is $E = E_1 + E_2 = 8\pi(\sigma + \alpha)/3$.

5.3.1.2 Second model

In the second model we take $f = \sec^2(n\pi\psi)$ following the lines of Sec.3.1.2, where n is an integer. The first-order equations associated support solutions similar to Eqs.(5.40a) and (5.40b)



Figure 5.10 The radial component of the electric field (left, blue) with $e = 1$ and the energy density (right, orange) associated to the model in Sec. 5.3.1.1 depicted in the plane for $\sigma = 5$ and $\alpha = 2$, with $k = 1$ (top), and $k = 2$ (bottom). The intensity of the blue and orange colors increases with the increasing of the electric field and energy density, respectively.

with a new geometrical coordinate $\eta(r)$ replacing $\xi(r)$ given by

$$\eta(r) = k \ln(r) + \frac{k}{2\alpha} [\text{Ci}(\xi_+(r)) - \text{Ci}(\xi_-(r))], \quad (5.64)$$

where C_i denotes the cosine integral function defined in Eq. (3.44) and $\xi_{\pm}(r) = 2\pi n[1 \pm (r^{2\alpha} - 1)/(r^{2\alpha} + 1)]$. In Fig. 5.11, we depicted the solutions $\phi(r)$ and $\chi(r)$ for the new geometrical coordinate. In this situation, the scalar fields show $2n$ inflection points that appear due to the form of $f(\psi)$. The energy density in Eq. (5.51a) reads

$$\rho_1 = \left[4k^2 \text{sech}^2(\eta) \cos^2 \left(n\pi \left(\frac{r^{2\alpha} - 1}{r^{2\alpha} + 1} \right) \right) \left(\text{sech}^2(\eta) + \tanh^2(\eta) \left(\frac{\sigma}{k} - 2 \right) \right) \right] \frac{1}{r^2}, \quad (5.65)$$

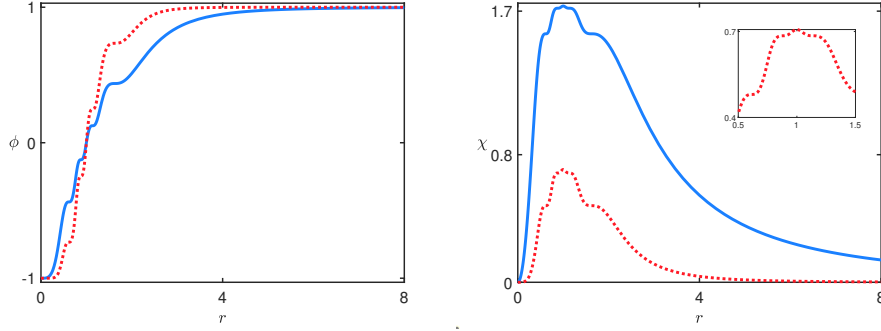


Figure 5.11 The solutions $\phi(r)$ (left) and $\chi(r)$ (right) associated to the model in Sec. 5.3.1.2 for $\sigma = 5$, $\alpha = 2$ and $n = 2$, with $k = 1$ (solid, blue line) and 2 (dotted, red line). The inset in the bottom figure shows the interval $r \in [0.5, 1.5]$ for $k = 2$.

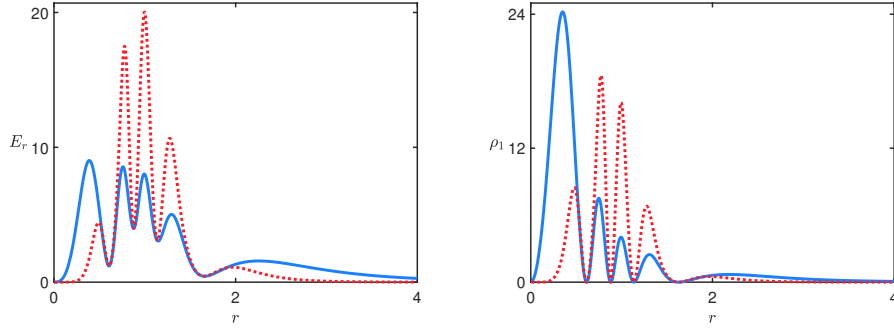


Figure 5.12 The radial component of the electric field (left) with $e = 1$ and the energy density (right) associated to the model in Sec. 5.3.1.2 for $\sigma = 5$, $\alpha = 2$ and $n = 2$, with $k = 1$ (solid, blue line) and $k = 2$ (dotted, red line).

and the electric field in Eq. (5.7) takes the form

$$E_r = \left[4k^2 \operatorname{sech}^2(\eta) \cos^2 \left(n\pi \left(\frac{r^{2\alpha} - 1}{r^{2\alpha} + 1} \right) \right) \left(\operatorname{sech}^2(\eta) + \tanh^2(\eta) \left(\frac{\sigma}{k} - 2 \right) \right) + \frac{16\alpha^2 r^{4\alpha}}{(r^{2\alpha} + 1)^4} \right] \frac{1}{re}. \quad (5.66)$$

In Fig. 5.12, we illustrate the electric field and energy density. Notice that these new configurations are richer than the previous ones, presenting a multi-ring structure controlled by k . To better illustrate these features, we plot them on the plane in Fig. 5.13. Here one can see that as k grows, the inner ring becomes diffuse. On the other hand, the following two rings become more concentrated. The total energy for this structure is the same as the previous case since it no depends on the function $f(\psi)$. Next, we explore modifications generated by the function $f(\psi)$ in three dimensions scenario.



Figure 5.13 The electric field (left, blue) with $e = 1$ and the energy density (right, orange) associated to the model in Sec. 5.3.1.2 depicted in the plane for $\sigma = 5$, $\alpha = 2$ and $n = 2$, with $k = 1$ (top) and 2 (bottom). The intensity of the blue and orange colors increases with the increasing of the electric field and energy density, respectively.

5.3.2 Three spatial dimensions

We continue our investigation of the model (5.44), studying it in three spatial dimensions. As before, we explore the unusual behavior of the electrical structure induced by the electric permittivity controlled by scalar fields. Here we consider the same functions $f(\psi)$ shown in the previous section. The first-order equation in Eq. (5.53c) is given by

$$\psi' = \pm \frac{\alpha(1 - \psi^2)}{r^2}. \quad (5.67)$$

In this case, we get

$$\psi = -\tanh\left(\frac{\alpha}{r}\right), \quad (5.68)$$

the energy density in Eq. (5.51b) for this configuration is given by

$$\rho_2 = \frac{\alpha^2}{r^4} \operatorname{sech}^4\left(\frac{\alpha}{r}\right). \quad (5.69)$$

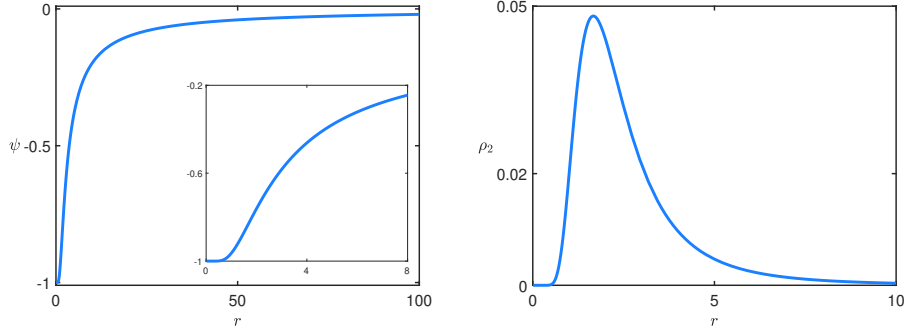


Figure 5.14 The solution $\psi(r)$ in Eq. (5.68) (left) and the energy density ρ_2 in Eq. (5.69) (right) for $\alpha = 2$. The inset in the top figure shows the solution near the origin.

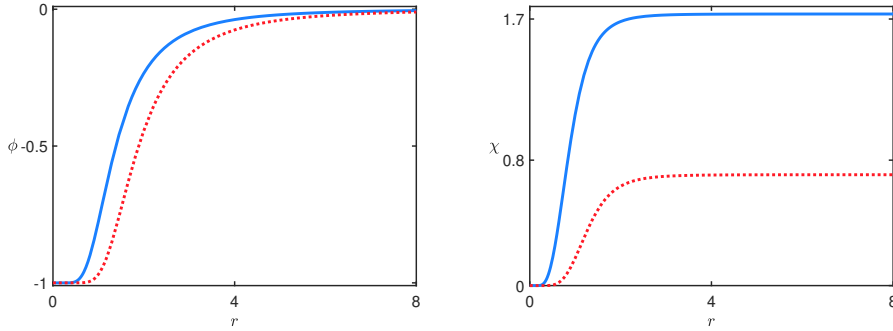


Figure 5.15 The solution $\phi(r)$ (left) and $\chi(r)$ (right) associated to the model in Sec. 5.3.2.1 for $\sigma = 5$ and $\alpha = 2$ with $k = 1$ (solid, blue line) and 2 (dotted, red line).

In Fig. 5.14, we plot the solution (5.68) and the energy density (5.69) for $\alpha = 2$. Notice that contrary to the case for $D = 2$, here α is not required in order to avoid divergences.

5.3.2.1 First model

Consider $f = 1/\psi^2$. In this case, the first-order equation (5.54) supports solution $\phi(r)$ similar to (5.53a), which leads to solution $\chi(r)$ in Eq. (5.53b) with geometrical coordinate replaced by

$$\xi(r) = \frac{2k}{\alpha} \left(\tanh\left(\frac{\alpha}{r}\right) - \frac{\alpha}{r} \right). \quad (5.70)$$

In Fig. 5.15 we depicted $\phi(r)$ and $\chi(r)$ for $\sigma = 5$, $\alpha = 2$ and some values of k . The energy density associated to this configuration in Eq. (5.51a) is

$$\rho_1 = \left[4k^2 \operatorname{sech}^2(\xi) \tanh^2\left(\frac{\alpha}{r}\right) \left(\operatorname{sech}^2(\xi) + \tanh^2(\xi) \left(\frac{\sigma}{k} - 2 \right) \right) \right] \frac{1}{r^4}, \quad (5.71)$$

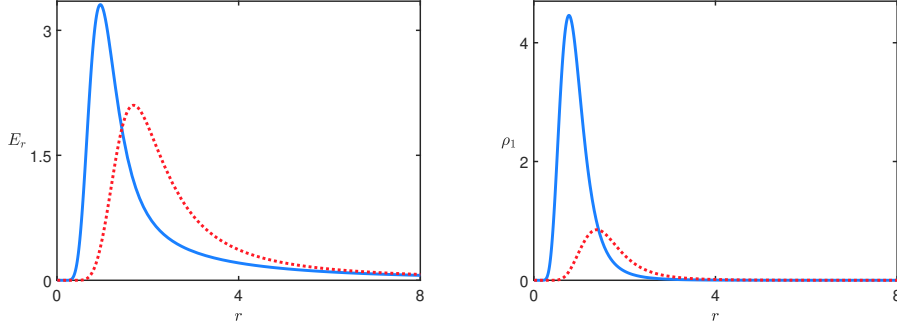


Figure 5.16 The radial component of the electric field (left) with $e = 1$ and the energy density (right) associated to the model in Sec. 5.3.2.1 for $\sigma = 5$, $\alpha = 2$, and $k = 1$ (solid, blue line) and 2 (dotted, red line).



Figure 5.17 The section passing through the center of the structure, representing the electric field (left, blue) with $e = 1$ and the energy density (right, orange) associated to the model in Sec. 5.3.2.1 for $\sigma = 5$, $\alpha = 2$ and $k = 2$. The intensity of the blue and orange colors increases with the increasing of the electric field and energy density, respectively.

and the electric field (5.22) is given by

$$E_r = \left[4k^2 \operatorname{sech}^2(\xi) \tanh^2\left(\frac{\alpha}{r}\right) \left(\operatorname{sech}^2(\xi) + \tanh^2(\xi) \left(\frac{\sigma}{k} - 2 \right) \right) + \alpha^2 \operatorname{sech}^4\left(\frac{\alpha}{r}\right) \right] \frac{1}{er^2}. \quad (5.72)$$

In order to illustrate the behavior of the physics quantities, we plot them in Fig. 5.16. One can see that the electric field and the energy density show a hole near the origin controlled by k . Moreover, k also controls the height of the peaks. We depicted these structures on the plane in Fig. 5.17 to better illustrate the behavior.

5.3.2.2 Second model

The other model investigates three spatial dimensions considering $f = \sec^2(n\pi\psi)$. Following the lines of the previous example, we get solutions similar to Eqs. (5.40a) and (5.40b) with

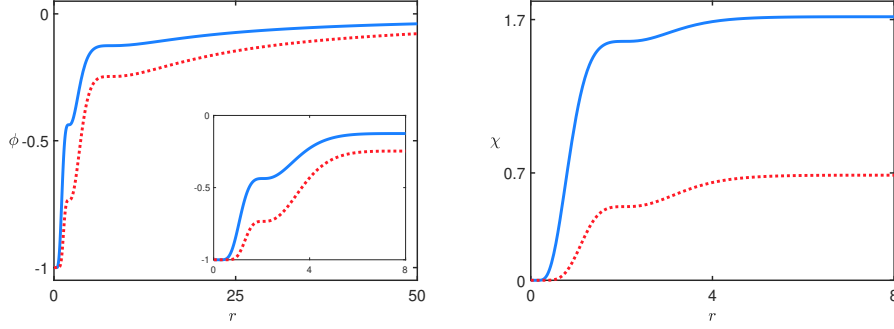


Figure 5.18 The solutions $\phi(r)$ (left) and $\chi(r)$ (right) associated to the model in Sec. 5.3.2.2 for $\sigma = 5$, $\alpha = 2$ and $n = 2$ with $k = 1$ (solid, blue line) and 2 (dotted, red line). The inset in the top figure shows the behavior for small r .

geometrical coordinate ξ given by

$$\eta(r) = -\frac{k}{r} + \frac{k}{2\alpha} [\text{Ci}(\xi_+(r)) - \text{Ci}(\xi_-(r))], \quad (5.73)$$

where $\xi_{\pm}(r) = 2n\pi(1 \mp \tanh(\alpha/r))$. The solutions $\phi(r)$ and $\chi(r)$ can be visualized in Fig. 5.18. In this case, the energy density is written in the form

$$\rho_1 = \left[4k^2 \text{sech}^2(\eta) \cos^2(n\pi \tanh(\alpha/r)) \left(\text{sech}^2(\eta) + \tanh^2(\eta) \left(\frac{\sigma}{k} - 2 \right) \right) \right] \frac{1}{r^4}, \quad (5.74)$$

and the electric field is

$$E_r = \left[4k^2 \text{sech}^2(\eta) \cos^2(n\pi \tanh(\alpha/r)) \left(\text{sech}^2(\eta) + \tanh^2(\eta) \left(\frac{\sigma}{k} - 2 \right) \right) + \alpha^2 \text{sech}^4(\alpha/r) \right] \frac{1}{er^2}. \quad (5.75)$$

5.4 Global Monopole in the presence of electric charge

Ref. [20] introduces a new way to construct localized structures, such as the global monopole. Here, we propose a model inspired by previous results, which considers a single-point charge in a medium whose electric permittivity is controlled by a family of scalar fields. For that, we replace the Bloch Wall in Sec. 5.2 by the global monopole. The Lagrangian density for this model is inspired by the ones in (4.16) and (5.8). Its form is given by

$$\mathcal{L} = -\frac{1}{2} \partial_\mu \phi^a \partial^\mu \phi^a - \frac{1}{4} P(|\phi|) F_{\mu\nu} F^{\mu\nu} - A_\mu j^\mu. \quad (5.76)$$

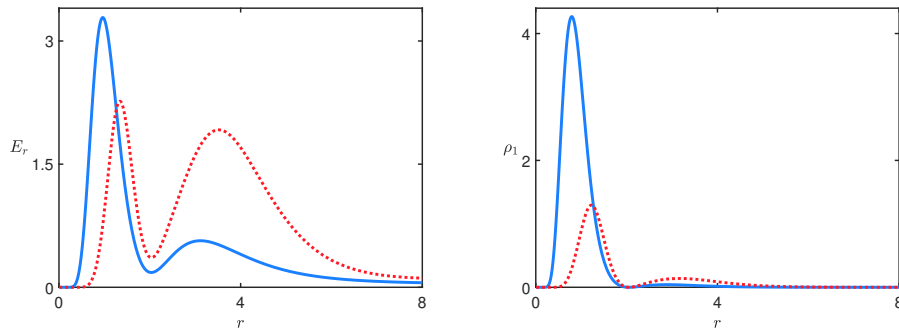


Figure 5.19 The radial component of the electric field (left) with $e = 1$ and energy density (right) associated to the model in Sec. 5.3.2.2 for $\sigma = 5$, $\alpha = 2$ and $n = 2$, with $k = 1$ (solid, blue line) and 2 (dotted, red line). For $k = 2$, we have depicted $2E_r$ and $2\rho_1$ to illustrate the behavior better.

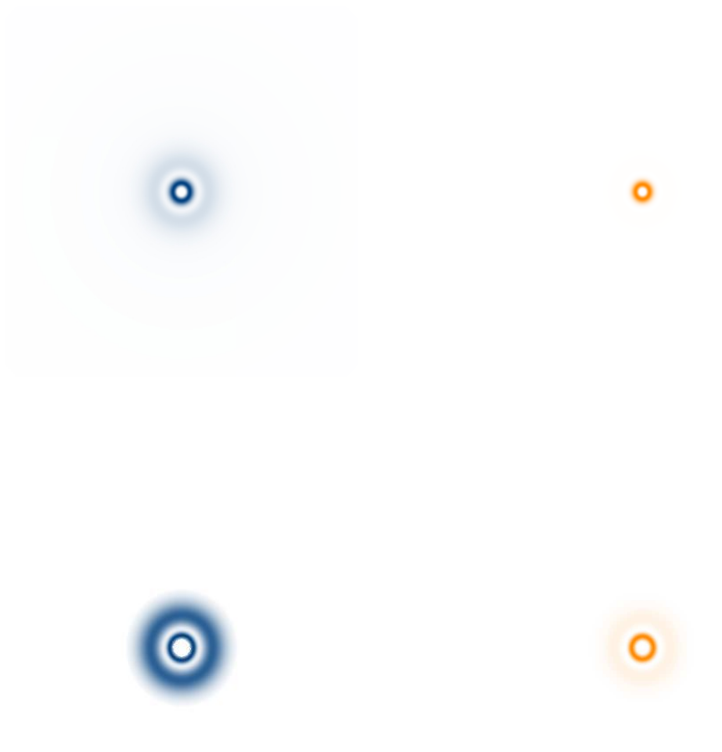


Figure 5.20 The section passing through the center of the structure, representing the electric field (left, blue) with $e = 1$ and the energy density (right, orange) associated to the model in Sec. 5.3.2.2 for $\sigma = 5$, $\alpha = 2$, with $k = 1$ (top) and 2 (bottom). The intensity of the blue and orange colors increases with the increasing of the electric field and energy density, respectively.

Here we use a coupling inspired by Ref. [16], where the family of fields is coupled to the gauge field A^μ through a dielectric function that describes a generalized electric permittivity $P(|\phi|)$. The equations of motion associated are given by

$$\partial_\mu \partial^\mu \phi^a - \frac{\phi^a}{4|\phi|} P_{|\phi|} F_{\mu\nu} F^{\mu\nu} = 0 \quad (5.77)$$

$$\partial_\mu (P(|\phi|) F^{\mu\nu}) - j^\nu = 0. \quad (5.78)$$

Consider the scenario of a single point charge at the origin in the absence of currents described by the current $j^0 = e\delta(r)/r^{D-1}$ and $j^i = 0$, where e denotes the electric charge, as in Eq. (5.3). There is no magnetic field, in this case. The electric field is written as $E^i = F^{i0}$. Thus, the Gauss law in Eq (5.78) becomes

$$\partial_i (P(|\phi|) F^{i0}) - j^0 = 0, \quad (5.79)$$

or yet

$$\partial_i (P(|H|) E^i) - e \frac{\delta(r)}{r^{D-1}} = 0, \quad (5.80)$$

which leads to

$$\mathbf{E} = \frac{e}{r^{D-1} P(H)} \hat{r}. \quad (5.81)$$

By the ansatz (4.18), we get the equation of motion (5.77) in the form

$$\frac{1}{r^{D-1}} (r^{D-1} H')' - (D-1) \frac{H}{r^2} + \frac{1}{2} P_H |\mathbf{E}|^2 = 0, \quad (5.82)$$

where $P_H = \partial P / \partial H$. This equation can be written in a compact form

$$\frac{1}{r^{D-1}} (r^{D-1} H')' = \frac{1}{2r^2} \frac{d}{dH} \left[(D-1) H^2 + \frac{e^2}{r^{2D-4} P} \right]. \quad (5.83)$$

The energy density associated to the structure is given by

$$\rho = \frac{1}{2} H'^2 + \frac{D-1}{2} \frac{H^2}{r^2} + \frac{1}{2P} \frac{e^2}{r^{2D-2}}. \quad (5.84)$$

The steps for getting follow the lines in A. Following the previous line, we introduce an auxiliary function in the energy density, which becomes

$$\rho_f = \frac{1}{2} \left(H' \mp \frac{W_H}{r^{D-1}} \right)^2 + \frac{1}{2P(H)} \frac{e^2}{r^{2D-2}} + \frac{D-1}{2} \frac{H^2}{r^2} - \frac{1}{2} \frac{W_H^2}{r^{2D-2}} \pm \frac{1}{r^{D-1}} W'. \quad (5.85)$$

In order to get the boundary conditions for the energy, we suppose that the dielectric function has the form

$$P = e^2 \left(W_H^2 - (D-1) H^2 r^{2D-4} \right)^{-1}. \quad (5.86)$$

In this way, the energy density becomes

$$\rho_f = \frac{1}{2} \left(H' \mp \frac{W_H}{r^{D-1}} \right)^2 \pm \frac{1}{r^{D-1}} W'. \quad (5.87)$$

The procedure is similar to that performed previously, where the potential is written as a function of radial coordinates. Notice that the energy bounded, $E \geq E_B$, and the minimum is reaching for configurations that meet the first-order equation $H' = \pm W_H/r^{D-1}$, which leads to energy density $\rho = W'/r^{D-1}$. Since the electric field in Eq. (5.81) is written in terms of $P(H)$, one might expect the negative terms in the dielectric function to modify its behavior. In addition, the negative term in $P(H)$ breaks the translational invariance.

In order to illustrate these results, we take the auxiliary function in Eq. (4.52) associated to the $|\phi|^4$ model studied in this chapter. The dielectric function then takes the form

$$P = e^2 \left((1 - H^2)^2 - (D - 1)H^2 r^{2D-4} \right)^{-1}. \quad (5.88)$$

We need to feed it with solution H To get the dielectric function. The first-order with solution H is the same in Eq. (4.36), and we know that it supports the solution (4.55). Therefore, we can replace the known solution H and get the dielectric function

$$P = e^2 \left(\operatorname{sech}^4 \left(\frac{1}{(D-2)r^{D-2}} \right) - (D-1) \tanh^2 \left(\frac{1}{(D-2)r^{D-2}} \right) r^{2D-4} \right)^{-1}. \quad (5.89)$$

Thus, the electric field in Eq. (5.81) takes the form

$$\mathbf{E} = \frac{1}{e} \left[\frac{1}{r^{D-1}} \operatorname{sech}^4 \left(\frac{1}{(D-2)r^{D-2}} \right) - \tanh^2 \left(\frac{1}{(D-2)r^{D-2}} \right) (D-1)r^{D-3} \right] \hat{r}. \quad (5.90)$$

One can get the gauge field A_0 through the expression $dA_0/dr = -E_r$ from the electric field. For simplicity, we take $A_0(0) = 0$. In Fig. 5.21, we display the electric field \mathbf{E} and A_0 for $D = 3$ and $e = 1$. An interesting behavior is observed. At the origin, the electric field is null. However, as we move away from the origin it grows, becoming positive, and then falls quickly becoming negative, even for a positive charge. This particular behavior is observed in Fig. 5.22, where the spatial section of the electric field passing through the center of the structure is plotted, with the color purple representing $E_r = -2$, the color white $E_r = 0$, and the color blue for $E_r \approx 0.079$. The special behavior is the opposite of Coulomb's law since the field attracts positive charge. In addition, the electric field non diverge at the origin. Actually, it is null at this point for $D \geq 3$. The energy density in Eq. (5.87) associated to this structure has the same form as Eq. (4.56). Therefore by integrating, we get the energy $E = 2\Omega(D)/3$.

In a second example, we consider the auxiliary function W in Eq. (4.58) associated to the $|\phi|^6$ model. For this case, the dielectric function (5.86) is written as

$$P = e^2 \left(|\phi|^2 \left((1 - |\phi|^2)^2 - (D-1)r^{2D-4} \right) \right)^{-1}, \quad (5.91)$$

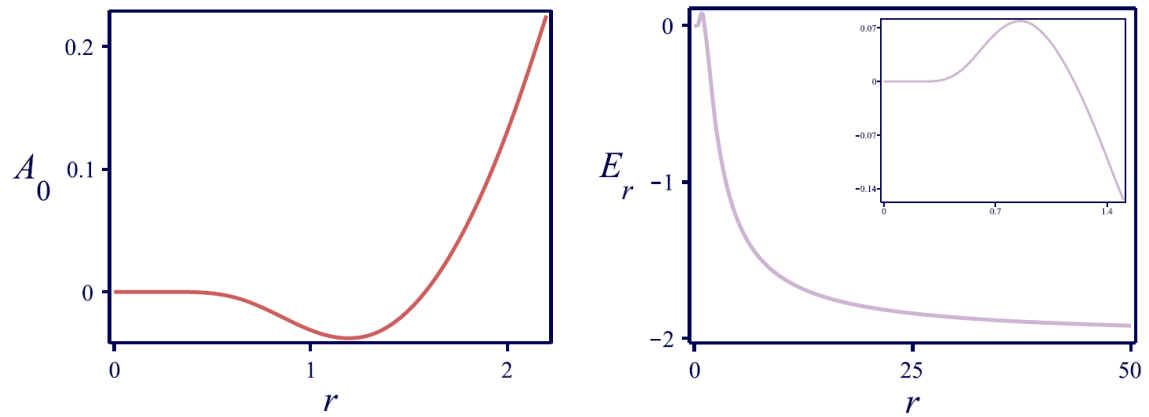


Figure 5.21 Gauge field (left) and the radial component of the electric field in Eq.(5.90) (right) associated to the system with electric permittivity in Eq.(5.89), for $D = 3$ and $e = 1$.**

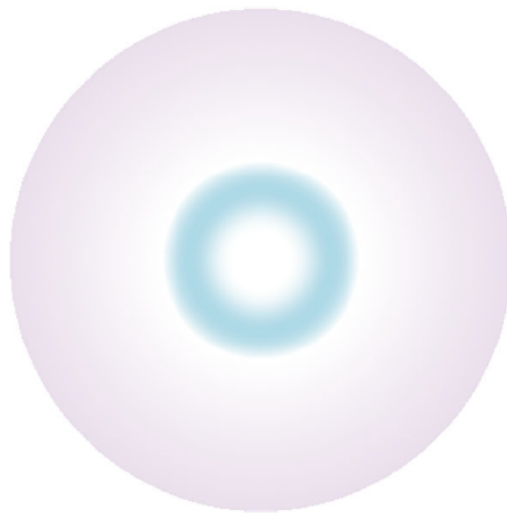


Figure 5.22 Section of the electric field passing through the center of the structure in the interval $r \in [0, 3]$ for $D = 3$ and $e = 1$. White, blue and purple are used to represent $E_r = 0$, $E_r = 0.079$ and $E_r = 2$, respectively.

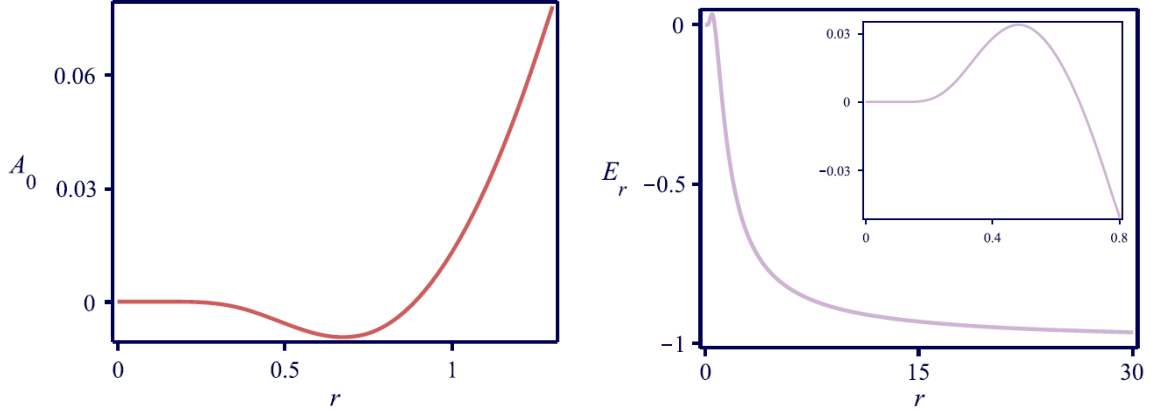


Figure 5.23 Gauge field (left) and the electric field in Eq. (5.92) (right) associated to the system with electric permittivity in Eq. (5.91), for $D = 3$ and $e = 1$. The inset in the right panel highlights the behavior of the electric field near the origin.

and the electric field in Eq. (5.81) becomes

$$\mathbf{E} = \frac{1}{8e} \left\{ \frac{1}{r^{D-1}} \left[\operatorname{sech}^2 \left(\frac{1}{(D-2)r^{D-2}} \right) + 4(D-1)r^{2D-4} \right] \right. \\ \left. \times \left[1 + \tanh \left(\frac{1}{(D-2)r^{D-2}} \right) \right] - 8(D-1)r^{D-3} \right\} \hat{r}. \quad (5.92)$$

In order to illustrate the electric field behavior, we plot it and A_0 for $D = 3$ and $e = 1$ in Fig. 5.23. Similar to the previous case, the electric field is null at the origin and grows as r gets bigger, then cross the zero and flips the signal reaching its minimum value of -1 asymptotically. However, in this case, the electric field performs this faster, forming a smaller positive shell-like structure than in the previous case; see Fig. 5.24. The energy density associated is the same as obtained in Eq. (4.62), and its energy is $E = 3\Omega(D)/16$.

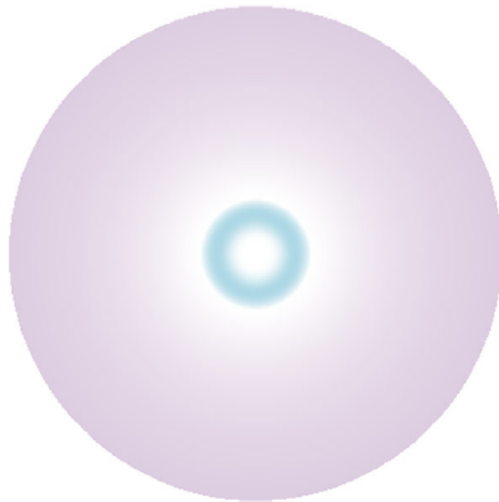


Figure 5.24 Section of the electric field passing through the center of the structure in the interval $r \in [0, 3]$ for $D = 3$ and $e = 1$. White, blue and purple are used to represent $E_r = 0$, $E_r = 0.034$ and $E_r = 1$, respectively.

Conclusions and perspectives

In this thesis, we investigated localized structures in different scenarios. We started with a review of scalar field theory in $(1, 1)$ -dimension, considering an action with standard Lagrangian density in Ch. 2. The first part establishes tools used throughout the thesis. Key themes, such as the Bogomol'nyi procedure, first-order formalism for energy minimization, stability of solutions, and structures (kinks, lumps, domain walls, Néel walls), are also discussed. Also, this chapter briefly commented on topology and topological charge. In the following pages, we introduce a model of coupled scalar fields used to describe Bloch Walls, known as BNRT, in order to motivate the investigations in the next chapter. Furthermore, we presented the trial orbit method as a mathematical tool to decouple the first-order equations.

In chapter 3, we explore modifications in the internal structure of the Bloch Walls developed by us in Ref. [20]. For that, we proposed a model with three scalar fields, where two areas were coupled by the potential describing the Bloch Wall structure. The third field is coupled to the other non-minimally through a function $f(\psi)$ that multiplies the dynamic terms, producing effects that mimic geometrical constrictions in a medium that involves the other fields. We developed a first-order formalism that minimizes energy and decouples the fields. In order to illustrate the procedure, we propose different possibilities for the function, such as $f(\psi) = 1/\psi^2$ producing a plateau in the core of solution matching with recent experiments involving domain walls in micrometer-sized $\text{Fe}_{20}\text{Ni}_{80}$, $f = \sec^2(n\pi\psi)$ inspired by the work that considers fermions in the presence of topological structures in Ref. [23] and another model that involves the Bessel function of the first kind. The procedure studied brings the possibility of another geometrical deforming of the medium, giving rise to configurations with new modifications in the profile's structures.

Chapter 4 is marked by topological structures in D spatial dimensions. Following Ref. [19], we developed a novel way to construct topological structures in D dimensions that avoid the Derrick and Hobart Theorem. We started with a Lagrangian density involving a family of scalar fields showing that usually, these structures diverge, which matches Derrick and Hobart's Theorem. Then, we proposed a first-order formalism inspired by [22], which considers the potential depends on the radial coordinate r regularizing the energy of the solutions. This procedure allowed the construction of localized structures with finite energy, such as the Global Monopoles. The first-order equations led us to a connection between global monopoles in D -dimensions with kinks in one spatial dimension. In order to illustrate the procedure, we took the auxiliary function $W(|\phi|)$ associated with the $|\phi|^4$ and $|\phi|^6$ models. In addition, we investigate two extended models. The first considered two families of fields inspired by the recent works that involve the Higgs portal, where one family is in the visible sector and the other in the hidden or dark sector. The second extended model dealt with a scalar field χ coupled non-

minimally to the family of fields ϕ^a that simulate geometrical constrictions similar to those investigated in Chapter 3. This procedure, which is the result of our work in Ref. [19], brings the light new possibilities for topological structures that may have existed in the early universe.

In chapter 5, we investigated electrically charged multi-field configurations introduced in our recent work [20]. We started with the review of electromagnetism in the presence of point charge in D spatial dimensions. Then, we propose a procedure that regularizes the divergence of the electric field at the origin. For that, we considered a point charge in a medium with electric permittivity controlled by scalar fields that mimic Bloch Walls. The procedure executed led to first-order equations and solutions with minimum energy. We use the trial orbit method to decouple the equations and get the expression of the electric field in two and three spatial dimensions. The investigations showed that the electric field presented a particular behavior forming structures of the type ring and shell for two and three dimensions, respectively. In addition, we investigated an extended model with three scalar fields, which dealt with geometrical constrictions in the Bloch Wall that controls the electric permittivity inspired in chapter 3 and Ref. [21]. Finally, we investigate a model with a family of fields inspired by the global monopole in chapter 4, in which the electric permittivity is controlled by the modulus of ϕ^a . The results led to an electric field with an unusual behavior contrary to Coulomb's law since the field attracts positive charge. The results have motivated our group to explore new possibilities, as in Ref. [17], where the authors investigate the electric field of a dipole immersed in a medium with permittivity controlled by scalar fields.

The current study inspires us to explore new possibilities of structures immersed in a medium controlled by electric permittivity, the Q-balls are an example. These are non-topological charge structures that need particular conditions to be stable. Modifications in the medium can change these conditions, giving rise to new possibilities. Other objects of our interest are the cuscuton models. Introduced in Ref. [3], cuscuton is a scalar field dark energy model with a non-standard dynamical term. In Ref. [4], the authors investigated how the cuscuton term modifies the usual behavior of kinks, showing that the solution stays the same while the energy is modified. Currently, we keep working on a paper about cuscuton following these lines of investigation.

Integrating factor for BPS equations

A.1 Integrating factor

The integrating factor method finds a function that multiplies both sides of the differential equation, making integrating the problem simpler; see Ref. [66]. In Ref. [50], the authors demonstrate that for certain first-order differential equations, it is possible to find an integrating factor that enables us to uncover all the BPS states of the system. This method of integrating factor to solve differential equations is a powerful technique that can help us gain insight into the underlying physics of various systems. We aim is to use it to decouple the BPS first-order equations (2.60) and (2.61). For that, we start with a review of the general case. Consider the differential equation bellow

$$f'(x) + a(x)f(x) = b(x) , \quad (\text{A.1})$$

Here, $f(x)$ denotes a real function, a and b are parameters that can depend on x and $f' = df/dx$. Consider the integrating factor μ to be determined. Multiplying both sides by it leads us to

$$\mu f' + \mu a f = \mu b , \quad (\text{A.2})$$

Suppose that the above equation can be written in the form

$$(\mu f)' = \mu b . \quad (\text{A.3})$$

The task of getting the function $f(x)$ becomes to solve the integral

$$\mu f = \int \mu b dx + c , \quad (\text{A.4})$$

or yet

$$f = \frac{\int \mu b dx + c}{\mu} , \quad (\text{A.5})$$

where c is an integration constant. Then the next step is to find μ in terms of the parameters a and b . For that, we rewrite the differential equation (A.3) explicitly using the chain rule as follow

$$\mu f' + \mu' f = \mu b. \quad (\text{A.6})$$

Using the Eq. (A.2) in the above equation allows rewriting the right side in the form

$$\mu f' + \mu' f = \mu f' + \mu a f . \quad (\text{A.7})$$

Thus, we can identify the integrating factor derivative as

$$\mu' = \mu a , \quad (\text{A.8})$$

and finally by integration we get

$$\mu = \exp \left\{ \int a \, dx \right\} . \quad (\text{A.9})$$

In order to use the method of integrating factors to solve our problem, we must first manipulate the differential equations (2.60) and (2.61):

$$\begin{aligned} \phi' &= 1 - \phi^2 - k\chi^2, \\ \chi' &= -2k\phi\chi, \end{aligned}$$

so that they have the same form as equation (A.1). To do this, we can identify the variable f as ϕ and x as χ . Next, we can divide equation (2.60) by equation (2.61) to bring them into the desired form for solving using integrating factors:

$$\frac{\phi'}{\chi'} = \frac{1 - \phi^2 - k\chi^2}{-2k\phi\chi}, \quad (\text{A.10})$$

regrouping terms

$$\phi_\chi + \left(-\frac{1}{2k\chi} \right) \phi = \frac{1}{\phi} \left(\frac{k\chi^2 - 1}{2k\chi} \right), \quad (\text{A.11})$$

where

$$\begin{aligned} \frac{\phi'}{\chi'} &= \frac{d\phi}{dx} \frac{dx}{d\chi} \\ &= \frac{d\phi}{d\chi} \\ &= \phi_\chi . \end{aligned} \quad (\text{A.12})$$

By analyzing the equation (A.1) in comparison to (A.11), we can identify the parameters $a = -1/2k\chi$ and $b = (k\chi^2 - 1)/2k\chi$. Thus, the differential equation (A.11) become

$$\phi_\chi + a\phi = \frac{1}{\phi} b . \quad (\text{A.13})$$

Now with the expression has the shape of the equation (A.1) we can perform the procedure. We start multiplying the above expression by μ , as follows

$$\phi(\mu\phi_\chi + \mu a\phi) = \mu b . \quad (\text{A.14})$$

Then, as before, we suppose that

$$\frac{1}{2}(\mu\phi^2)_\chi = \mu b. \quad (\text{A.15})$$

By integrating, we get

$$\phi^2 = \frac{2 \int \mu b d\chi + C}{\mu}, \quad (\text{A.16})$$

where C is a constant determining the orbit connecting the minima. From the equations (A.14) and (A.16) we can identify

$$\frac{1}{2}\mu_\chi\phi^2 + \mu\phi\phi_\chi = \mu\phi\phi_\chi + \mu a\phi^2, \quad (\text{A.17})$$

which leads us to

$$\mu = \exp\left\{2 \int a d\chi\right\}. \quad (\text{A.18})$$

Replacing the parameter a in the above equation, we get

$$\mu = \exp\left\{-2 \int \frac{1}{2k\chi} d\chi\right\}. \quad (\text{A.19})$$

This equation supports the solution

$$\mu = \chi^{-1/k}. \quad (\text{A.20})$$

We can use the above expression for μ and the parameter b to feeding the equation (A.16) as follows

$$\phi^2 = \frac{2}{\chi^{-1/k}} \int [\chi^{-1/k}(k\chi^2 - 1)(2k\chi)^{-1}] d\chi + \frac{C}{\chi^{-1/k}}. \quad (\text{A.21})$$

By integration, we get the expression

$$\phi^2 = -\frac{1}{1/k-2}\chi^2 + 1 + C\chi^{1/k}, \quad (\text{A.22})$$

or yet

$$\phi^2 + \frac{1}{1/k-2}\chi^2 = 1 + C\chi^{1/k}. \quad (\text{A.23})$$

This orbit equation can be used to decouple the first-order equations that involve the scalar fields. In Ref. [50], the authors find a critical value and analyze the orbit behavior for different values of C . Here, we consider the case for $C \rightarrow \infty$ and $C = 0$. To investigate it, we consider the analysis in Sec. 2.5.3, which leads to the topological sector formed by $W_1 = (1, 0)$ and

$W_2 = (-1, 0)$. In this sector configuration, the scalar field $\phi = \pm 1$ implies in $\chi = 0$. The regime where $C \rightarrow \infty$ must consider $\chi = 0$ in Eq. (A.23) to satisfy the topological sector condition, which leads (2.60) to

$$\phi' = 1 - \phi^2. \quad (\text{A.24})$$

The pair of solutions that involve this regime is given by

$$\phi(x) = \tanh(x), \quad (\text{A.25})$$

$$\chi(x) = 0. \quad (\text{A.26})$$

On the other hand, the regime where $C = 0$ leads to the orbit

$$\phi^2 + \frac{1}{1/k - 2} \chi^2 = 1, \quad (\text{A.27})$$

and therefore, the solutions

$$\phi(x) = \tanh(2kx), \quad (\text{A.28})$$

$$\chi(x) = \pm \sqrt{\frac{1}{k} - 2} \operatorname{sech}(2kx), \quad (\text{A.29})$$

where one must take $k \in (0, 1/2)$.

Conserved quantities

A.1 Noether Current

Continuous symmetry can be related to conserved physical quantities through the Noether Theorem. This appendix, inspired by the book [43], focuses on the steps to get the Noether Current that leads to these quantities, such as the energy-momentum tensor.

Here, we will consider the action in $(3, 1)$ -dimensions that remains unchanged after a continuous transformation on the coordinates

$$S = \int \mathcal{L}(\phi(x^\mu), \partial_\mu \phi(x^\mu)) d^4x. \quad (\text{A.1})$$

A small continuous variation can be written as a change in the coordinates that leads x^μ in x'^μ , where we denote $x'^\mu = x^\mu + \delta x^\mu$. The fields also feel the effect of variation going from $\phi(x^\mu)$ to $\phi'(x'^\mu)$, where $\phi'(x'^\mu)$ represents the field $\phi(x^\mu)$ with a shape variation at the transformed coordinate x'^μ . In order to not carry the notation, we define $\mathcal{L}(\phi, \partial_\mu \phi) \equiv \mathcal{L}(x)$, also omitting the index μ in the coordinate x . Thus varying the action, we get

$$\begin{aligned} \delta S &= \delta \int \mathcal{L}(\phi, \partial_\mu \phi) d^4x \\ &= \int \delta(\mathcal{L}(x) d^4x) \\ &= \int_{\Omega'} \mathcal{L}'(x') d^4x' - \int_{\Omega} \mathcal{L}(x) \delta d^4x, \end{aligned} \quad (\text{A.2})$$

where

$$\delta \mathcal{L}(x) = \mathcal{L}'(x') - \mathcal{L}(x). \quad (\text{A.3})$$

The volume element variation in the integral becomes

$$\begin{aligned} \delta d^4x &= d^4x' - d^4x \\ &= J(x, x') d^4x - d^4x \\ &= d^4x (J(x, x') - 1), \end{aligned} \quad (\text{A.4})$$

where $J(x, x')$ is the is the Jacobian determinant that relates x^μ with x'^μ . It is written in the form

$$J(x, x') = \det \left(\frac{\partial x'^\mu}{\partial x^\mu} \right), \quad (\text{A.5})$$

where

$$\begin{aligned}\frac{\partial x'^{\mu}}{\partial x^{\alpha}} &= \delta_{\alpha}^{\mu} + \frac{\partial(\delta x^{\mu})}{\partial x^{\alpha}} \\ &= \delta_{\alpha}^{\mu} + \partial_{\alpha} \delta x^{\mu} .\end{aligned}\tag{A.6}$$

Thus, the Jacobian determinant in Eq. (A.5) can be written in matrix form as follows

$$J(x, x') = \det \begin{pmatrix} 1 + \partial_0 \delta x^0 & \partial_1 \delta x^0 & \partial_2 \delta x^0 & \partial_3 \delta x^0 \\ \partial_0 \delta x^1 & 1 + \partial_1 \delta x^1 & \partial_2 \delta x^1 & \partial_3 \delta x^1 \\ \partial_0 \delta x^2 & \partial_1 \delta x^2 & 1 + \partial_2 \delta x^2 & \partial_3 \delta x^2 \\ \partial_0 \delta x^3 & \partial_1 \delta x^3 & \partial_2 \delta x^3 & 1 + \partial_3 \delta x^3 \end{pmatrix}, \tag{A.7}$$

Notice that non-nulls terms are in the diagonal. In this way, we can use it to rewrite the Jacobian determinant in the form

$$J(x, x') = 1 + \partial_{\mu}(\delta x^{\mu}). \tag{A.8}$$

Replacing the above expression in the volume element variation (A.4) leads us to

$$\begin{aligned}\delta d^4 x &= d^4 x (1 + \partial_{\mu}(\delta x^{\mu}) - 1) \\ &= \partial_{\mu}(\delta x^{\mu}) d^4 x .\end{aligned}\tag{A.9}$$

In the same way, the scalar field transforms as

$$\phi'(x') = \phi(x) + \delta \phi(x), \tag{A.10}$$

where this expression compares the variation of the field shape in the new coordinate and the field in the original coordinate x . It is interesting to define another kind of variation, which we denote by $\tilde{\delta}$. It operating in $\phi(x)$, compares the field variation at the same point as follows

$$\begin{aligned}\tilde{\delta} \phi(x) &= \phi'(x) - \phi(x) \\ &= \delta \phi(x) - (\phi'(x') - \phi'(x)) \\ &= \delta \phi(x) - \left[\phi'(x) + \frac{\partial \phi'(x)}{\partial x'_{\mu}} (x'_{\mu} - x_{\mu}) - \phi'(x) \right] \\ &= \delta \phi(x) - \frac{\partial \phi(x)}{\partial x_{\mu}} \delta x_{\mu} .\end{aligned}\tag{A.11}$$

As seen, the Lagrangian density depends on the field derivative, so we need to be careful when applying the operator because it may not commute. Consider the analysis below

$$\begin{aligned}\frac{\partial}{\partial x_{\mu}} (\tilde{\delta} \phi(x)) &= \frac{\partial}{\partial x_{\mu}} (\phi'(x) - \phi(x)) \\ &= \frac{\partial \phi'(x)}{\partial x_{\mu}} - \frac{\partial \phi(x)}{\partial x_{\mu}} \\ &= \tilde{\delta} \left(\frac{\partial \phi(x)}{\partial x_{\mu}} \right) .\end{aligned}\tag{A.12}$$

Therefore, we can conclude that the operators $\tilde{\delta}$ and ∂_μ commute. On the other hand, the same non-occurs with the derivative and the operator δ as follows

$$\begin{aligned}
\frac{\partial}{\partial x_\mu}(\delta\phi(x)) &= \frac{\partial}{\partial x_\mu}(\phi'(x') - \phi(x)) \\
&= \frac{\partial\phi'(x')}{\partial x'_\mu} - \frac{\partial\phi(x)}{\partial x_\mu} + \frac{\partial\phi'(x')}{\partial x_\mu} - \frac{\partial\phi'(x')}{\partial x'_\mu} \\
&= \delta\left(\frac{\partial\phi(x)}{\partial x_\mu}\right) + \frac{\partial\phi'(x')}{\partial x'_\nu} \frac{\partial x'_\nu}{\partial x_\mu} - \frac{\partial\phi'(x')}{\partial x'_\mu} \\
&= \delta\left(\frac{\partial\phi(x)}{\partial x_\mu}\right) + \frac{\partial\phi'(x')}{\partial x'_\nu} \left(g^{\nu\mu} + \frac{\partial\delta x_\nu}{\partial x_\mu}\right) - \frac{\partial\phi'(x')}{\partial x'_\mu} \\
&= \delta\left(\frac{\partial\phi(x)}{\partial x_\mu}\right) + \frac{\partial\phi'(x')}{\partial x'_\nu} \frac{\partial\delta x_\nu}{\partial x_\mu}.
\end{aligned} \tag{A.13}$$

The extra term impedes the operator's commute. Then we rewrite the variation in terms of $\tilde{\delta}$, starting with the Lagrangian density

$$\begin{aligned}
\delta\mathcal{L}(x) &= \mathcal{L}'(x') - \mathcal{L}(x) \\
&= \mathcal{L}'(x) + \frac{\partial\mathcal{L}'(x)}{\partial x_\mu} \delta x_\mu - \mathcal{L}(x) \\
&= \tilde{\delta}\mathcal{L}(x) + \frac{\partial\mathcal{L}'(x)}{\partial x_\mu} \delta x_\mu.
\end{aligned} \tag{A.14}$$

Replacing the above expression and volume element variation (A.9) in the action in Eq. (A.2) leads us to

$$\begin{aligned}
\delta S &= \int \left(\tilde{\delta}\mathcal{L}(x) + \frac{\partial\mathcal{L}'(x)}{\partial x_\mu} \delta x_\mu \right) d^4x + \int \mathcal{L}'(x) \frac{\partial\delta x_\mu}{\partial x_\mu} d^4x \\
&= \int \left(\tilde{\delta}\mathcal{L}(x) + \frac{\partial}{\partial x_\mu}(\mathcal{L}'(x)\delta x_\mu) \right) d^4x.
\end{aligned} \tag{A.15}$$

The next step is to calculate $\tilde{\delta}\mathcal{L}(x)$. It is important to remember that this variation is considered at the same point. Therefore, variations will be only in the field, and its derivative will be as follows

$$\tilde{\delta}\mathcal{L}(x) = \tilde{\delta}\phi \frac{\partial\mathcal{L}}{\partial\phi} + \tilde{\delta}\left(\frac{\partial\phi}{\partial x_\mu}\right) \frac{\partial\mathcal{L}}{\partial(\partial^\mu\phi)}. \tag{A.16}$$

Thus, the action variation in Eq. (A.15) becomes

$$\begin{aligned}
\delta S &= \int \left\{ \tilde{\delta}\phi \frac{\partial \mathcal{L}}{\partial \phi} + \tilde{\delta} \left(\frac{\partial \phi}{\partial x_\mu} \right) \frac{\partial \mathcal{L}}{\partial (\partial^\mu \phi)} + \frac{\partial}{\partial x_\mu} (\mathcal{L} \delta x_\mu) \right\} d^4x \\
&= \int \left\{ \frac{\partial}{\partial x_\mu} \left(\frac{\partial \mathcal{L}}{\partial (\partial^\mu \phi)} \right) \tilde{\delta}\phi - \frac{\partial}{\partial x_\mu} \left(\frac{\partial \mathcal{L}}{\partial (\partial^\mu \phi)} \right) \tilde{\delta}\phi + \tilde{\delta}\phi \frac{\partial \mathcal{L}}{\partial \phi} + \frac{\partial}{\partial x_\mu} (\tilde{\delta}\phi) \frac{\partial \mathcal{L}}{\partial (\partial^\mu \phi)} + \frac{\partial}{\partial x_\mu} (\mathcal{L} \delta x_\mu) \right\} d^4x \\
&= \int \left\{ \left[\frac{\partial \mathcal{L}}{\partial \phi} - \frac{\partial}{\partial x_\mu} \left(\frac{\partial \mathcal{L}}{\partial (\partial^\mu \phi)} \right) \right] \tilde{\delta}\phi + \frac{\partial}{\partial x_\mu} \left[\frac{\partial \mathcal{L}}{\partial (\partial^\mu \phi)} \tilde{\delta}\phi \right] + \frac{\partial}{\partial x_\mu} (\mathcal{L} \delta x_\mu) \right\} d^4x. \quad (\text{A.17})
\end{aligned}$$

Now if we take the action invariant by the small variation, that is, $\delta S = 0$, the integrand in the above expression will be null

$$\left[\frac{\partial \mathcal{L}}{\partial \phi} - \frac{\partial}{\partial x_\mu} \left(\frac{\partial \mathcal{L}}{\partial (\partial^\mu \phi)} \right) \right] \tilde{\delta}\phi + \frac{\partial}{\partial x_\mu} \left[\frac{\partial \mathcal{L}}{\partial (\partial^\mu \phi)} \tilde{\delta}\phi \right] + \frac{\partial}{\partial x_\mu} (\mathcal{L} \delta x_\mu) = 0. \quad (\text{A.18})$$

Notice that the first term in the above expression is the Euler-Lagrange equation, which is null. In this way, we can write

$$\begin{aligned}
\frac{\partial}{\partial x_\mu} \left(\frac{\partial \mathcal{L}}{\partial (\partial^\mu \phi)} \tilde{\delta}\phi \right) + \frac{\partial}{\partial x_\mu} (\mathcal{L} \delta x_\mu) &= 0 \\
\frac{\partial}{\partial x_\mu} \left(\frac{\partial \mathcal{L}}{\partial (\partial^\mu \phi)} \tilde{\delta}\phi + \mathcal{L} \delta x_\mu \right) &= 0 \\
\frac{\partial}{\partial x_\mu} f_\mu(x) &= 0. \quad (\text{A.19})
\end{aligned}$$

Note that for the above expression to be obeyed, the term in parentheses must be constant. Therefore, this term describes a quantity conserved that we define as Noether Current:

$$f_\mu(x) \equiv \frac{\partial \mathcal{L}}{\partial (\partial^\mu \phi)} \tilde{\delta}\phi + \mathcal{L} \delta x_\mu, \quad (\text{A.20})$$

or yet

$$\begin{aligned}
f_\mu(x) &= \frac{\partial \mathcal{L}}{\partial (\partial^\mu \phi)} (\delta\phi(x) - \partial^\nu \phi(x) \delta x_\nu) + \mathcal{L} \delta x_\mu \\
&= \frac{\partial \mathcal{L}}{\partial (\partial^\mu \phi)} \delta\phi(x) - \left(\frac{\partial \mathcal{L}}{\partial (\partial^\mu \phi)} \partial^\nu \phi(x) \delta x_\nu - \mathcal{L} \delta x_\nu \delta x^\nu \delta x_\mu \right) \\
&= \frac{\partial \mathcal{L}}{\partial (\partial^\mu \phi)} \delta\phi(x) - \left(\frac{\partial \mathcal{L}}{\partial (\partial^\mu \phi)} \partial_\nu \phi(x) \delta x^\nu - g_{\mu\nu} \delta x^\nu \mathcal{L} \right). \quad (\text{A.21})
\end{aligned}$$

Thus we finally get

$$f_\mu(x) = \frac{\partial \mathcal{L}}{\partial (\partial^\mu \phi)} \delta\phi(x) - \left(\frac{\partial \mathcal{L}}{\partial (\partial^\mu \phi)} \partial_\nu \phi(x) - g_{\mu\nu} \mathcal{L} \right) \delta x^\nu. \quad (\text{A.22})$$

A.2 Energy-momentum tensor

The energy-momentum tensor is a quantity related to invariant translations. To see that, we consider that the scalar field is invariant by coordinate transformation $x'^{\mu} = x^{\mu} + \varepsilon^{\mu}$, we can understand it as $\phi(x)$ does not change its shape on transformation. This can write as $\phi'(x') = \phi(x)$, and the consequence of that is $\delta\phi = 0$, which allows us to discard the first term. Multiplying the equation (A.22) by ε_{ν} and differentiating we get

$$\frac{\partial}{\partial x_{\mu}} T_{\mu\nu} = 0, \quad (\text{A.23})$$

where

$$T_{\mu\nu} = \pm \frac{\partial \mathcal{L}}{\partial (\partial^{\mu} \phi)} \partial_{\nu} \phi(x) \mp g_{\mu\nu} \mathcal{L}. \quad (\text{A.24})$$

The sign respect the metric ($\pm, \mp, \mp, \dots, \mp$), but by convention, we choose the energy density T_{00} with a positive sign.

The above expression can present problems in the case of vector fields. In the gauge field A^{μ} , the energy-momentum tensor is non-gauge invariant and non-symmetric. A modification can be done in the tensor to respect these conditions leading to the Belinfante-Rosenfeld tensor. Another way to get the energy-momentum tensor for a vector field without putting a term by hand is through a general relativity approach. Here, we present this other way following the way outlined in books [88] and [46]. As a model, we will use the Lagrangian density in Eq. (5.8) without the source.

Consider the Einstein–Hilbert action in general relativity for this model

$$S = \int \left[-\frac{1}{4} P(\phi) g^{\mu\rho} g^{\nu\sigma} F_{\rho\sigma} F_{\mu\nu} + \frac{1}{2} g^{\mu\nu} \partial_{\mu} \phi \partial_{\nu} \phi \right] \sqrt{-g} d^D x. \quad (\text{A.25})$$

Here, g denotes the metric determinant. A variation in this model leads to

$$\begin{aligned} \delta S = & \int \left[-\frac{1}{4} P(\phi) \delta(g^{\mu\rho} g^{\nu\sigma}) F_{\rho\sigma} F_{\mu\nu} + \frac{1}{2} \delta(g^{\mu\nu}) \partial_{\mu} \phi \partial_{\nu} \phi \right] \sqrt{-g} d^D x \\ & + \int \left[-\frac{1}{4} P(\phi) F_{\rho\sigma} F^{\rho\sigma} + \frac{1}{2} \partial_{\alpha} \phi \partial^{\alpha} \phi \right] \delta(\sqrt{-g}) d^D x, \end{aligned} \quad (\text{A.26})$$

which leads us to

$$\begin{aligned} \delta S = & \int \left[-\frac{1}{4} P(\phi) \left(2g^{\rho\sigma} F_{\mu\rho} F_{\nu\sigma} - \frac{1}{2} g_{\mu\nu} F_{\rho\sigma} F^{\rho\sigma} \right) \right. \\ & \left. + \frac{1}{2} \partial_{\mu} \phi \partial_{\nu} \phi - \left(\frac{1}{4} \partial_{\alpha} \phi \partial^{\alpha} \phi \right) g_{\mu\nu} \right] \delta g^{\mu\nu} \sqrt{-g} d^D x, \end{aligned} \quad (\text{A.27})$$

where $\delta\sqrt{-g} = -(1/2)\sqrt{-g}g_{\mu\nu}\delta g^{\mu\nu}$. The term between square brackets is identified as

$$\begin{aligned} \frac{1}{2} T_{\mu\nu} = & -\frac{1}{4} P(\phi) \left(2g^{\rho\sigma} F_{\mu\rho} F_{\nu\sigma} - \frac{1}{2} g_{\mu\nu} F_{\rho\sigma} F^{\rho\sigma} \right) \\ & + \frac{1}{2} \partial_{\mu} \phi \partial_{\nu} \phi - \left(\frac{1}{4} \partial_{\alpha} \phi \partial^{\alpha} \phi \right) g_{\mu\nu}, \end{aligned} \quad (\text{A.28})$$

or yet

$$T_{\mu\nu} = -\frac{1}{4}P(\phi)\left(4F_{\mu\rho}F_{\nu}^{\rho} - g_{\mu\nu}F_{\rho\sigma}F^{\rho\sigma}\right) + \partial_{\mu}\phi\partial_{\nu}\phi - \frac{1}{2}g_{\mu\nu}\partial_{\alpha}\phi\partial^{\alpha}\phi. \quad (\text{A.29})$$

The energy density T_{00} in this case is given by

$$T_{00} = -\frac{1}{4}P(\phi)\left(4F_{0\rho}F_0^{\rho} - g_{00}F_{\rho\sigma}F^{\rho\sigma}\right) + \partial_0\phi\partial_0\phi - \frac{1}{2}g_{00}\partial_{\alpha}\phi\partial^{\alpha}\phi. \quad (\text{A.30})$$

This expression in terms of the electric field takes the form

$$T_{00} = -\frac{1}{4}P(\phi)\left(-4|\mathbf{E}|^2 - (-2|\mathbf{E}|^2)\right) + \frac{1}{2}\phi'^2, \quad (\text{A.31})$$

where static configurations were considered. Thus, we write the energy density for this model in the form

$$T_{00} = \frac{1}{2}P|\mathbf{E}|^2 + \frac{1}{2}\phi'^2. \quad (\text{A.32})$$

The above expressions can serve as a guide to obtain the other energy density for the other models.

Bibliography

- [1] Vortex-line models for dual strings. *Nuclear Physics B*, 61:45–61, 1973.
- [2] Magnetic monopoles in unified gauge theories. *Nuclear Physics B*, 79(2):276–284, 1974.
- [3] N. Afshordi, D. J. H. Chung, and G. Geshnizjani. Cuscuton: A Causal Field Theory with an Infinite Speed of Sound. *Phys. Rev. D*, 75:083513, 2007.
- [4] I. Andrade, M. A. Marques, and R. Menezes. Cuscuton kinks and branes. *Nucl. Phys. B*, 942:188–204, 2019.
- [5] G. Arcadi, A. Djouadi, and M. Kado. The Higgs-portal for vector dark matter and the effective field theory approach: A reappraisal. *Phys. Lett. B*, 805:135427, 2020.
- [6] A. Avelar, D. Bazeia, W. Cardoso, and L. Losano. Lump-like structures in scalar-field models in 1+1 dimensions. *Physics Letters A*, 374(2):222–227, 2009.
- [7] A. T. Avelar, D. Bazeia, L. Losano, and R. Menezes. New Lump-like Structures in Scalar-field Models. *Eur. Phys. J. C*, 55:133–143, 2008.
- [8] M. Barriola and A. Vilenkin. Gravitational field of a global monopole. *Phys. Rev. Lett.*, 63:341–343, Jul 1989.
- [9] D. Bazeia, M. dos Santos, and R. Ribeiro. Solitons in systems of coupled scalar fields. *Physics Letters A*, 208(1):84–88, 1995.
- [10] D. Bazeia, W. Freire, L. Losano, and R. F. Ribeiro. Topological defects and the trial orbit method. *Modern Physics Letters A*, 17(29):1945–1953, 2002.
- [11] D. Bazeia and A. R. Gomes. Bloch brane. *Journal of High Energy Physics*, 2004(05):012, may 2004.
- [12] D. Bazeia, M. A. Liao, and M. A. Marques. Geometrically constrained kinklike configurations. *Eur. Phys. J. Plus*, 135(4):383, 2020.
- [13] D. Bazeia, L. Losano, and R. Menezes. First-order framework and generalized global defect solutions. *Physics Letters B*, 668(3):246–252, 2008.
- [14] D. Bazeia, L. Losano, R. Menezes, and J. Oliveira. Generalized global defect solutions. *The European Physical Journal C*, 51:953–962, 2007.

- [15] D. Bazeia, M. A. Marques, and R. Menezes. Stable finite energy global vortices and asymptotic freedom. *Europhysics Letters*, 122(6):61001, jul 2018.
- [16] D. Bazeia, M. A. Marques, and R. Menezes. Electrically charged localized structures. *Eur. Phys. J. C*, 81(1):94, 2021.
- [17] D. Bazeia, M. A. Marques, and R. Menezes. Maxwell-scalar device based on the electric dipole. *Phys. Rev. D*, 104:L121703, Dec 2021.
- [18] D. Bazeia, M. A. Marques, and G. J. Olmo. Small and hollow magnetic monopoles. *Phys. Rev. D*, 98:025017, Jul 2018.
- [19] D. Bazeia, M. A. Marques, and M. Paganelly. Novel way to construct spatially localized finite energy structures. *Eur. Phys. J. Plus*, 136(10):990, 2021.
- [20] D. Bazeia, M. A. Marques, and M. Paganelly. Electrically charged multi-field configurations. *Eur. Phys. J. C*, 82(11):1036, 2022.
- [21] D. Bazeia, M. A. Marques, and M. Paganelly. Manipulating the internal structure of Bloch walls. *Eur. Phys. J. Plus*, 137(10):1117, 2022.
- [22] D. Bazeia, J. Menezes, and R. Menezes. New global defect structures. *Phys. Rev. Lett.*, 91:241601, Dec 2003.
- [23] D. Bazeia, A. Mohammadi, and D. C. Moreira. Fermions in the presence of topological structures under geometric constrictions. *Phys. Rev. D*, 103:025003, Jan 2021.
- [24] D. Bazeia, J. R. Nascimento, and D. Toledo. Alternate route to soliton solutions in hydrogen-bonded chains. *Physics Letters A*, 228:357–362, 1996.
- [25] D. Bazeia, J. R. S. Nascimento, R. F. Ribeiro, and D. Toledo. Soliton stability in systems of two real scalar fields. *Journal of Physics A: Mathematical and General*, 30(23):8157–8166, dec 1997.
- [26] D. Bazeia and E. Ventura. Topological twistons in crystalline polyethylene. *Chemical Physics Letters*, 303(3):341–346, 1999.
- [27] E. B. Bogomolny. Stability of Classical Solutions. *Sov. J. Nucl. Phys.*, 24:449, 1976.
- [28] P. Braga, M. Guimaraes, and M. Paganelly. Multivalued fields and monopole operators in topological superconductors. *Annals of Physics*, 419:168245, 2020.
- [29] G. Chen, J. Zhu, A. Quesada, J. Li, A. T. N’Diaye, Y. Huo, T. P. Ma, Y. Chen, H. Y. Kwon, C. Won, Z. Q. Qiu, A. K. Schmid, and Y. Z. Wu. Novel chiral magnetic domain wall structure in Fe/Ni/Cu(001) films. *Phys. Rev. Lett.*, 110:177204, Apr 2013.
- [30] J. M. D. Coey. *Magnetism and Magnetic Materials*. Cambridge University Press, 2010.

- [31] S. R. Coleman. Q-balls. *Nucl. Phys. B*, 262(2):263, 1985. [Addendum: *Nucl.Phys.B* 269, 744 (1986)].
- [32] S. R. Coleman. Q-balls. *Nucl. Phys. B*, 262(2):263, 1985. [Addendum: *Nucl.Phys.B* 269, 744 (1986)].
- [33] F. Dalfovo, S. Giorgini, L. P. Pitaevskii, and S. Stringari. Theory of bose-einstein condensation in trapped gases. *Rev. Mod. Phys.*, 71:463–512, Apr 1999.
- [34] M. de Montigny, H. Hassanabadi, J. Pinfeld, and S. Zare. Exact solutions of the generalized Klein–Gordon oscillator in a global monopole space-time. *Eur. Phys. J. Plus*, 136(7):788, 2021.
- [35] G. H. Derrick. Comments on nonlinear wave equations as models for elementary particles. *Journal of Mathematical Physics*, 5(9):1252–1254, 1964.
- [36] F. Diebel, M. Boguslawski, T. Dadalyan, R. Drampyan, and C. Denz. Controlled soliton formation in tailored bessel photonic lattices. *Opt. Express*, 24(12):12933–12940, Jun 2016.
- [37] P. A. M. Dirac. Quantised singularities in the electromagnetic field,. *Proc. Roy. Soc. Lond. A*, 133(821):60–72, 1931.
- [38] P. A. M. Dirac. The relation between mathematics and physics. *Proceedings of the Royal Society of Edinburgh*, 59:122–129, 1940.
- [39] B. Felsager. *GEOMETRY, PARTICLES AND FIELDS*. Graduate Texts in Contemporary Physics. Univ.Pr., Odense, 1981.
- [40] R. Friedberg and T. D. Lee. Fermion-field nontopological solitons. *Phys. Rev. D*, 15:1694–1711, Mar 1977.
- [41] R. Friedberg, T. D. Lee, and A. Sirlin. Class of scalar-field soliton solutions in three space dimensions. *Phys. Rev. D*, 13:2739–2761, May 1976.
- [42] A. S. Goldhaber. Collapse of a “global monopole”. *Phys. Rev. Lett.*, 63:2158–2158, Nov 1989.
- [43] W. Greiner and J. Reinhardt. *Field quantization*. 1996.
- [44] H. A. Haus and W. S. Wong. Solitons in optical communications. *Rev. Mod. Phys.*, 68:423–444, Apr 1996.
- [45] R. H. Hobart. 82(2):201, aug 1963.
- [46] M. P. Hobson, G. P. Efstathiou, and A. N. Lasenby. *General relativity: An introduction for physicists*. 2006.

- [47] J. Hong, Y. Kim, and P. Y. Pac. Multivortex solutions of the abelian chern-simons-higgs theory. *Phys. Rev. Lett.*, 64:2230–2233, May 1990.
- [48] A. Hook, S. Kachru, and G. Torroba. Supersymmetric Defect Models and Mirror Symmetry. *JHEP*, 11:004, 2013.
- [49] G. T. Horowitz, J. E. Santos, and D. Tong. Optical Conductivity with Holographic Lattices. *JHEP*, 07:168, 2012.
- [50] A. A. Izquierdo, M. A. G. León, and J. M. Guilarte. Kink variety in systems of two coupled scalar fields in two space-time dimensions. *Phys. Rev. D*, 65:085012, Mar 2002.
- [51] R. Jackiw and E. J. Weinberg. Self-dual chern-simons vortices. *Phys. Rev. Lett.*, 64:2234–2237, May 1990.
- [52] P.-O. Jubert, R. Allenspach, and A. Bischof. Magnetic domain walls in constrained geometries. *Phys. Rev. B*, 69:220410, Jun 2004.
- [53] B. Julia and A. Zee. Poles with both magnetic and electric charges in non-abelian gauge theory. *Phys. Rev. D*, 11:2227–2232, Apr 1975.
- [54] Y. V. Kartashov, A. Ferrando, A. A. Egorov, and L. Torner. Soliton topology versus discrete symmetry in optical lattices. *Physical review letters*, 95 12:123902, 2005.
- [55] Y. V. Kartashov, V. A. Vysloukh, and L. Torner. Rotary solitons in besel optical lattices. *Phys. Rev. Lett.*, 93:093904, Aug 2004.
- [56] Y. V. Kartashov, V. A. Vysloukh, and L. Torner. Stable ring-profile vortex solitons in besel optical lattices. *Phys. Rev. Lett.*, 94:043902, Feb 2005.
- [57] T. W. B. Kibble. Topology of cosmic domains and strings. *Journal of Physics A: Mathematical and General*, 9(8):1387, aug 1976.
- [58] T. Lancaster and S. J. Blundell. *Quantum Field Theory for the Gifted Amateur*. Oxford University Press, 2014.
- [59] L. D. Landau. On the theory of phase transitions. *Zh. Eksp. Teor. Fiz.*, 7:19–32, 1937.
- [60] T. D. Lee and G. C. Wick. Vacuum stability and vacuum excitation in a spin-0 field theory. *Phys. Rev. D*, 9:2291–2316, Apr 1974.
- [61] J. Léonard, A. Morales, P. Zupancic, T. Esslinger, and T. Donner. Supersolid formation in a quantum gas breaking a continuous translational symmetry. *Nature*, 543:87–90, 2016.
- [62] K. W. Madison, F. Chevy, W. Wohlleben, and J. Dalibard. Vortex formation in a stirred bose-einstein condensate. *Phys. Rev. Lett.*, 84:806–809, Jan 2000.
- [63] N. S. Manton and P. Sutcliffe. *Topological solitons*. Cambridge Monographs on Mathematical Physics. Cambridge University Press, 2004.

- [64] M. A. Marques. Novel lump-like structures. *Europhysics Letters*, 125(1):11001, Jan 2019.
- [65] D. Mihalache, D. Mazilu, F. Lederer, B. A. Malomed, Y. V. Kartashov, L.-C. Crasovan, and L. Torner. Stable spatiotemporal solitons in Bessel optical lattices. *Phys. Rev. Lett.*, 95:023902, Jul 2005.
- [66] P. M. Morse and H. Feshbach. Methods of theoretical physics. *American Journal of Physics*, 22(6):410–413, 1954.
- [67] M. Nakahara. *Geometry, topology and physics*. 2003.
- [68] L. Perivolaropoulos. Instabilities and interactions of global topological defects. *Nuclear Physics B*, 375(3):665–693, 1992.
- [69] S. D. Pollard, J. A. Garlow, K.-W. Kim, S. Cheng, K. Cai, Y. Zhu, and H. Yang. Bloch chirality induced by an interlayer dzyaloshinskii-moriya interaction in ferromagnetic multilayers. *Phys. Rev. Lett.*, 125:227203, Nov 2020.
- [70] A. M. Polyakov. Particle Spectrum in Quantum Field Theory. *JETP Lett.*, 20:194–195, 1974.
- [71] M. K. Prasad and C. M. Sommerfield. Exact classical solution for the 't Hooft monopole and the Julia-Zee dyon. *Phys. Rev. Lett.*, 35:760–762, Sep 1975.
- [72] J. P. Preskill. Cosmological production of superheavy magnetic monopoles. *Phys. Rev. Lett.*, 43:1365–1368, Nov 1979.
- [73] R. Rajaraman. Solitons of coupled scalar field theories in two dimensions. *Phys. Rev. Lett.*, 42:200–204, Jan 1979.
- [74] L. Randall and R. Sundrum. An alternative to compactification. *Phys. Rev. Lett.*, 83:4690–4693, Dec 1999.
- [75] G. W. Rayfield and F. Reif. Evidence for the creation and motion of quantized vortex rings in superfluid helium. *Phys. Rev. Lett.*, 11:305–308, Oct 1963.
- [76] S. H. Rhie and D. P. Bennett. Global monopoles do not “collapse”. *Phys. Rev. Lett.*, 67:1173–1173, Aug 1991.
- [77] L. H. Ryder. *Quantum Field Theory*. Cambridge University Press, 2 edition, 1996.
- [78] Q. Shafi and A. Vilenkin. Inflation with $su(5)$. *Phys. Rev. Lett.*, 52:691–694, Feb 1984.
- [79] T. Shinjo, T. Okuno, R. Hassdorf, K. Shigeto, and T. Ono. Magnetic vortex core observation in circular dots of permalloy. *Science*, 289(5481):930–932, 2000.
- [80] T. Skyrme. A unified field theory of mesons and baryons. *Nuclear Physics*, 31:556–569, 1962.

- [81] T. H. R. Skyrme. A Nonlinear field theory. *Proc. Roy. Soc. Lond. A*, 260:127–138, 1961.
- [82] D. Tong and K. Wong. Vortices and Impurities. *JHEP*, 01:090, 2014.
- [83] T. Vachaspati. *Kinks and Domain Walls: An Introduction to Classical and Quantum Solitons*. Cambridge University Press, 2006.
- [84] D. Vegh. Holography without translational symmetry. 1 2013.
- [85] A. Vilenkin. Cosmic strings and domain walls. *Physics Reports*, 121(5):263–315, 1985.
- [86] A. Vilenkin and E. P. S. Shellard. *Cosmic strings and other topological defects*. Cambridge monographs on mathematical physics. Cambridge Univ. Press, Cambridge, 1994.
- [87] A. Wachowiak, J. Wiebe, M. Bode, O. Pietzsch, M. Morgenstern, and R. Wiesendanger. Direct observation of internal spin structure of magnetic vortex cores. *Science*, 298(5593):577–580, 2002.
- [88] R. M. Wald. *General Relativity*. Chicago Univ. Pr., Chicago, USA, 1984.

